THE EFFECTS OF LOW-LEVEL ELECTROMAGNETIC FIELDS AND ULTRAWEAK PHOTON EMISSION ON BIOLOGICAL SYSTEMS

by

Lukasz M. Karbowski

A thesis submitted in partial fulfillment
of the requirements for the degree of
Doctor of Philosophy (PhD) in Biomolecular Sciences

The Faculty of Graduate Studies
Laurentian University
Sudbury, Ontario

THESIS DEFENCE COMMITTEE/COMITÉ DE SOUTENANCE DE THÈSE
Laurentian Université/Université Laurentienne
Faculty of Graduate Studies/Faculté des études supérieures

Title of Thesis Titre de la thèse	THE EFFECTS OF LOW-LEVEL ELECTROMAGNETIC FIELDS AND ULTRAWEAK PHOTON EMISSION ON BIOLOGICAL SYSTEMS
Name of Candidate Nom du candidat	Karbowski, Lukasz
Degree Diplôme	Doctor of Philosophy Science
Department/Program Département/Programme	Biomolecular Sciences
Date of Defence Date de la soutenance	March 17, 2017

APPROVED/APPROUVÉ

Thesis Examiners/Examinateurs de thèse:

Dr. Michael Persinger
(Supervisor/Directeur(trice) de thèse)

Dr. Rob Lafrenie
(Committee member/Membre du comité)

Dr. Abdel Omri
(Committee member/Membre du comité)

Dr. Carl Blackman
(External Examiner/Examinateur externe)

Dr. Cynthia Whissell
(Internal Examiner/Examinateur interne)

Approved for the Faculty of Graduate Studies
Approuvé pour la Faculté des études supérieures
Dr. David Lesbarrères
Monsieur David Lesbarrères
Dean, Faculty of Graduate Studies
Doyen, Faculté des études supérieures

ACCESSIBILITY CLAUSE AND PERMISSION TO USE

Abstract

The functionality of biological organisms is a product of minute-invisible forces and structures, which together form a cohesive ensemble that initiate the processes of life. The electromagnetic and photonic nature of biological life and its basic unit the cell may be considered a viable option for communication, survival and senescence. The basis of this investigation considers the dynamic nature of low-level electromagnetic fields and ultraweak photon emission as a mechanism for intracellular and intercellular interactions, which work under the premise of only demanding small quanta of energy. Metastatic cancerous cells have been observed to emit specific frequencies of photon emission compared to healthy cells and increase this emission in unfavorable conditions. The application of a specific sequence of patterns (MuKarb) at a specific intensity, observed in the dissolution of planarian worms, when applied to cancerous cells produce complete death of the exposed metastatic cells but not healthy cells. When such patterns of light at specific wavelengths are pulsed into the aforementioned cells, the emitted light from the cells in the pulsed pattern is observed relative to the duration of the light exposure. These effects become critical to the specificity of the appropriate pattern and intensity of the field, which has been linked to the importance of appropriate equipment configuration. The smallest

changes in the current/voltage flow within the circuitry of the digital to analogue converter and electromagnetic field devices can make drastic changes with respect to the elimination of cancerous cells being observed or not. This phenomenon reflects the Aharanov-Bohm phase shifts in voltage within the electromagnetic field equipment and its importance in producing effects as a result of low-level electromagnetic fields. The application of specificity within low-level electromagnetic generating equipment has also been shown through the process of non-locality (entanglement) where appropriate and tuned apparatus are required to produce specific non-local effects. Successful non-local effects were observed through observing decreases in growth of melanoma cells through nontangible means, comparable to the manipulate local melanoma cells. These results converge on the premise and importance of properly tuned equipment for successful low-level electromagnetic field and photon exposures. Furthermore the interaction between the use of low-level electromagnetic fields and photons at specific pattern has shown the importance of interfering with the propagation of metastatic cells.

Acknowledgements

The development process and completion of this dissertation would not be possible without the presence of the many people in my life, which helped in cultivating my experiences and unforgettable memories.

My immediate gratitude to my supervisor and mentor Dr. Michael Persinger whose guidance, patience and perseverance helped me obtain a drive for excellence. Your passion and dedication in the pursuit of discovery is one that one wishes to replicate.

I am truly grateful to my thesis committee, Dr. Robert Lafrenie and Dr. Abdelwahab Omri and my examiners Dr. Carl F. Blackman and Dr. Cynthia Whissell for their insights and constructive criticisms. Thank you for your guidance and support during the creation of this dissertation.

Great thanks is also credited to my research colleagues and friends within the Neuroscience Research Group, with whom exploring the unknown gives us the ability to create the world we envision in our dreams.

I would also like to thank my brothers and parents for their constant support and words of encouragement throughout this journey.

Table of Contents

Title. i
Signature Page ii
Abstract iii
Acknowledgements v
Table of Contents. vi
List of Tables ix
List of Figures. x
List of Abbreviations. xiii

Chapter One: 1.0 – Introduction. 1
1.1 Water Viscosity. 3
1.2 Electromagnetic Fields 6
1.3 Ultraweak Photon Emission in Biological Organisms. . . 11
1.4 Irena Cosic's Resonance Recognition Model. 14
1.5 Low-level Electromagnetic Fields and Excess Correlations 17
1.6 Thesis Objective 21
1.7 References 22
1.8 Preamble to Chapter 2. 32

Chapter Two: 2.0 - Variable Viscosity of Water as the Controlling Factor in Energetic Quantities That Control Living Systems: Physicochemical and Astronomical Interactions. 33
Abstract. 34
2.1 Introduction 35
2.2 Intrinsic Energy Derived from the Viscosity of Water . 38
2.3 Fluorescence Spectrometry Evidence 40
2.4 Estimating Intrinsic Frequencies 44
2.5 Application to the S-E Relationship. 45
2.6 Intramolecular Pressure and Photon Emission. 46
2.7 Gravitational Variants 48
2.8 Conclusion 50
2.9 References 52
2.10 Preamble to Chapter 3. 55

Chapter Three: 3.0 - Experimental Evidence That Specific Photon Energies Are "Stored" In Malignant Cells For an Hour: The Synergism of Weak Magnetic Field-LED Wavelength Pulses 56
Abstract. 57
3.1 Introduction 59
3.2 Procedure. 63
3.3 Results. 73
3.4 Discussion 81
3.5 References 88

3.6 Preamble to Chapter 4. 94
Chapter Four: 4.0 - Only 1% Melanoma Proportion in Non-Malignant Cells Exacerbates Photon Emissions: Implications for Tumor Growth and Metastases 95
Abstract. 96
4.1 Introduction 98
4.2 Methods. 99
4.3 Results. 101
4.4 Discussion 102
4.5 Summary at a Glance. 107
4.6 References 108
4.7 Preamble to Chapter 5. 111

Chapter Five: 5.0 - Novel Cosic Resonance ("Standing Wave") Solutions for Components of the JAK-STAT Cellular Signaling Pathway: A Convergence of Spectral Density Profiles. 112
Abstract. 113
5.1 Letter 114
5.2 References 131
5.3 Preamble to Chapter 6. 133

Chapter Six: 6.0 - Seeking the Source of Transience for a Unique Magnetic Field Pattern That Completely Dissolves Cancer Cells *in Vitro*. 134
Abstract. 135
6.1 Introduction 137
6.2 Materials and Methods. 140
6.2.1 General Experimental Protocol. 140
6.2.2 Biochemical Measures 141
6.2.3 Equipment. 142
6.3 Results. 149
6.4 Discussion 157
6.4.1 Potential Mechanisms 159
6.4.2 Potential Sources for Inconsistency of Effects. 160
6.5 General Conclusion 165
6.6 References 166
6.7 Preamble to Chapter 7. 173

Chapter Seven: 7.0 - Temporal Precision and Instrumental Complexity Determine the Efficacy of Cancer Treatment by Weak, Complex Patterned Magnetic Fields. 174
Abstract. 175
7.1 Introduction 177
7.2 Methods. 182
7.2.1 Cells. 182
7.2.2 Mouse Exposures. 184

7.2.3 Equipment Design and Specifications. 185
7.3 Results. 191
7.4 Discussion 197
7.5 References 203
7.6 Preamble to Chapter 8. 211

Chapter Eight: 8.0 - Experimental Demonstration That Aharanov-Bohm Phase Shift Voltages In Optical Coupler Circuits of Tuned Patterned Magnetic Fields Is Critical for Inhibition of Malignant Cell Growth. 212
Abstract. 213
8.1 Introduction 214
8.2 Methods and Materials. 216
8.3 Results. 220
8.4 Discussion and Conclusion. 222
8.5 References 228
8.6 Preamble to Chapter 9. 233

Chapter Nine: 9.0 - Elimination of growth inhibition of malignant cells by specific patterned magnetic fields when source solenoids are wrapped with copper: implications for quantum (Aharanov-Bohm) effects. 234
Abstract. 235
9.1 Introduction 237
9.2 Methods and Materials. 244
9.3 Results. 252
9.4 Discussion 255
9.5 References 261
9.6 Preamble to Chapter 10 265

Chapter Ten: 10.0 - Experimentally-Induced Inhibition of Growth in Melanoma Cell Cultures Separated by ~Two Kilometers When Both Share Excess Correlation Magnetic Fields: Macroscopic Evidence of Free-Space Quantum Teleportation?. 266
Abstract. 267
10.1 Introduction 269
10.2 Materials and Methods. 273
10.3 Results. 278
10.4 Discussion 284
10.5 Conclusion 291
10.6 References 293

Chapter Eleven: 11.0 – Discussion. 297
Discussion. 297
Future Direction. 305

List of Tables

Chapter Six:

Table 1A. Percent dropout of malignant cells for specific magnetic field configurations. 151

Table 1B. Continuation of summary of results from Table 1A. . 153

Chapter Seven:

Table 1. Percentages of indicated proportions of cell growth suppression compared to shame field controls 193

List of Figures

Chapter Three:

Figure 1. Exposure and measurement diagram 65

Figure 2. The actual LED and Magnetic Field exposure device. . 67

Figure 3. The frequency-modulated or "Thomas" pattern. 68

Figure 4. The general shape of the "geomagnetic pattern" . . . 69

Figure 5. The "LTP" pulse derived from Rose et al for stimulating hippocampal slices generated as a magnetic field. 70

Figure 6. Log base 10 of the mean numbers of photons per minute from the cell plates. 74

Figure 7. The mean numbers of photon emissions per s per min. .76

Figure 8. Emission values (photons per min) 77

Figure 9. Vertical axis indicates the numbers of photon counts by fluorescent spectrometry measurements for the media only as a function of wavelength of emissions. 78

Figure 10. Fluorescence spectrometry for cells (sham field) as a function of the wavelength of emissions. 79

Figure 11. Fluorescence spectrometry of cells exposed to specific parameters of the low intensity magnetic field plus light. . . 80

Chapter Four:

Figure 1. Photon emission of cell mixtures 102

Figure 2. Spectral Power Density for photon emissions for the amplitude enhanced at the 22 Hz band 103

Chapter Five:

Figure 1. Fluorescence (photon) counts predicted by Cosic's Recognition Resonance Model. 118

Figure 2. Stylized shapes and descriptions of the proteins composing the JAK-STAT 122

Figure 3. Predicted Spectral Density Profile for CASP-9 . . . 125

Figure 4. Congruence of distribution of Spectral Power Densities profiles. 126

Figure 5. Maximum congruence of SPD profiles for CASP-9 . . . 127

Chapter Six:

Figure 1. The three main components of the DAC system 143

Figure 2. Colorized measurement of the strength of the Thomas pattern magnetic field. 145

Figure 3. Comparisons between frequency-modulated patterns . .147

Figure 4. Cell plate positions. 150

Figure 5. Presence of melanin formation. 154

Figure 6. Appearance of melanin in melanoma cells. 155

Figure 7. Fluorescence staining for phalloidin 156

Figure 8. Acridine orange stain results. 156

Chapter Seven:

Figure 1. The shape of the frequency shifting magnetic field .188

Figure 2. An example of the acrylic exposure box 190

Figure 3. Percentage suppression of growth of melanoma cells .196

Chapter Eight:

Figure 1. Exposure device where culture plates were placed . .218

Figure 2. Temporal structure of the magnetic field pattern . .219

Figure 3. Numbers of cells present after 5 days. 221

Chapter Nine:

Figure 1. Relative (uv) emission fluorescence spectrometry ratios 243

Figure 2. The typical plastic exposure chambers for cell cultures 246

Figure 3. Temporal structure of the magnetic field pattern . .248

Figure 4. Shape of the copper foil sectioned for wrapping. . .249

Figure 5. Exposure box apparatus. 250

Figure 6. Cell counts post magnetic field manipulation 253

Figure 7. Numbers of cells per day over the five days. 254

Figure 8. Numbers of cells on day 5 for sham 255

Figure 9. Depiction of flux lines propagating through and around the exposure area. 258

Chapter Ten:

Figure 1. Pictures of the actual toroids and microcontroller system 277

Figure 2. Closer view of the micro-control (Arduino) system that operated the toroids 277

Figure 3: Cell counts post magnetic field exposure 279

Figure 4: Cell counts post non locality paradigm exposure. . .280

Figure 5. Cell counts without non-local paradigm 282

Figure 6: Cell counts for the non-local paradigm separated by 1.7 km 283

List of Abbreviations

$A \cdot m^2$	Ampere Meter Squared
A·s	Ampere Seconds
B	Strength of Field Change
CASP-9	Caspase-9
cm	Centimeter
cm·deg/°K	Centimeter Degree/Kelvin
cc	Cubic Centimeter
c	Velocity (speed of light)
D	Diffusion Constant
DAC	Digital to Analogue Converter
DMEM	Dulbecco's Modified Eagle Medium
E	Energy
EM	Electromagnetic
EMF	Electromagnetic Field
ELF	Extremely Low Frequency
eV	Electronvolt
EZ	Exclusion Zone
f	Frequency
γ	Gamma
gm	Grams
G	Gravitational Constant
h	Plank's Constant

ħ	Modified Planck's Constant
hr	Hours(s)
Hz	Hertz
IR	Infrared
IL-2	Interleukin-2
IL-6	Interleukin-6
JAK	Janus Kinase
J	Joules
J·s	Joules Seconds
k	Boltzmann Constant
$kg \cdot m^{-1} \cdot s^{-2}$	Kilogram Meter per Second Squared
km	Kilometer
LED	Light-Emitting Diode
L	Liter
mG	Milligauss
M	Magnitude
mA	MilliApmere
μ	Magnetic Susceptibility
m^2	Meter Squared
mg/kg	Milligram per Kilogram
mg/ml	Milligrams per Milliliter
μL	Microliter
mL	Milliliters
μm	Micrometer

uM	Micromolar
ms	Millisecond
mm	Millimeter
mM	Millimolar
µT	Microtesla
MuKarb-EMF	MuKarb-Electromagnetic Field
nm	Nanometer
nT	Nanotesla
Ω	Ohm
ε	Permittivity
PBS	Phosphate Buffered Saline
pH	Potential of Hydrogen
q	Unit Charge
r	Radius
RRM	Resonance Recognition Model
s	Seconds
SD	Standard Deviation
SFU	Solar Flux Unit
SPD	Spectral Power Density
STAT	Signal Transducer and Activator of Transcription
T	Temperature
t	Time
TYK2	Tyrosine Kinase 2

UPE	Ultraweak Photon Emission
UV	Ultraviolet
η	Viscosity
V	Volts
W	Watts
$W \cdot m^{-2}$	Watts per Meter Squared
λ	Wavelength (m)

Chapter One

1.0 Introduction

The means by which energy is transformed is reflected in the structure of both biological and machine-based systems. Biology is modeled from a mechanistic perspective where the structure is distinguished from the qualia of energy maintaining the system. As a result, it is assumed that the structure is of utmost importance and not the energy. If matter did not exist, energy as a form of life would dissipate instantly, as energy requires a specific arrangement in space in order to exist over time.

The law of conservation of energy states "energy can be neither created nor destroyed. Energy possesses the capacities to change forms within the matter it occupies and to flow from one place to another (Feynman 1970, Grove 1874). Using this approach it is assumed that energy propagates based on the geometry of the system and becomes irrelevant outside of a power source to maintain the functionality of material construct. This becomes an important concept in the development and senescence of life where communication within the simplest form of life, the cell, conservers and transfers energy from one form to another in order to maintain its viability (Alberts et al. 2002, Harold 1972).

In order for a cell and its aggregates to survive it requires two different approaches to communication in order to maintain proliferation, homeostasis and senescence. The first is internal, where the cell maintains its structure and function through a plethora of biomolecular pathways within the domain of the "cell". This includes DNA replication, transcription, translation and other biomolecular processes. The second is an external form of communication when cells form aggregates. They communicate with each other through membrane receptors and biomolecules in order to maintain the structure and function of higher order tissue. The propagation of electrical impulses through axons between neurons is an important form of communication where energy is transferred from a cascade of molecular matter (proteins) to an electrical signal following a final transition / response by the receiving neuron (Bean 2007). This change between matter and energy is classified as the main form of communication between neurons separated over specific distances.

The difference between the properties and functions of matter, which is often depicted according to spatial structure, and energy, which is often represented as temporal structure, may reflect critical components that must be considered in concert to fully understand the physical bases to cellular phenomena. The energies involved with the mechanisms of "cellular machinery"

that facilitate the structural changes that reflect function are self-contained within the system. However the energies that initiate this massive machinery may involve more subtle quantities that reflect fundamental physical properties. These properties are expected to be subject to the influence of temporal patterns of energy.

One analogy might be the operation of an automobile. The massive energies converted from petroleum products to operate the highly structured mechanics that move the car are substantial. In comparison the quantity of energies required to start this process, such as the turning of the ignition key, is orders of magnitude less intense. This dissertation explores the contribution and characteristics of the subtle energies presented as low intensity temporally patterned magnetic fields that initiate the powerful sequences of molecular pathways. From the perspective of the most fundamental component within which life systems occur, the substrate for this mechanism may begin within the ubiquitous substance: water.

1.1 Water Viscosity

Life on Earth as we know it would not exist with the absence of water (H_2O). The importance of water is generally appreciated from a macro-perspective as it is *the* fundamental solvent that drives systemic function. However its importance at

the micro-level, with protein and other biomolecular interactions has not been a major focus of investigation. The presence of water is observed in almost every biomolecular pathway from the initiation of a reaction to the final product. Water becomes the fundamental necessity within all chemical reactions associated with biology. Without the presence of water in the cell, not only would the cell not survive, but also no reactions would take place to maintain the functionality of the cellular architecture.

The unique properties that arise in this solvent are primarily due to the ability of water to form hydrogen bonds within itself and other molecules. (Maksyutenko et al. 2006). These bonds give rise to unique geometries that water display consistent rearrangement based on the surrounding environment (Soper and Phillips 1986). Water is made up of 2 hydrogen atoms, which are covalently bonded to an oxygen atom. This unique structure allows the H_2O molecule to possess polar properties and an electrical dipole moment (Nilsson and Pettersson 2015). Furthermore, the hydrogen bonding seen in water can create other epiphenomenon such a water tension or viscosity (DeCoursey 2003).

Water is also capable of exhibiting periodicities and oscillations as a result of its properties in forming coherent domains, especially around boundary conditions (Zheng et al. 2006). These conditions allow for the structure of water to store energy and even information within its electromagnetic domain.

Recent work by Bellissent-Funel and colleagues showed the capability of water to determine the structure and dynamics of proteins (Beliissent-Funel et al. 2016). The authors argue that water may possess a blueprint for enhancing the formation of protein molecules. Del Giudice and Preparata (1994) showed that water possesses the potential to rearrange in the interfacial phases where its structure may resemble an early form of plasma membrane due to its function in separating ions. This interfacial surface was later measured by researchers to possess 10 times the viscosity of bulk water and contains a film of proton charges between a boundary and the bulk water (Pollack 2003).

Murugan and colleagues showed that the exposure of ionized water to a low-level pattern magnetic field produced an increase in pH towards alkalinity over a 24-hour period (Murugan et al. 2015). The energies associated with these changes were with in the range of 10^{-20} Joules, which correspond with both theoretical and experimental observations. The variability of viscosity within water may be considered as the mediating property for the storage of information or for energy obtained from an external source. Both pH and viscosity are proportional to each other and as a result can influence the mediating properties of water. As a result the variability in viscosity present in water may be the foundation by which electromagnetic properties influence biological tissue.

1.2 Electromagnetic Fields

The electromagnetic spectrum is defined as infinite, though it has been categorized and organized along a continuum of frequencies. These frequencies correspond to qualitative shifts in the effects of the associated electromagnetic energy. The energy is directly proportional to the frequency of the electromagnetic field. For example γ-rays are the most energetic and also have the highest associated frequency (1.93×10^{-13} J, 10^{18} Hz), compared to extremely low frequency-EMF (ELF-EMF; 1.93×10^{-33} J, 3 Hz) such as those found in biological organisms (Cifra et al. 2010). An important component of the electromagnetic spectrum is the visible spectrum, which centers around $4\text{-}8 \times 10^{14}$ Hz (1.24×10^{-19} J).

Misrepresentations of electromagnetic fields (EMFs) within the media has led to negative perceptions and caution when considering their use in medical applications. Only recently has this view changed towards an acceptance of using EMFs as a potential treatment in several different fields. The literature supporting the beneficial effects of specific or designed EMFs exists with respect to numerous fields. Certain scientific disciplines that have introduced electromagnetic field technology into their treatment paradigms include osteopathology, oncology, microbiology and neuroscience (Galkowski et al. 2009, Hu et al. 2010, Buckner et al. 2015, Lai and Singh 2010). When comparing

all the different studies involving electromagnetic fields with each other, the studies differ in the application and generation of the EMF. This stands as evidence to the importance of the spatial and temporal components of the electromagnetic field. This is analogous to that of chemical effects on biological systems, as they are determined by the complexity of spatial (molecular) structure.

There is accumulating evidence to suggest that the use of temporally patterned low-level magnitudes may be a different yet viable form of cancer treatment. It is known to influence malignant cells with minimal damage to healthy tissue. For example, with the use of a specific patterned EM field at a weak intensity of 1 – 5 microT researchers were able to suppress the growth of injected melanoma cells into C57BL6 mice (Hu et al. 2010). Buckner et al (2015) have shown that a specific activation of T-type calcium channels in *in-vitro* models govern weak electromagnetic effects. This T-type channel modulation by the specific electromagnetic field has been linked to the decreases in cancer cell proliferation. A major discovery following the decrease in cancer cell proliferation is the ability of the electromagnetic field to differentially affect cancerous and healthy cells. Healthy cells were not affected by the electromagnetic field (Buckner et al. 2015). It is important to note that a major discrepancy between the *in-vivo* and *in-vitro*

experiments is the capacity at which the cancerous cells are affected. The *in-vitro* models exposed to low-level time varying fields produce a maximum of ~48% decrease in cell proliferation (Buckner et al. 2015). On the other hand *in-vivo* models can produce complete suppression when using the same exposure paradigm and electromagnetic field (Hu et al. 2010). This discrepancy points towards further synergistic mechanisms, between the *in-vivo* model and the EM field.

A major hypothesis in explaining this phenomenon can include the recruitment of other physiological systems within the organism, as this component is absent in the *in-vitro* systems. Hu and colleagues predict that the complete suppression of tumor growth in the *in vivo* models may be due to the recruitment of the immune system. It may also help to eliminate the malignant growth. The immune system has been shown to respond in positive ways through the role of calcium signaling with respect to electromagnetic field treatments (Walleczek 1992).

The complexity of malignant cell lines can be observed not only with respect to pharmacological treatments, where resistance to treatment agents is common, but also with respect to more alternative treatment approaches such as electromagnetic fields. In electromagnetic field applications there are two different yet common approaches, which are dependent on the intensity of the field. With respect to intensity EM treatments

can be categorized into high or low-level intensity exposure where high intensity can be within the range of milliTesla and higher while low-level treatments include intensities between nanoTesla to microTesla. With respect to high-level EM exposures, associated patterns seem to be simple where they do not contain information within the structure. These effects are usually dependent on the intensity. The patterns are usually sinusoidal- or jigsaw-shaped.

On the other hand low-level EM treatments are highly efficient when associated with specific tuned properties such as timing, intensity, and pattern (Persinger et al. 2016, Buckner et al. 2015, Mach and Persinger 2009). These properties in low-level electromagnetic field treatments become critical in a positive final outcome. This can be compared to the analogy of opening up a door by kicking it in (using a large amount of force) or by using a key where the appropriate pattern can be implemented with very low amounts of energy.

The effects of electromagnetic fields with respect to low-level EM upon biology systems have been frequently challenged by pre-existing assumptions. The primary argument was the lack of "strength" within the generated field to produce observable results in a biological system by overcoming latent thermal energies or even penetrate into the area of interest. Past research argues that any observable results could only be

attributed to molecular agitation or thermal energy. Weak EM effects were considered below or at the threshold of the kT boundary where k is the variable representing the Boltzmann constant and T representing absolute temperature in Kelvin degrees. Cifra et al (2010) refuted these assumptions and identified the weakness in the traditional assumptions. Persinger and Saroka (2013) showed that a patterned 1 microTesla field showed minimal or no attenuation in intensity when passing through a simulated skull. The authors also provided evidence for the pattern of the generated magnetic field to be consistent and not distorted with that of a regular exposure void of material.

The importance of pattern becomes critical in low-level electromagnetic field treatments. Buckner et al demonstrated a ~45% decrease in malignant cell growth when the cells were exposed to a decelerating temporal pattern at a 3 millisecond point duration (Buckner et al 2015). This decrease in malignant cell growth was not observed when the pattern is reversed or with other similar signals and intensities. Murugan and her colleagues provided evidence for the importance of pattern in exposing planarian worms to two successive (tandem) patterned fields (6.5 hours per day for 5 days to one frequency-modulated pattern followed by an additional 6.5 hour exposure of a very complex magnetic pattern with an accelerated modulated amplitude). The

exposures produced complete dissolution of planarian worms (Murugan et al. 2013). When the order of the applied fields or the reversal of the fields was presented to the planarian worms the dissolution did not occur. Other researchers suggested the same importance of pattern with respect to low-level electromagnetic field treatments.

1.3 Ultraweak Photon Emission in Biological Organisms

Work over the last century by a plethora of different scientists provided the foundations for biophoton research that exists today (Gurwitch 1923, Popp 1979ab). The basis of their research considers the "photon" as a potential mechanism of communication between biological organisms. A photon can be described as a packet of energy that possesses particle-wave duality (Einstein 1905). This definition of duality has been associated to a photon as its prosperities, depending on the external forces, allow the photon to be represented as a wave or as a particle at different states. The energy of a photon can be directly related to it's wavelength and as a result calculated through the equation $E=hc/\lambda$. Within this formula the variable "E" represents energy being equivalent to Plank's constant "h" multiplied by the speed of light "c" over a specific wavelength "λ". The wavelength of a photon can be obtained from a range of energies between UV [ultraviolet] (~200nm) up to IR [infrared]

(~1500nm). These wavelength energies can range anywhere within the range of 10^{-19} Joules. The wavelengths in the UV range yield higher energy when compared to IR.

Dotta et al (2014) found that specific wavelengths of photons that were emitted within the visible range from B16BL6 cells corresponded to particular molecular pathways/structures and were increased or decreased by specific agonists and antagonists. Within this study the authors showed that the wavelength of the specific component of the pathway was exactly predicted by the Cosic's Resonance Recognition Model equations (Cosic, 1994). The authors also correlated the dominant frequencies to be within the ranges of ultraviolet, through the visible and to near infrared. The experiments showed that specific molecular structures exhibited specific patterns of electromagnetic energies. These specific patterns of photon emissions may be classified as a form of language or code by the biomolecular architecture within the cellular domains.

These photon emissions involve very little amounts of energy but are capable of activating the nuances of molecular components, which initiate the cascade of reactions observed in molecular pathways. They possess their own intrinsic energy. In other words the ultraweak photon emission between cells possess the ability to spark an intracellular process without affecting them once initiated. Such observable interactions of photons

within molecules, cells and/or whole tissue can be influenced by photons which possess quantum like particle properties which in turn through electromagnetic forces are capable of interacting with the surrounding environment (Gabrielli et al. 2006).

Further work in UPE (Ultraweak Photon Emission) research shows the ability of melanoma and other malignant cell lines are capable of producing greater proportions of light when compared to non-malignant cell lines (Dotta et al. 2011, Dotta et al. 2016, Murugan et al. 2016). Melanoma cell lines divide at a much more rapid pace. When measured (over a million cells) the photon emissions are equivalent to 10^{-20} Joules per second per cell (Dotta et al 2011). Other researchers found that the human body is capable of producing ultraweak photon emission irrelevant of heat or IR emission (Cohen and Popp 2003, Popp 1988, Ives et al. 2014).

This particular researcher goes back as far as the early 1900s where Walter John Kilner was the first to publish the *Human Aura* in western medicine. Through the use of a constructed apparatus (the "Kilner Screen") Kilner was capable of observing the human aura or by modern definition ultraweak photon emission from the body (Kilner 1965). In his work Kilner describer the ability to distinguish ill people from healthy people with respect to numerous different diseases based on the premise of the "aura" emission coming from the individuals body (Kilner

1965). Even at its infancy the work produced by Kilner presented the phenomenon of UPE from the human body as criteria for distinguishing the ill.

Modern UPE researchers have been gathering evidence in support of Kilner's predictions within the application of cancer detection with respect to wavelength properties of the photon emission (Dotta et al. 2014, Cohen and Popp 2003). Murugan and colleagues (2016) used a photomultiplier tube and a specific filter for the wavelength of 500 nm in order to differentiate between malignant and non-malignant cells based on the bio-photon emissions. The work by Dotta et al and Murugan et al produced concrete validity towards a new form of technology for the detection of malignant cellular debris within healthy tissue. The unknown factor within this technology, which will be an important portion of this dissertation, is the threshold for the presence of malignancy that photomultiplier measurements can discern within healthy tissue.

1.4 Irena Cosic's Resonance Recognition Model

The Resonance Recognition Model (RRM) takes a different approach at visualizing structural proteins. Instead of observing them based on their structural properties this model focuses more on the protein sequence as a discrete signal, rather that it's eventual geometry. The basis of the model rests upon representing

any specific protein's primary structure as a numerical series (Cosic 1994). This is done by allocating a physical value to each amino acid. Each allocated value is based upon the obtained energy of a delocalized electron within each amino acid. These values within the amino acids when compounded together represent the folding motifs and structural architecture of a protein in its quaternary state. As a result the final product produces a unique spectral signal for the protein including specific peak wavelengths representing the structural components in protein dynamics.

Wu and Persinger (2011) provided evidence of cytochrome C and cytochrome oxidase II activation by exposing a regenerating blastema within a planarian worm to an array of infrared LEDS with the wavelength of 880 nm. The use of the 880 nm wavelength paradigm produced an increase in rate of regrowth of sectioned planarian worms (Wu and Persinger 2011). The resonance recognition model (RRM) accurately predicted both proteins with respect to their activation within this experiment. With the use of the RRM model Murugan et al (2015) were capable of distinguishing and differentiating non-lethal from lethal strains of Ebola viruses. Not only were the researchers capable of identify unique structures within the different strains of viruses (which differentiated them by lethality); the authors

were able to obtain a theoretical treatment option for infected individuals.

Cosic and colleagues mapped out a classification schema for proteins within the cellular boundaries with respect to the RRM model. The group found that the plethora of biological signals/pathways could be categorized by their resonant frequency into larger groups based on their functions (Cosic et al. 2016). Their work supported and aligned very well with the findings of Dotta at el (2014) where specific wavelengths of photons within the visible range emitted from B16 cells corresponded to particular molecular pathways/structures. To give stronger validity to these mechanisms the pathways/structures were increased or decreased by specific agonists and antagonists. The study showed that the wavelength of the specific component of the pathway was exactly predicted by the resonance recognition model equations. The study by Dotta et al was one of the first to show that the dominant frequencies found with the use of the RRM model classified observed biological protein molecules in a spectrum of ultraviolet, through the visible, and to the near infrared.

The resonance recognition model shows great potential in the application of biology and medicine and may be a start in obtaining the Rosetta stone code for biomolecular molecules. It is important to show the RRM model can theoretically and experimentally predict concrete pathways and molecules. With this

particular proof at hand, the RRM model may gain the required support to accelerate its approaches in predicting biomolecular behavior and correlating them to biomolecular structure/pathways. This approach may produce the required circumstances to finally link the material components of biomolecular with the energy-based phenomenon within the sciences.

1.5 Low-level Electromagnetic Fields and Excess Correlations

Excess correlation or quantum entanglement has been described by Albert Einstein as the "spooky action at a distance" with respect to theoretical physics as a limit in not being able to explain unique phenomenon of communication between particles, which did not follow the theoretical physic's principles at the time. Contemporary theoretical principles work under the premise of locality with respect to the tangible building blocks making up the universe. The basis of locality affecting space and time in modern physics and other hard sciences is the assumption by which matter interacts with other parts of matter by a causal effect or a direct link between the two.

With respect to non-locality, the definition is transposed where two units acting in a similar fashion, separated by space where no intermediate mechanism is observed, can produce a measurable outcome. Julgaard et al (2001) have experimentally demonstrated principles of non-locality where entanglement was

produced between two macroscopic objects of cesium gas samples containing about 10^{12} atoms. Further experiments by several researchers showed that macroscopic objects could display excess correlations through principles of non-locality. Dotta et al (2009) found that when two cultures of melanoma cells were separated by 10 meters and were simultaneously exposed to a circulatory rotating magnetic field the application of light flashes to one dish resulted in the emission of photons as measured by photomultiplier tubes in the other melanoma cell dish.

This unique research also provided proof of the specificity within this phenomenon by showing that the excess correlation did not occur when the circularly rotating fields were not present. The researchers also proved the importance of specificity within the magnetic field generation and successful results. When the generated magnetic field was presented in the reverse pattern the excess correlation did not occur. Several other researchers have also observed the phenomenon of pattern specificity in producing reliable results in magnetic field exposure (Murugan et al. 2013, Buckner et al. 2015).

The mechanism behind excess correlation at this point is theoretical. It is a condition that can exist in quantum theory and can reflect the properties of the photon interacting with magnetic fields. Vaziri et al (2002) indicated that the primary

means for producing quantum communication (excess correlation) within the boundaries of our technology will take advantage of the photon as the initiator (Vaziri et al 2002). Persinger and his colleagues suggest that the group and phase velocities of photons play a critical role by affecting emerging properties of photons. Persinger and colleagues in pursuit of understanding the photonic mechanisms of excess correlation, measured non-local photon radiant flux densities during a number of experiments employing different models including the mixture of hydrogen peroxide and sodium hypochlorite solutions in the local setting, malignant cell cultures and human cerebrum activity (Persinger et al. 2015, Dotta et al. 2011, Dotta and Persinger 2012). Within these experiments the two loci for which excess correlations paradigms were separated by 10 m to 3 km. The spaces only shared simultaneous rotating magnetic fields in a specific sequence.

Dotta and colleagues (2013) also demonstrated excess correlation in two beakers of water. The following beakers were separated by non-local distances and simultaneously exposed to the appropriate patterned magnetic fields, which have been shown to elicit excess correlations for photon reactions. Introduction of an acidic compound into the local beaker of spring water produced the expected shift in pH in the solution. On the other hand the non-local beaker of spring water (no injection of acid), drifted in the exact same proportion as the local beaker but

towards alkalinity. The occurrence of similar excess correlation properties in several different experiments produce evidence towards the potential quantum properties of a photon and the interactions with a magnetic field may govern this unique phenomenon.

Melanoma cells and other malignant cells lines emit a substantial amount of ultralow level photons during habituation to room temperature after removal from incubation when compared to healthy tissue (Dotta et al. 2011; 2016). The peak wavelengths of photons are within the visible range and include UV and IR wavelengths where they periodically shift as a function of time post removal from the incubator (Dotta et al. 2014). Murugan et al (2014) found that certain drugs, for example morphine, elicit strong bursts of photons from malignant cell cultures. Morphine has been linked to increasing the metastatic potential of existing tumors in in vivo models (Simon and Tracey 1986), which may support the metastatic potentials being governed by excess correlation paradigms. For this reason it is possible that this burst firing of photons is an important and observable component in excess correlation and cancer physiology. If one considers that excess correlation and its congruent relationship between local and non-local space reflects a window of communication than then a potential is seen for using this technology in the medical environment. This technology may possess the ability interfere

with the interactions and communicating malignant cells growing and thriving in order to form a tumor masses in its host.

1.6 Thesis Objective

Malignancies have been the disdain of human health over the many centuries of medical history. There were numerous breakthroughs with regards to their understanding and treatment but this category of disease still plagues the longevity of the human species. Recent research has shown promise with approaching malignancies from a biophysical perspective with the use of low-level electromagnetic fields and biophotonic emission for both detection and treatment. The objective of this thesis is to approach malignancies from a biophysical perspective and enhance treatment and detection options. A look at the electrical components of the Digital to Analogue converters and EMF generators will also be tested and manipulated in order to narrow in on the appropriate conditions that govern the specificities in their positive cancer effects.

1.7 References

Alberts, B., Johnson, A., Lewis, J., Raff, M., Roberts., K., and Walter, P. (2002) Molecular biology of the cell: chapter 14 energy conversion: mitochondria and chloroplasts. Garland Science. 4th Edition.

Bean, BP. (2007) The action potential in mammalian central neurons. Nature Reviews Neuroscience. Vol 8: 451-465.

Bellissent-Funel, MC., Hassanali, A., Havenith, M., Henchman, R., Phol, P., Sterpone, F., van der Spoel, D., Xu, Y., Garcia, AE. (2016) Water determines the structure and dynamics of proteins. Chemical Reviews. Vol 116(13): 7673-7697.

Buckner, CA., Buckner, AL., Koren, SA, Persinger, MA, Lafrenie, RM. (2015) Inhibition of cancer cell growth by exposure to a specific time-varying electromagnetic field involves t-type calcium channels. PLOS One. Vol 10(4): e0124136.

Cifra, M., Fields, JZ., Farhadi, A. (2010) Electromagnetic cellular interactions. Progress in Biophysics and Molecular Biology. Vol 105(3): 223-246.

Cohen S., Popp, FA. (2003) Biophoton emission of human body. Indian Journal of Experimental Biology. Vol 41: 440-445.

Cosic, I. (1994) Macromolecular bioactivity: is it resonant interaction between macromolecules? theory and application. IEEE Transactions on Biomedical Engineering. Vol 41: 1101-1114.

Cosic, I., Cosic, D., Lazer, K. (2016) Environmental light and its relationship with electromagnetic resonances of biomolecular interactions, as predicted by the resonant recognition model. Environmental Research and Public Health. Vol 13: 647.

DeCoursey, TE. (2003). Voltage-gated proton channels and other proton transfer pathways. Physiological Reviews. Vol 83(2): 475-579.

Del Giudice, E., Preparata, G. (1994) Coherent domains in water as a possible explanation of biological membrane formation. Journal of Biological Physics. Vol 20: 105-116.

Dotta, BT., Buckner, CA., Lafrenie, RM., Persinger, MA. (2011) Photon emissions from human brain and cell culture exposed to distally rotating magnetic fields shared by separate light-stimulated brains and cells. Brain Research. Vol 1388: 77-88.

Dotta, BT., Karbowski, LM., Murugan, NJ., Vares, DAE., Persinger, MA. (2016) Ultra-weak photon emissions differentiate malignant cells from non-malignant cells in vitro. Archives in Cancer Research. Vol 4(2).

Dotta, BT., Mulligan, BP., Hunter, MD., Persinger, MA. (2009) Evidence of macroscopic quantum entanglement during double quantitative electroencephalographic measurements of friends vs strangers. NeuroQuantology. Vol 4: 548-551.

Dotta, BT., Murugan, NJ., Karbowski, LM., Lafrenie, RM., Persinger, MA. (2014) Shifting wavelengths of ultraweak photon emissions from dying melanoma cells: their chemical enhancement and blocking are predeicted by cosic's theory of resonant recognition model for macromolecules. Naturwissenschaften. Vol 101(2):87-94.

Dotta, BT., Murugan, NJ., Karbowski, LM., Persinger, MA. (2013) Excessive correlated shifts in pH within distal solutions sharing phase-uncoupled angular accelerating magnetic fields: Macro-entanglement and information transfer. International Journal of Physical Sciences. Vol 8(36): 1783-1787.

Dotta, BT., Persinger, MA. (2012) "Doubling" of local photon emissions when two simultaneous, spatially separated, chemoluminescent reactions share the same magnetic field configurations. Journal of Biophysical Chemistry. Vol 3. 72-80.

Einstein, A. (1905/1965) Concerning an heuristic point of view toward the emission and transformation of light. American Journal of Physics. Vol 33(5): 1-16.

Feynman, R. (1970) The Feynman lectures on physics vol i. Addison Wesley Longman.

Gabrielli, E., Huitu, K., Roy, S. (2006) Photon propagation in magnetic and electric fields with scalar/pseudoscalar couplings: a new look. Physical Review D. Vol 74: 1-21.

Galkowski, V., Petrisor, B., Drew, B., Dick, D. (2009) Bone stimulation for fracture healing: what's all the fuss? Indian Journal of Orthopedics. Vol 43(2): 117-120.

Grove, WR. (1874) The correlation of physical forces (6^{th} ed.) London. Longmans, Green.

Gurwitch, AG. (1923) Das Problem der zellteilung physiologisch betrachtet, in a. g. gurwitsch et al. Monorgraphien asu dem Gesamtgebiet der Physiologie der Pflanzen und der Tiere. 473-475.

Harold, FM. (1972) Conservation and transformation of energy by bacterial membranes. Bacteriological Reviews. Vol 36(2): 172-230.

Hu, JH., St-Pierre, LS., Buckner, CA., Persinger, MA. (2010) Growth of injected melanoma cells is suppressed by whole body exposure to specific spatial-temporal configurations of weak intensity magnetic fields. International Journal of Radiation Biology. Vol 86(2): 79-88.

Ives, JA., van Wijk, EPA., Bat N., Crawford, C., Walter, A., Jonas, WB., van Wijk, R. (2014) Ultraweak photon emission as a non-invasive health assessment: a systematic review. PLOS One. Vol 9(2): e87401.

Julgaard, B., Kozehekin, A., Polzik, ES. (2001) Experimental long-lived entanglement of two macroscopic objects. Nature. Vol 413. 400-403.

Kilner, WJ. (1911-1965) The human aura - The human atmosphere, or the aura made visible by the acid of chemical screens. Citadel Press. New York.

Lai, HC., Singh, NP. (2010) Medical applications of electromagnetic fields. Electromagnetic Phenomena and Health. Vol 10(1): 012006.

Mach, QH., Persinger, MA. (2009) Behavioral changes with brief exposures to weak magnetic fields patterned to simulate long-term potentiation. Brain Research. Vol 1261: 45-53.

Maksyutenko, p., Rizzo, TR., Boyarkin, OV. (2006) A direct measurement of the dissociation energy of water. The Journal of Chemical Physics. 125.

Murugan, NJ., Karbowski, LM., Lafrenie, RM., Persinger, MA. (2015) Maintained exposure of spring water but not double distilled water in darkness and thixotropic conditions to weak (~1uT) temporally patterned magnetic fields shift photon spectroscopic wavelengths: effects of different shield materials. Journal of Biophysical Chemistry. Vol 6: 14-28.

Murugan, NJ., Karbowski, LM., Lafrenie, RM., Persinger, MA. (2013) Temporally-patterned magnetic fields induce complete fragmentation in planaria. PLOS One. Vol 8(4): e61714.

Murugan, NJ., Karbowski, LM., Dotta, BT., Vares, DAE., Saroka, KS., Lafrenie, RM., Persinger, MA. (2016) Differentiation of malignant compared to non-malignant cells by their photon emissions may only require a specific filter around 500 nm. Journal of Cancer Science & Therapy. Vol 8 (6): 170-171.

Murugan, NJ., Dotta, BT., Karbowski, LM., Persinger, MA. (2014) Conspicuous bursts of photon emissions in malignant cell cultures following injections of morphine: implications for cancer treatment. International Journal of Current Research. Vol 6(12): 10588-10592.

Nilsson, A., Pettersson, LGM. (2015) The structural origin of anomalous properties of liquid water. Nature Communications Review. 6.

Pollack, GH. (2003) The role of aqueous interfaces in the cell. Advances in Colloid and Interface Science. Vol 103: 173-196.

Persinger, MA., Dotta, BT., Karbowski, LK., Murugan, NJ. (2015) Inverse relationship between photon flux densities and nanotesla magnetic fields over cell aggregates: quantitative evidence for energetic conservation. FEBS Open Bio. Vol 5: 413-418.

Persinger, MA., Dotta, BT., Murugan, NJ., Karbowski, LM., Koren, SA. (2016) Rotational frequency matching of the energy of the changing angular velocity magnetic field intensity and the proton magnetic moment produces a ten fold increased excess correlation in pH shifts in spring water. NeuroQuantology. Vol 14(1): 1-8.

Persinger, MA., Saroka, KS. (2013) Minimum attenuation of physiologically-patterned, 1 uTesla magnetic fields through simulated skull and cerebral space. Journal of Electromagnetic Analysis and Applications. Vol 5: 151-156.

Popp FA. (1988) Biophoton emission. Experientia. Vol 44: 543-630.

Popp, FA. (1979a) Photon storage in biological systems. Electromagnetic Bioinformation. Munich. Urban and Schwarzenberg: 123-149.

Popp, FA. (1979b) Photon storage in biological systems. Electromagnetic Bioinformation. New York. Urban and Schwarzenberg: 123-149.

Soper, AK., Phillips, MG. (1986) A new determination of the structure of water at 25°C. Chemical Physics. Vol 107(1): 47-60.

Simon, RH., Tracey, AE. (1986) Morphine increases metastatic tumor growth. Brain Research Bulletin. Vol 16: 363-367.

Walleczek, J. (1992) Electromagnetic field effects on cells of the immune system: the role of calcium signaling. The FASEB Journal. Vol 6(13): 3177-3185.

Wu, HP., Persinger, MA. (2011) Increased mobility and stem-cell proliferation rate in dugesia tigrina induced by 880 nm light emitting diode. Journal of Photochemistry and Photobiology. Vol 102(2): 156-160.

Vaziri, A., Weihs, G., Zeilinger, A. (2002) Experimental two-photon, three-dimensional entanglement between photons that have never co-existed. Physical Review Letters. Vol 89(24): 1-4.

Zheng, J., Chin, W., Khijniak, E., Pollack, GH. (2006) Surfaces and interfacial water: evidence that hydrophilic surfaces have long-range impact. Advances in Colloid and Interface Science. Vol 127(1): 19-27.

1.8 Preamble to Chapter 2: A Theoretical Approach to a Potential Model for Observed Low-level Electromagnetic Field Effects in Biological Systems.

The make up of the human body consists largely by the aggregation of dihydrogen oxide, making up the environment in which complex molecules interact with each other for the maintenance of life. Several studies involving electromagnetic fields provide evidence for the reconstruction of water molecules resulting with a change in diffusivity periods or pH changes towards alkalinity within a controlled H_2O system. Considering the different types of phenomenon observed as a result of the low-level electromagnetic fields a similar mechanism can be theorized pertaining to a biological system. A theoretical approach with taking consideration of the physical chemical principles of water may shine light into what components of H_2O are involved in observed changes. A phase of water involving viscosity of the aqueous solution may be congruent to such effects. An examination of the viscosity of water from a mathematical perspective may determine a theoretical explanation governing EMF effects within biological systems.

Chapter Two

Variable Viscosity of Water as the Controlling Factor in Energetic Quantities That Control Living Systems: Physicochemical and Astronomical Interactions

Published in International Letters of Chemistry, Physics and Astronomy (2015) - Vol: 43. Pg. 1-9

Reproduced with Permission from SciPress

Lukasz M. Karbowski and Michael A. Persinger

Abstract

The emergence of energy from the product of viscosity, volume and intrinsic or extrinsic frequency indicates that the ten fold difference in this property displayed by water could define the boundary of the physicochemical conditions of living systems. Intra-aqueous energy induced by geomagnetic variations and experimental time-varying magnetic fields within specific volumes of water maintained in static, dark conditions can be manifested as photon emissions with shifts in spectral power that approximate the width of the plasma cell membrane. Various manipulations of the viscosity of water accurately predicted the frequency required to affect intracellular organelles such as vesicles as well as the intramolecular pressures that affect interactions with photons. Application of the Smoluschowski-Einstein relation to the proton, the mediator of pH and the dynamics of the hydronium ion, potentially explained the vector characteristics of the frequency band of extremely low frequency magnetic fields that slow malignant cells. The derivation of viscosity from the inverse of the Newtonian Gravitational Constant, diffusivity and the square of the applied frequency indicates that resonant oscillations between the solid earth and the atmosphere and unit variations in solar flux density may be relevant variables.

Introduction

The importance of the intrinsic variations in values of viscosity (η) within aqueous systems for determining their intrinsic energies and subsequently the wavelengths spontaneously emitted as photons has not been explored systematically. If viscosity is the term employed to represent the resistance of a fluid to gradual deformation then there should be an energy contained within the system that is associated with this physical reluctance. One would anticipate that the intrinsic and transient organization within water that has been described as coherent domains within which applied magnetic fields can be contained [1] or geometric arrangements of oscillating arrays [2] require intrinsic energies. These energies would emerge not only from the thermal phenomena coupled to absolute temperature but also from the basic properties of protons and electrons that composed the molecular networks.

One of the assumptions of the general quantum concept is that the bases of information as digital or 0,1 sequences is mediated through packets of discrete energy that are shared by local and non-local mechanisms [3]. Thus changes in the properties of media within which physicochemical reactions should result in specific quantities of energy. Typically non-intercalated processes could interact to produce qualitatively different phenomena. The central manifestation of these phenomena

should be dependent upon photon emissions that reflect both measures of intensity (radiant flux density) and spectral power density. There is now strong evidence that photons are the primary mediators of inter-molecular, inter-cellular [4], inter-organismic [5] interactions through which complex information is conveyed.

We have assumed that photon-related viscosity phenomena should be related to the most fundamental physical and chemical properties of matter. For example the diffusivity value ($0.88 \cdot 10^{-7}$ $m^2 \cdot s^{-1}$) derived from the ratio of the unit magnetic moment of a proton ($1.41 \cdot 10^{-26}$ $A \cdot m^2$) and the unit charge ($1.6 \cdot 10^{-19}$ $A \cdot s$) multiplied by the viscosity ($8.94 \cdot 10^{-4}$ $kg \cdot m^{-1} \cdot s^{-1}$) of water around 25°C results in a force of $7.87 \cdot 10^{-11}$ $kg \cdot m \cdot s^{-2}$ [6]. When this force is applied over the distance of two O-H bounds ($1.92 \cdot 10^{-10}$ m) the energy is $1.5 \cdot 10^{-20}$ J. This is with range of the intrinsic energy associated with neuronal action potentials, agonist-receptor interaction, the potential between potassium ions that contribute to the resting membrane potential [7] and even the electron affinities between nucleobases for DNA [8].

According to Decoursey [9], the second shell hydrogen bonds are in the order of $1.8 \cdot 10^{-20}$ J per molecule and is consistent with the measurements of the mobility of protons (H^+) within water. These mobile protons function as a dynamic “thread” that maintain a matrix for interactions of chemical species

within a fixed volume of water by producing and moving through transient (~10^{-12} s) hydronium ions (H_3O^+). They determine pH which then affects chemical reactions. Very narrow ranges of pH between 6.2 and 7.2 can affect angiogenesis and metastasis [10].

There is theoretical and empirical evidence that proton flux [11] through proton channels within the plasma membrane may be the prototypic source for electrical potentials because of the emergent property of interfacial water that occurs along a surface. As demonstrated by the imaginative experiments of Pollack and his colleagues [12-14], the increased viscosity within the exclusion zone that emerges as an interface between the surface and bulk water and the formation of a concentrated layer of protons produces voltages that are the same order of magnitude as the resting plasma membrane potential of living cells.

Quantifying the role of viscosity at the most basic level of proton magnetic moment and the unit charge to mediate energy that may serve as the quanta of communication between chemical reactions at their large aggregates (such as the cell) may be revealing. In water the viscosity can range from $1.00 \cdot 10^{-3}$ Pa·s at 20°C to $6.3 \cdot 10^{-4}$ Pa·s for physiological (37° C) temperature. The viscosity of vital fluids such as blood is about 4 times greater than water. The corresponding viscosity for hematocrit values between 60 and 20 range from 7.2 to $2.6 \cdot 10^{-3}$ Pa·s, respectively,

according to Rand and Lacome [15]. Intracellular viscosity has been inferred to be about 1.4 greater [16] in one type of cell (fibroblasts) than extracellular water and as high as $6.8 \cdot 10^{-2}$ Pa·s. The viscosity of Pollack's Exclusion Zone where aggregated shells of protons produce as much as 100 mV potential differences can be a factor of 10 higher than bulk water. Here we develop the potential relevance of the narrow-band variations in viscosity from chemical, physical, and astronomical perspectives.

2.2 Intrinsic Energy Derived from the Viscosity of Water

The product of viscosity (η), the volume (V) under consideration and intrinsic frequency (Hz) is energy (J). In basic units this is:

$$J=(kg \cdot m^{-1}s^{-1}) \cdot m^3 \cdot s^{-1} \qquad (1).$$

It indicates that water of a specific volume that is oscillated by forces, internal or external, mechanically or electromagnetically has the potential to contain a specific quantity of energy.

In one of our experimental settings where quantities of 10 cc of spring water were placed in cell culture dishes and allowed to sit in the dark for several days to ensure thixotrophic effects [17], the determination of estimated

intrinsic energy contained within this volume, assuming ~10^{-3} Pa·s viscosity, would only required frequency. Assuming a low frequency associated with increased geomagnetic intensity, such as an equivalent 5 min periodicity (3.3 mHz), the quantity would be $3.3 \cdot 10^{-11}$J.

The potential relevance of this prediction was measured by a phenomenon observed initially by the second author while monitoring background photon flux density by analogue photomultiplier tubes (PMTs). He noted that when quantities of 10 cc (10^{-5} m^3) of spring water were placed over the aperture that the mean photon flux densities increased sufficiently to be discernable over the background of $5 \cdot 10^{-12}$ $W \cdot m^{-2}$ during some but not all increases in geomagnetic field intensity. The effect was transient and was maintained in the order of one or more kiloseconds after the onset of the geomagnetic activity as measured by a MEDA magnetometer whose sensor was 2 m away from the PMT sensor.

The inconsistency was later discerned to relate to the rise time for the maximum increase in local geomagnetic intensity. According to the intrinsic energy (J) for that space containing that quantity of water would be:

$$J=(B^2) \cdot (2\mu \cdot s)^{-1} \ m^3 \quad (2),$$

where B is the strength of the field change, μ is the magnetic susceptibility ($4\pi \cdot 10^{-7}$ $N \cdot A^{-2}$) s is the rise time and m^3 is the volume of water. For the occasional increase in magnetic field strength above 100 nT within 300 s the power ($J \cdot s^{-1}$) would be $1.3 \cdot 10^{-16}$ W. Given that the aperture of the PMT was ~10^{-4} m^2, this would be equivalent to about $1.3 \cdot 10^{-12}$ $W \cdot m^{-2}$. This value was at the margin of detection by the system. However it suggested that the stored magnetic field energy could be re-released as photons within a range that overlaps with the visible and near-ultraviolet and near-infrared.

The equivalent power within that volume of water due to the viscosity of the water (equation 1) requires the square of the frequency. If the same frequency (3.3 mHz) were applied, then the power would be $1.1 \cdot 10^{-13}$ W or about 10^3 more than the induced power from the increased geomagnetic intensity. For the maintained geomagnetic intensity to converge with this potential contained within the viscosity approximately 20 min (1 ks) would be required. This transience of the phenomenon would be congruent with the experimental observations [18,19].

2.3 Fluorescence Spectrometry Evidence

We have shown spring water that remains unmoved and in hyper-darkness for several days while being exposed to physiologically-patterned, weak (μT range) magnetic fields

created by specific point durations (3 ms) exhibits increase photon emission as measured by fluorescent spectrophotometer. The static condition of the spring water during the exposure to the magnetic field is essential because agitated movements (e.g., transport) before the measurement eliminate the effect. These observations are consistent with the production of thixotrophic phenomena or the increased viscosity that is associated with quantities of water that are not moved and remain in darkness. This effect has been reported by other researchers [17].

The 3 ms point durations refer to the time each point or value between 0 and 256 that is converted to between -5 V and 5 V (127=0 V) is generated by the computer software through the digital-to-analogue converters that result in the current applied through the application geometry. In these studies the field was applied through a large coil in order to increase the homogeneity of a given intensity across the volume of the water sample. The samples of water were placed approximately 1 m away from the vertical face of the coils. Point durations for the same patterned field that were 1 ms or 4 or 5 ms did not produce the enhancing photon emission.

The selection of the 3 ms point duration was derived from both theoretical concepts from basic astronomy as well as empirical verification. Persinger and Koren [20] had suggested that the expansion coefficient reflected in Hubble’s parameter

($2.4 \cdot 10^{-18}$ s^{-1}) could be related to the space occupied by a particle. For a proton the value would be $8 \cdot 10^{-33}$ $m \cdot s^{-1}$. Consequently the time to expand one Planck's length ($1.6 \cdot 10^{-35}$ m) from the context of this model would be that value divided by the expansion velocity. The median solution, given the range in Hubble's constant, was about 3 ms. On the other hand the solution for the electron was about 1 ms.

Subsequent experiments involving the "excess correlations" of photon emissions from chemical reactions separated by non-traditional distances supported the specific parameters [21]. This was tested by measuring the simultaneous output of two identical photochemical [3] or pH reactions [22] separated by 10 m but that shared the same changing magnetic fields with changing angular velocities generated around a circular array of solenoids. Proton-related phenomena were optimal with 3 ms point durations while electron-related phenomena were optimally evoked by point durations of 1 ms [23]. The selection of integer values was determined by the limits of the software that generated the magnetic fields.

As described by Murugan et al [24], the spectrophotometer registered the photon emissions for wavelengths between 350 nm and 470 nm. The major consequence of exposing spring water to the physiologically patterned magnetic fields was a shift of the peak in photon emissions by about 10 nm, the width of a plasma

cell membrane, towards longer wavelengths. The shift emerged at about 400 nm and slowly attenuated between this value and 450 nm. The calculated energy associated with this shift was about 10^{-20} J which is well within the range associated with second shell values of the hydrogen ion [9]. The mobility of H^{+} through the matrices of hydronium ions is associated with this energy.

If viscosity is the controlling value then its characteristics should be reflected in the dominant wavelength of the photons spontaneous emissions once energy (J), in this case the magnetic form, has been stored within the volume of water. Assuming $\eta=0.79\cdot10^{-3}$ $kg\cdot m^{-1}s^{-1}$ for the viscosity of spring water at 25°C and $1.8\cdot10^{-20}$ J for the second shell energies of hydrogen, and $3.33\cdot10^{2}$ Hz was the effective frequency of 3 ms point durations, then the volume (m^3) can be discerned by:

$$m^3=J(Hz\cdot\eta)^{-1} \qquad (3),$$

or, $0.68\cdot10^{-18}$ m^3. The cube root of this value is 408 nm which is well within the range of the wavelength where the shift occurred for the increased power flux density of photons from the water exposed to the weak temporally asymmetric magnetic fields in a static, hyper dark environment.

The total energy (J) as photons associated with the exposure to the magnetic fields within that environment was

predicted by the classic formula which is the same as equation 2 but with s^{-1} (frequency) removed. In this instance the total energy stored within the water matched the summed energy of the increased photon emission from that water as discerned by fluorescent spectrophotometer. However these calculations indicate that the wavelength of the energy emitted as photons was determined by the viscosity of the water within the volume within the cuvette.

2.4 Estimating Intrinsic Frequencies

Similarly we could predict frequency of the system (resonant or intrinsic) by knowing the implicit energy and the viscosity by:

$$f=E\ (\eta\ m^3)^{-1} \quad (4).$$

Discrete volumes of similar chemical structures are formed ubiquitously within discrete subsets or micro-boundaries or "vesicles". The Golgi apparatus contributes in large part to the concentration of proteins within these vesicles whose widths range from 70 to 300 nm. At presynaptic locations within the brain the widths of the vesicles range between 15 and 75 nm [25].

If we assumed the persistent energy value of $2{\cdot}10^{-20}$ J, the viscosity of water measured by Margraves et al [26] within

human brain tumor (T98G glioblastoma) cells ($6.8 \cdot 10^{-2}$ kg $\cdot m^{-1}$ s^{-1}) that display an average diameter of 496 nm then an intrinsic frequency can be estimated. Assuming the volume of the vesicles within these tumor cells would be $6.1 \cdot 10^{-23}$ m^3 the intrinsic frequency is ~5 Hz. This frequency solution is well within the range of the natural oscillation band that produces mobilization and release of vesicle pools at neuromuscular synapses [27].

The above equation predicts the time constant of asynchronous or spontaneous releases of the contents of synaptic vesicles should reflect the 5 Hz value in general even in other cell preparations with comparable vesicular dimensions. Goda and Stevens [28] measured time constants between 100 and 200 ms or 10 to 5 Hz for hippocampal synapses for cultured cells. Stevens and Williams [29] confirmed that only about 25 to 30 action potentials at 20 Hz are sufficient to elicit exocytosis from readily releasable pools of synaptic vesicles.

2.5 Application to the S-E Relationship

Brownian motion is classically defined by the Smoluchowski-Einstein (S-E) relation where the diffusion constant (D) in $m^2 \cdot s^{-1}$ is:

$$D = kT(6\pi\eta r)^{-1} \quad (5),$$

where k is the Boltzmann constant ($1.38 \cdot 10^{-23}$ $J \cdot T^{-1}$), T is temperature in Kevin, η is the viscosity of the medium and r is the particles radius.

If we assume a radius of $0.66 \cdot 10^{-15}$ m for a proton (1/2 the Compton λ) and the viscosity inside tumor cells is $6.8 \cdot 10^{-2}$ Pa·s then for the diffusion constant is $2.1 \cdot 10^{-6}$ m^2 $\cdot s^{-1}$. Multiplied by the mass of a proton ($1.67 \cdot 10^{-27}$ kg) all that is required is frequency to obtain energy. This produces an interesting "boundary condition" for the relationship between the first applied frequency and subsequently Planck-related energy. If the applied frequency is 6 Hz, the resulting energy is $21 \cdot 10^{-33}$ J. When divided by the central quantum value, Planck's constant ($6.626 \cdot 10^{-34}$ J·s), the functional frequency is 32 Hz. Interestingly, this is consistent with the upper and lower boundary for the frequency-modulated electromagnetic field configuration, presented with 3 ms point durations, that has produced the most effective diminishment of cancer cell proliferation. Reversing the presentation of the pattern (32 Hz to 6 Hz) produced no diminishment of malignant cell growth. Growth of normal or non-malignant cells was not affected by this configuration [19].

2.6 Intramolecular Pressure and Photon Emission

Viscosity is effectively pressure distributed over time, which means that it is force per unit area as a function of time.

The force (F) between two water molecules each with a unit charge can be estimated by classic formula:

$$F=(q^2) \cdot(4\pi\varepsilon r^2)^{-1} \quad (6),$$

where q is the unit charge, ε is permittivity and r is the distance between the charges.

For the distance between water molecules ($2.97\cdot10^{-10}$ m) and the permittivity complex ($4\pi\varepsilon_o$) equal to $1.11\cdot10^{-10}$ C^2 $N^{-1}m^{-1}$, the force would be $2.6\cdot10^{-9}$ N. When applied over the area of the water molecule ($8.8\cdot10^{-20}$ m^2) an inordinately high pressure of $0.29\cdot10^{11}$ Pa results. This pressure multiplied by the volume of the water molecule ($26\cdot10^{-30}$ m^3) results in an intrinsic energy of $7.7\cdot10^{-19}$ J or the frequency (by dividing by Planck's constant) $1.16\cdot10^{15}$ Hz. This is equivalent to a wavelength, assuming the velocity of light in a vacuum ($3\cdot10^8$ $m\cdot s^{-1}$) of ~260 nm.

This wavelength is within the ultraviolet component of the photon spectrum. More importantly it is within normal fluctuation of the peak (~270 nm) for absorption within the exclusion zone for a variety of substances as reported by Pollack and his colleagues [30]. Viscosity can be increased by a factor of 10 within the exclusion zone. The magnitude of the absorption peak was directly related to the molarity and hence indirectly to contributing factors to the narrow-band changes in viscosity. At

5.3 M NaCl within pure water (55.35 M) where there were 10 water molecules surround each solute molecule the 270 nm peak was maximum. At 1 M, or approximately 50 to 60 water molecules per salt molecule, the peak submerged into background.

The solutions from the calculations and Pollack's remarkable early research indicate that the pressure generated by the charges between water molecules per area of the molecule but then generated through its occupied volume can produce a condition that allows similar wavelength absorption. By implication the energy could be emitted at different (usually longer) wavelengths when triggered by appropriate stimuli that alter the supporting molecular configuration. The most typical candidate is the proportion of H^+ or hydronium ions that determine pH.

2.7 Gravitational Variants

An alternative derivation for viscosity involves the Gravitational constant $6.67 \cdot 10^{-11}$ m^3 $kg^{-1}s^{-2}$. Viscosity can be derived by:

$$\eta = G^{-1} \ (m^2 \cdot s^{-1}) \ s^{-2} \qquad (7).$$

In other words a natural viscosity emerges from the product of the inverse G, the target measure of diffusivity (δ) and the square of the frequency.

Hence if the viscosity is known, the intrinsic frequency from potentially any source that could affect the system can be estimated by:

$$f=\sqrt{(\eta(\delta\cdot G^{-1})^{-1}}) \quad (7).$$

The empirical H^+ diffusion constant at 20°C on earth is $8.65\cdot10^{-9}$ $m^2\cdot s^{-1}$ [9]. Assuming a general viscosity of functional fluid, for example the blood (~$2.5\cdot10^{-3}$ Pa·s), the frequency would be about 4.3 mHz. This periodicity is remarkably similar to one of the intrinsic resonant oscillations between the solid earth and atmosphere. Nishida et al [31] found that the average values of two of the fundamental spherical modes with amplitudes in the order of $0.5\cdot10^{-11}$ $m\cdot s^{-2}$ (0.5 nGal) showed marked annual variation with peak-to-peak values of about 0.1 to 0.2 (0.4 to 0.6) nGal. The two peak modes were 3.7 mHz and 4.3 mHz.

At the level of the average cell (10 μm width) with a mass of $5\cdot10^{-13}$ kg the force generated by a perturbation of $0.5\cdot10^{-11}$ $m\cdot s^{-2}$ is $2.5\cdot10^{-24}$ N. When applied across the 10^{-8} m of the plasma cell membrane the energy is $2.5\cdot10^{-32}$ J. The equivalent frequency, dividing by Planck's constant is about 38 Hz. The expected variation of the mass of a cell (assuming a standard deviation is about 30% of the mean) would indicate that most

(68%) of the cells would display intrinsic variations of between 27 Hz and 50 Hz.

The power associated with the resonant oscillations of the earth when coherent with the cell would not be trivial. The energy of $2.5 \cdot 10^{-32}$ J oscillating at 4.3 mHz would result in a power of $1.1 \cdot 10^{-34}$ W. When divided by the area of the membrane ($3.14 \cdot 10^{-12}$ m) the flux density would be $3.5 \cdot 10^{-23}$ $W \cdot m^{-2}$. If the frequency were congruent within the 2.8 GHz, range this means that a shift of only 1 SFU (solar flux unit) would share the quantitative values to intercalate with the typical cell. This increment of magnitude has been related to a number of geophysical and biological phenomena [32].

In the above equation (7) the controlling variable would be viscosity because G and δ would be effectively constant. Thus a range of viscosities within the cytoplasm or clearly within the interfacial water boundaries of exclusion boundaries would have the capacity to shift the intrinsic frequency into or outside from the fundamental oscillations associated with entire earth and its potential modulation by subtle changes in solar radiation.

2.8 Conclusion

The variable values of viscosities of water containing ions, that can range by a factor of 10 between bulk and interfacial (adjacency to surfaces) forms, could contain the

intrinsic energy that are functional boundaries for physiological changes important for cell survival. Temporally patterned and specific strengths of weak magnetic fields can interact with the viscosity-related energies to affect the spectral power density of photon emissions and absorptions that can simulate the essential geometric and temporal parameters of the living system including intracellular organelles such as vesicles and the width of the plasma cell membrane. The derivation of viscosity from a relationship that involves the Gravitational constant and the fundamental mode frequencies of the solid earth-atmospheric oscillations indicate flux densities from astronomical energies can be more significant than presently appreciated.

2.9 References

[1] E. Del Guidice, G. Preparata, *Journal of Biological Physics* 20 (1994) 105-116.

[2] C. R. House, *Water transport in cells and tissues*, Edward Arnold (Publishers) LTD, London, 1974.

[3] B. T. Dotta, M. A. Persinger, *Journal of Biophysical Chemistry* 3(2012) 72-80.

[4] M. V. Trushin, *Microbiological Research* 159 (2004) 1-10.

[5] R. Vogel, R. Suessmuth, *Bioelectrochemistry and Bioenergetics* 45 (1998) 93-101.

[6] M. A. Persinger, *International Letters of Chemistry, Physics and Astronomy* 14 (2014) 1-10.

[7] M. A. Persinger, *Current Medicinal Chemistry* 17 (2010) 3094-3098.

[8] J. Gu, Y. Xie, H. F. Schaefer III, *Nucleic Acids* 35 (2007) 5165-5172.

[9] T. E. Decoursey, *Physiological Reviews* 83 (2003) 475-579.

[10] C. W. Song, R. Griffin, H. J. Park, in B. Teicher (ed) *Cancer drug discovery and development: cancer drug resistance*, Humana Press, N.J., 2006.

[11] C. A. Wright, *Biochemica et Biophysica Acta* 1757 (2006) 886-912.

[12] C. Chai, H. Yoo, G. H. Pollack, *Journal of Physical Chemistry* 113 (2009) 13953-13958.

[13] G. H. Pollack, *Advances in Colloid and Interface Science* 103 (2003) 173-196.

[14] G. H. Pollack, X. Figueroa, Q. Zhao, *International Journal of Molecular Sciences* 10 (2009) 1419-1429.

[15] P. W. Rand, E. Lacombe, *Journal of Clinical Investigation* 43 (1964) 2214-2226.

[16] K. Fushimi, A. S. Verkman, *Journal of Cell Biology* 112 (1991) 719-725.

[17] N. Verdel, P. Bukovec, *Entropy* 16 (2014) 2146-2160.

[18]. N. Rouleau, T. N. Carniello, M. A. Persinger, *Journal of Biophysical Chemistry* 5 (2014) 44-53.

[19] N. J. Murugan, L. M. Karbowski, B. T. Dotta, M. A. Persinger, *International Journal of Pure and Applied Chemistry* 5 (2015) 131-139.

[20] M. A. Persinger, S. A. Koren, *International Journal of Neuroscience*, 2007 (117, 157-175.

[21] S. A. Koren, B. T. Dotta, M. A. Persinger, *The Open Astronomy Journal* 7 (2014) 1-6.

[22] B. T. Dotta, N. J. Murugan, L. M. Karbowski, M. A. Persinger, *International Journal of Physical Sciences* 8 (2013) 1783-1787

[23] B. T. Dotta, S. A. Koren, M. A. Persinger, *Journal of Consciousness Exploration & Research* 4 (2013) 25-34.

[24] N. J. Murugan, L. M. Karbowski, R. M. Lafrenie, M. A. Persinger, *Journal of Biophysical Chemistry*, in press.

[25] S. M. Blinkov, I. I. Glezer, *The human brain in figures and tables: a quantitative handbook*, Plenum Press, N.Y., 1968.

[26] C. Margraves, K. Kihm, S. Y. Yoon, C. K, Choi, S. Lee, J. Liggett, S. J. Baek, *Biotechnology and Bioengineering* 108 (2011) 2504-2508.

[27] R. Delgado, C. Maureira, C. Oliva, Y. Kidokoro, P. Labarca, *Neuron* 28 (2000) 941-953.

[28] Y. Goda, C. F. Stevens, *Procedings of the National Academy of Sciences* 91 (1994) 12942-12946.

[29]C. F. Stevens, J. H. Williams, *Journal of Neurophysiolgy* 98 (2007) 3221-3229.

[30] B. Chai, J-m. Zheng, Q. Zhao, G. H. Pollack, *Journal of Physical Chemistry* 112 (2008) 2242-2247.

[31] K. Nishida, N. Kobayashi, Y. Fukao, *Science* 287 (2000) 2244-2246.

[32] D. A. E. Vares, M. A. Persinger, *International Journal of Geosciences* 5 (2014) 1503-1508.

2.10 Preamble to Chapter 3: Storing Electromagnetic Energy in Biological Organisms: Can the Viscosity Water be Responsible?

In consideration of our observations with respect to viscosity, pH, electromagnetism, and gravity, it was necessary to investigate how fundamental biological units (i.e. cells) might process experimentally applied energy quanta. Just as water occupying a volume in space was shown to express properties characteristic of cells given certain environmental conditions, we wanted to know if these properties were in any way relevant to biological systems beyond coincidental approximations to relevant wavelengths. We operated upon the assumption that light emissions shared between cells constituted signals with specificity and utility analogous to molecular ligands. Our approach involved exposing cells to pulsed light and electromagnetic fields. Insofar as aqueous solutions are susceptible to light emission frequency shifts, and photonic energies are biologically relevant information, it was necessary to determine whether cells (primarily composed of water and operating within aqueous media) could be induced to alter their function in the presence of experimentally manipulated electromagnetic energy.

Chapter Three

Experimental Evidence That Specific Photon Energies Are "Stored" In Malignant Cells For an Hour: The Synergism of Weak Magnetic Field-LED Wavelength Pulses

Published in Biology and Medicine (2016) – Vol: 8 (1). Pg. 1-8

Lukasz M. Karbowski, Nirosha J. Murugan and Michael A. Persinger

Abstract

According to the Trushin hypothesis light emissions between cells and microorganisms could be a major mechanism for "interunit" communication. The capacity for particularly patterned electromagnetic magnetic fields with specific temporal parameters to remain or to be "trapped" within the cell's aqueous environments that facilitate interfacial water was postulated by Del Giudice and Preparata and shown experimentally by Murugan and her colleagues. We reasoned that specific pulsing patterns of photon energies coupled to weak magnetic fields would facilitate photon representations within cells. We found that melanoma cells *in vitro* exposed for one hour to a specific temporally complex pattern of weak magnetic fields coupled with LED 470 nm (blue) light flashes (1 ms point durations) demonstrated this capacity. During the 120 min following the one hour of exposure this magnetic-light paired stimulation 100 to 1000 fold increases in emissions of photons from cells were measured compared to any of the other field patterns which did not differ from sham field conditions. The delayed emissions began about 30 to 40 min after field+light termination, peaked around 70 min later and approached the values of other conditions after about 100 min. The total photon energy emitted was quantitatively similar to the energy induced by the effective magnetic field. Additional

measurements by fluorescence spectrophotometry indicated that the wavelengths of the photons during this post-stimulation interval peaked around the 470 nm which corresponded to the wavelength to which the cells had been exposed in combination with a magnetic field. The emission peak for sham field exposed cells was around Pollack's value of ~270 nm for interfacial water. These results are consistent with models predicting that under special conditions coupled magnetic fields and pulsed photons can be maintained within the aqueous state of living tissue and can be re-emitted long after that stimulation has terminated. The results suggest a potential mechanism for intercellular communication that is applicable to biology and medicine.

3.1 Introduction

The capacity for aqueous systems such as those found within living cells to maintain specific patterns from applied electromagnetic energy as well as information for protracted periods has both theoretical and practical implications. Although "flickering clusters" of transient structures of water molecules with half-lives in the tens of picoseconds have been inferred for decades [1], the maintenance of quasi-stable structures for periods of kiloseconds was considered highly unlikely due to the intrinsic thermal agitation. This argument was reviewed and refuted by Cifra [2]. The brilliant reasoning and insights of Del Giudice and Preparata [3] indicated that classical electromagnetic fields could become constrained "or trapped" within the ensemble of atoms oscillating in phase with transitions between ground states and particularly excited states. The duration of this "entrapment" could be significant for influencing the biomolecular pathways that control cellular dynamics and intercellular communication as well as Trushin's "conversations" among microorganisms [4].

The representation of "photon temporal patterns" as information within the cells is particularly relevant in light of recent theoretical, quantitative and experimental evidence that "molecular resonance recognition" as defined by Cosic [5]. Specific combinations of narrow-band wavelengths within the

visible [6] and paravisible (near infrared and near ultraviolet) may connect the different discrete structure of molecules that constitute these pathways such as JAK-STAT [7] and MAP-ERK [8]. The flux densities of light emissions from cells are usually within the 10^{-12} $W \cdot m^{-2}$ range [9] but can be enhanced pharmacologically by adding morphine [10] or appropriately patterned magnetic fields within the 1 μT range. Recently Dotta et al [11] applied the equation for the magnetic moment of a Bohr atom to the plasma cell membrane. The quantitative solution for the lateral diffusion of charges of lipids within the plasma membrane around the cell's perimeter resulted in a "membrane magnetic moment" that when multiplied by a specific intensity magnetic field resulted in energy that would be expected by photons within the visible wavelength.

The repeated demonstrations of the ordered structure of interfacial water that can exist for kiloseconds or more near surfaces, such as cell membranes, by Pollack and his colleagues [12,13] indicates that there are aggregate conditions that could maintain optimal patterns of applied electromagnetic fields. The property of thixotrophy whose physical mechanisms have been reviewed recently by Persinger [14] whereby water maintained in the dark and not disturbed produces stable aggregates of water molecules that can be maintained for days reiterates the potential for this "solvent of life" to represent applied

energies for protracted periods. Murugan et al [15] demonstrated an intensity-dependent (within the 1 μT range) increase of the "holding effect" in spring water in which small aliquots of protons were added while the solution was exposed to a specific type of magnetic field. Whereas sham field exposed water displayed the expected incremental decreases in pH with each addition of protons, the water exposed to the specific magnetic fields exhibited no such shift until a sudden change occurred after a "holding" latency of 6 to 15 min. They inferred this latency reflected the maintenance of the proton injections within structure water before the charge accumulation exceeded the intrinsic domains within water molecules induced by the energy from the applied magnetic fields.

Murugan et al [16] showed that undisturbed spring water maintained in the dark and exposed continuously to weak (μT) physiologically patterned, frequency-modulated magnetic fields displayed enhanced photon emissions as measured by spectrophotometer within range of 320 nm to 470 nm with most of the shift occurring between 400 nm and 455 nm. Spectral analyses indicated a specific enhanced peak of power in photon emissions around 10 nm, the width a plasma membrane. The shift in energy was equivalent to about 10^{-20} J. Neither the shift nor the SPD was evident in double distilled water exposed to the same conditions. Del Giudice and Preparata's theoretical approach

extended Hepp and Lieb's discovery that above a specific atomic density and within biologically temperatures a spontaneous phase transition emerged that could maintain the electromagnetic A vector potential within the coherent domain of liquid water. The ground state whose frequency was assumed to be ~0.26 eV or the scaled equivalent of $4.2 \cdot 10^{-20}$ J, is within the range of the energy associated with the second shell of hydrogen that is directly involved with the mobility of protons within the hydronium ion [17]. Murugan et al [18], employing the same patterned magnetic fields as those that produce the enhanced of spectrophotometer measurements, found that spring water displayed progressive shifts towards alkalinity over two or three hours and that the shifts occurred in increments of about 20 ms.

Emissions of photons from cells have been considered the primary means by which intercellular communications modulate aggregate behavior [4, 19]. The demonstration that cells can "store" photons as virtual representations as suggested by Popp [20] or the information associated with specific wavelengths of photons could be "represented" for protracted periods only to be re-emitted hundreds of seconds to minutes later would alter perspectives of cell-to-cell communication. The maintained state could create the condition for information within the storing cell to affect the substrate that is transiently maintaining the photon energies and superimpose its characteristics onto the re-

emitted photon field. Here we present experimental evidence for protracted photon storage and markedly delayed re-emission within malignant cell cultures.

3.2 Procedure

General Light Emission as Measured by Digital Photometers

We employed the same procedure that resulted in diminishment of growth of malignant cells but not normal cells in several previous studies [21]. In the present experiments plastic plates (5.5 cm wide) of 10^5 to 10^6 (95% confluence) B16Bl6 were exposed to different weak magnetic fields and blue LED (470 nm) light that were flashed in synchrony from the top of the plates that had been maintained at 37°C, within a standard (dark) incubator (Figure 1). The device that generated the magnetic fields or LED patterns is shown in Figure 2. The structures of the different patterns (Figures 3-5) were programmable from the outside of the incubator by a personal computer [22]. The different patterns were generated by converting columns of numbers between 0 and 256 to between -5 to +5 V (with 127=0 V). The duration that each number (and voltage) was generated was called the point duration. The point duration, usually 1 ms or 3 ms, has been shown to produce significant alterations in calcium influx via T-type calcium channels [23], slowing of cancer but normal cell growth, and affect analgesia in rodents [24] and invertebrates [25]. We

[26, 27] have shown quantitatively and by experiment the potential cosmological sources of these temporal values and their relationships to the intrinsic properties of the electron and the proton. They are associated with point durations of ~1 ms and ~3 ms, respectively.

Examples of the different shapes of the field patterns delivered to the cells are shown in Figure 1. They included a frequency-modulated pattern often described as the Thomas pattern. It was composed of 849 points (values from 1 through 256). The second pattern was the geomagnetic pattern composed of 5071 points that had been intended to be applied as 69 ms point durations to imitate the amplitude modulation in mHz range of a 7 Hz fundamental variation for a duration of 6 min to simulate an average sudden impulse [28]. However when Murugan et al [29] shifted the point duration to 1 ms they found that this pulse duration produced complete fragmentation and dissolution of planarian when they were exposed to combinations of this field and the Thomas pattern.

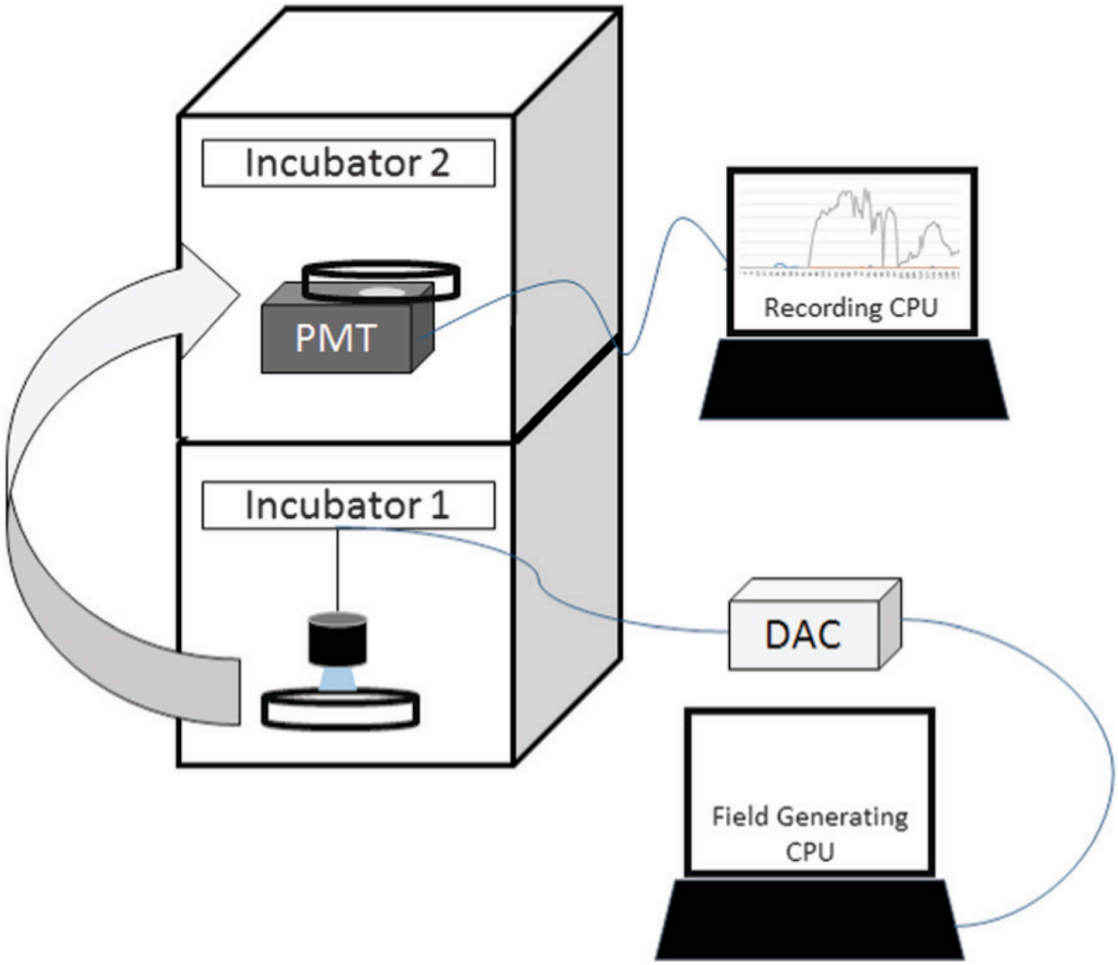

Figure 1. Exposure and measurement diagram. The cells were first placed in incubator 1 and exposed to the magnetic field, light pulses, or both magnetic field and light pulses simultaneously for 1 hr. They were then placed without treatment into incubator 2 where photon counts were measured for 2 hr.

The third pattern was the LTP (Long Term Potentiation) pattern that was the magnetic field equivalent of the electrical current pattern developed by Rose et al [30] to induce long term potentiation in hippocampal slices. Whole body exposure of rats to the magnetic field equivalent of that pattern resulted in marked disruption of behaviors that required LTP [31]. This "LTP" pattern facilitates the formations of the aggregate cellular substrate that synthesize or alter of synaptic spines. The spatial patterns of the volumetric distribution of these novel spines in the brain are considered the physical correlate of memory formation.

Figure 2. The actual exposure device. The 8 LEDs (each 470 nm) were placed over the plate of cells (Figure 1). The nails heads which served as the source of the magnetic field could be activated singly, the LEDs could be activated singly, or both the field and LEDs could be activated simultaneously.

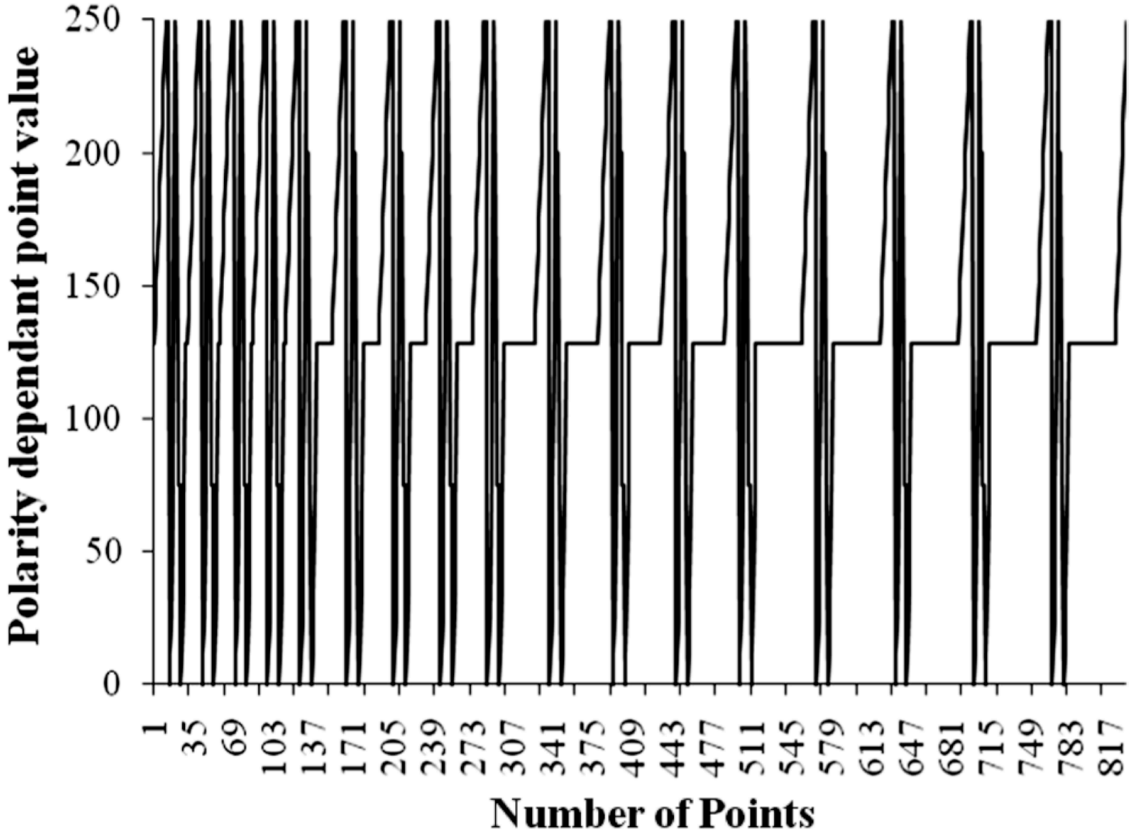

Figure 3. The frequency-modulated or "Thomas" pattern. Vertical lines indicate the value between 0 and 256 that was transformed to voltage to produce the pattern. Horizontal axis indicates the sequences of points each with a value between 0 and 256.

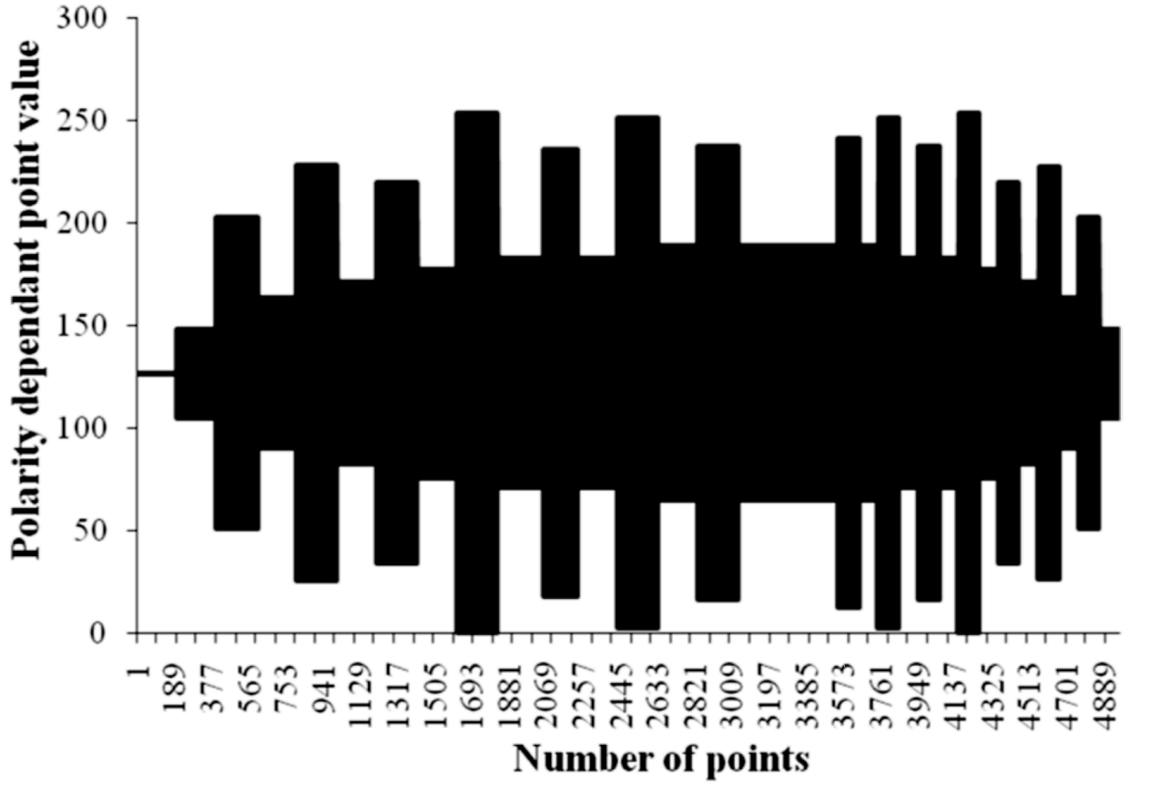

Figure 4. The general shape of the "geomagnetic pattern" which was an amplitude-modulated pattern composed of over 5,000 points (horizontal axis). The vertical axis indicates the values between 0 and 256 that were transformed to voltages.

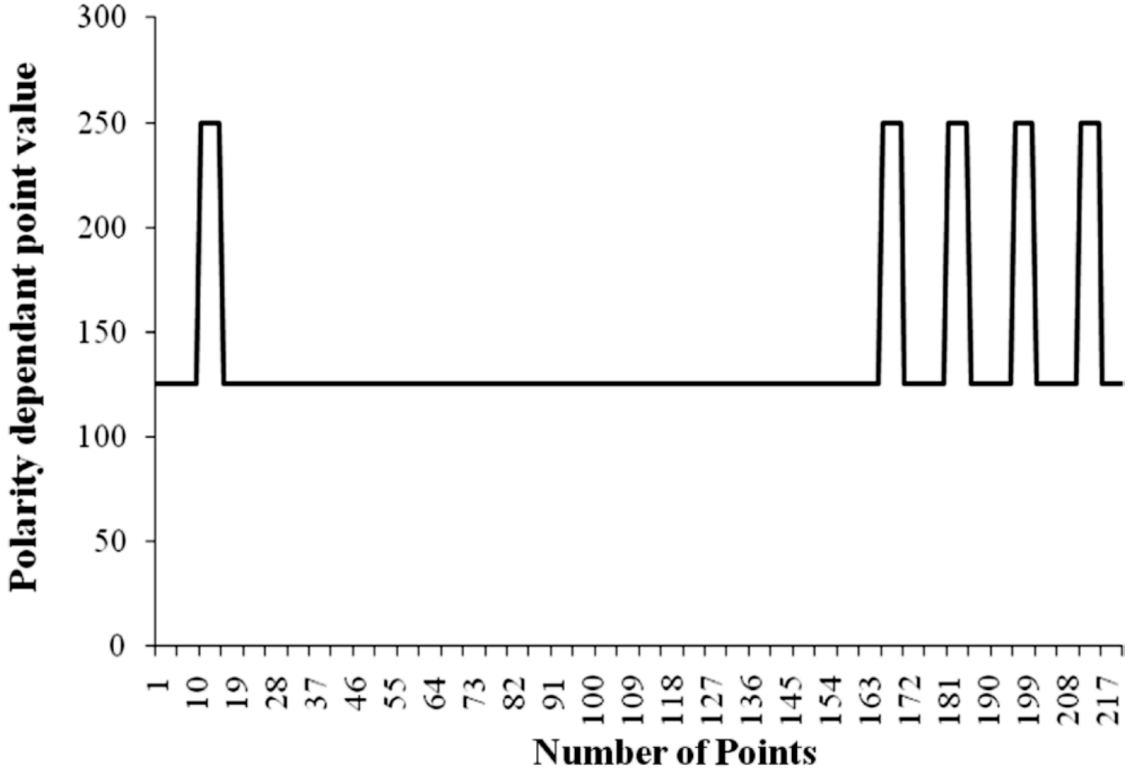

Figure 5. The "LTP" pulse derived from Rose et al [30] for stimulating hippocampal slices but here was generated as a magnetic field. Vertical axis is the values between 0 and 256 transformed to voltages. The horizontal axis refers to the sequence of numbers.

In summary the cells were exposed to one of three different patterns of signals each of which were composed of point durations of either 1 ms or 3 ms. The output from the digital-to-analogue converter from the computer containing the number sequences was delivered to the custom-constructed device shown in Figure 2. As the computer program progressed in discrete temporal steps through each of the numbers between 0 and 256 that composed the pattern specific voltages (and hence electric currents) were delivered to the LED/solenoid points. The output was directed either to: 1) the LEDs only, 2) the magnetic circuit only, or 3) the LEDs and the magnetic field circuit. This means that both the LED and magnetic field pulsed for the same duration along the series of values that defined the complex pattern.

The final variable was intensity for the magnetic field only, the light only or the coupled magnetic field plus the light. The low intensity condition was associated with a magnetic field strength (as measured by a 3-axis power meter) of ~2.7 to 2.8 μT within the volume (3 cc) containing the cells and simultaneous flux power density from the LED of between ~51 and 66 lux for all conditions. For the high intensity condition the magnetic field strength averaged ~7 μT and the radiant flux density from the LED ranged between 932 and 1774 lux. The total exposure time for each pattern was 60 min. Each pattern was tested at least three times (triplicate).

When the 60 min of exposure had been completed, the dish was removed and placed within 10 s into another incubator (same size and company and the in which the cells were exposed) that was maintained at 37°C (Figure 1). The aperture of a 2.5 cm^2 type digital photomultiplier sensor (Sens Tech LTD DM0090C) was placed over the top of the covered dish containing the cells that had been exposed to one of the patterned fields or to no field (the sham condition) during the previous one hour. The numbers of photon counts per 20 ms (the upper limit for the software of the equipment), i.e., 50 times per s were recorded externally as photon counts per s for 120 min. The data were averaged into blocks of 1 min and 10 min for convenience for analyses. The single most persistent and largest effects were repeated at least five times on different days.

Specific Wavelength Emission as Measured by Fluorescence Spectrophotometer

After the most optimal pattern (geomagnetic pattern), point duration (1 ms) intensity (low) and coupled patterns of light (470 nm, 50 Lux, 1 uT) was discerned that generated the greatest number of post-exposure photons, the procedure was repeated but measured by fluorescent spectroscopy to isolate the specific wavelengths of the photon emissions. The cells were removed and placed in a fluorescence spectrometer (Olis RS M1000 F1) where photon emission counts per s between 200 and 600 nm were measured

as described previously by Murugan et al [16]. The results (mean of triplicates) of the profiles for the media, cells only and cells that had been exposed to the field plus the light pattern were calculated. The data for each of the triplicates for each condition (media only, cells only, cells after exposure to the light+magnetic field) were z-scored. The means of the z-scores for each condition were then averaged.

3.3 Results

The experimental design involved 3 types of field patterns, two point durations, two amplitudes, and either magnetic field only, light (450 nm) only, or both light and magnetic field combinations. This was a total of 36 experimental conditions. The results were conspicuous and reliable. Only the cells that had been exposed to the low intensity, 1 ms, geomagnetic pattern *and* 450 nm LED **simultaneously** displayed evidence of delayed photon emissions during the subsequent 100 min of removal from these conditions. The effects were so large that the raw photon data emissions were $\log_{10}$ transformed. The results are shown in Figure 6.

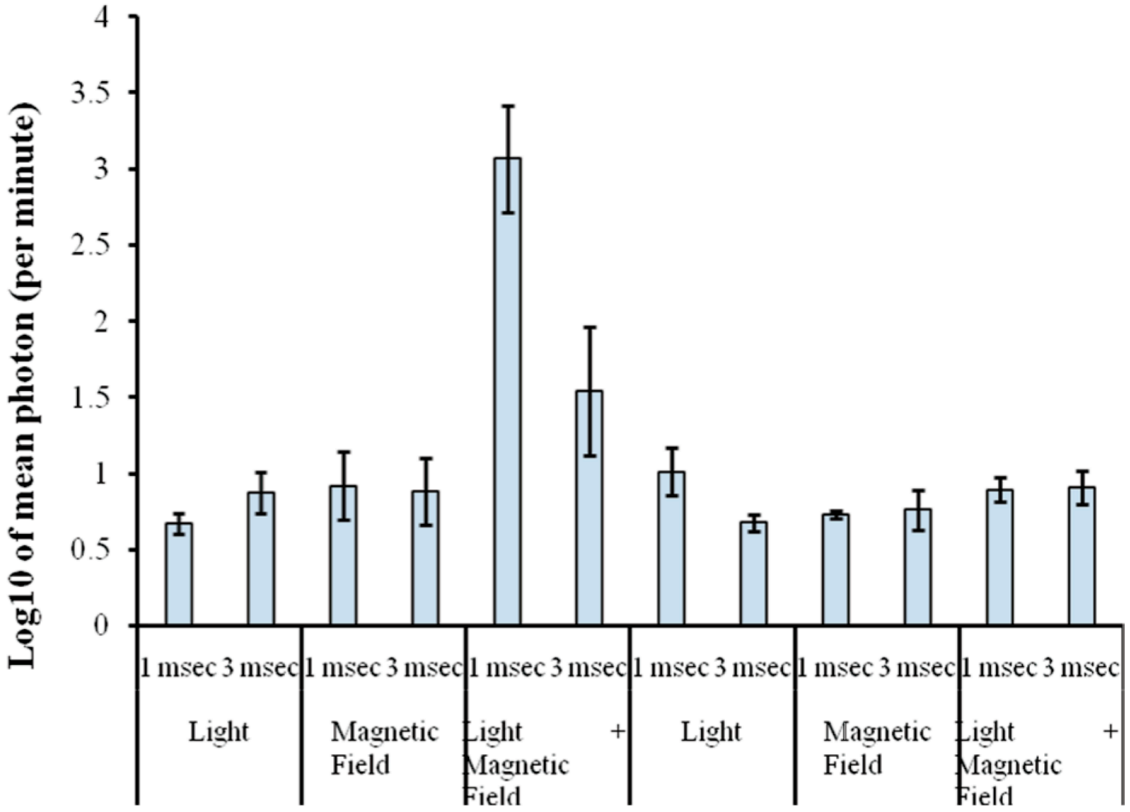

Figure 6. Log base 10 of the mean numbers of photons per minute from the cell plates for the 100 min after 60 min exposure to the geomagnetic pattern with either 1 ms or 3 ms point durations for the low intensity and high intensity condition for the light only, magnetic field only or light+magnetic field condition. Note the low intensity, 1 ms light+magnetic field exposure was associated with a subsequent 1000 fold increase in photon emissions from the cells over the subsequent approximately 100 min.

The light+magnetic field effect for the geomagnetic pattern with 1 ms point durations and low intensity was associated with total photon emissions exceeding 1000 per minute compared to the other variations of combinations. There was a marginally significant increase in delayed photon emissions for the low intensity 3 ms point duration for the magnetic field-light combination. However the high intensity light flash-magnetic field intensity was not associated with any significant emissions of photons. These values did not differ appreciably from any of the other treatments, which did not differ significantly from the sham field conditions.

Figure 7 shows the timing of the photon emissions from the cells that had been exposed to the low intensity light+magnetic field patterns (green) and to the higher intensity light+magnetic field configuration (blue). Samples from the other conditions (brown) which all ranged from 7 to 8 photons per min for the serial blocks of ten minutes overlapped with the previous group. Approximately 30 min elapsed before the delayed release of photons occurred. The peak occurred approximately 60 to 80 min after termination of exposure. Within about 110 min the photon emissions had declined to near reference group levels.

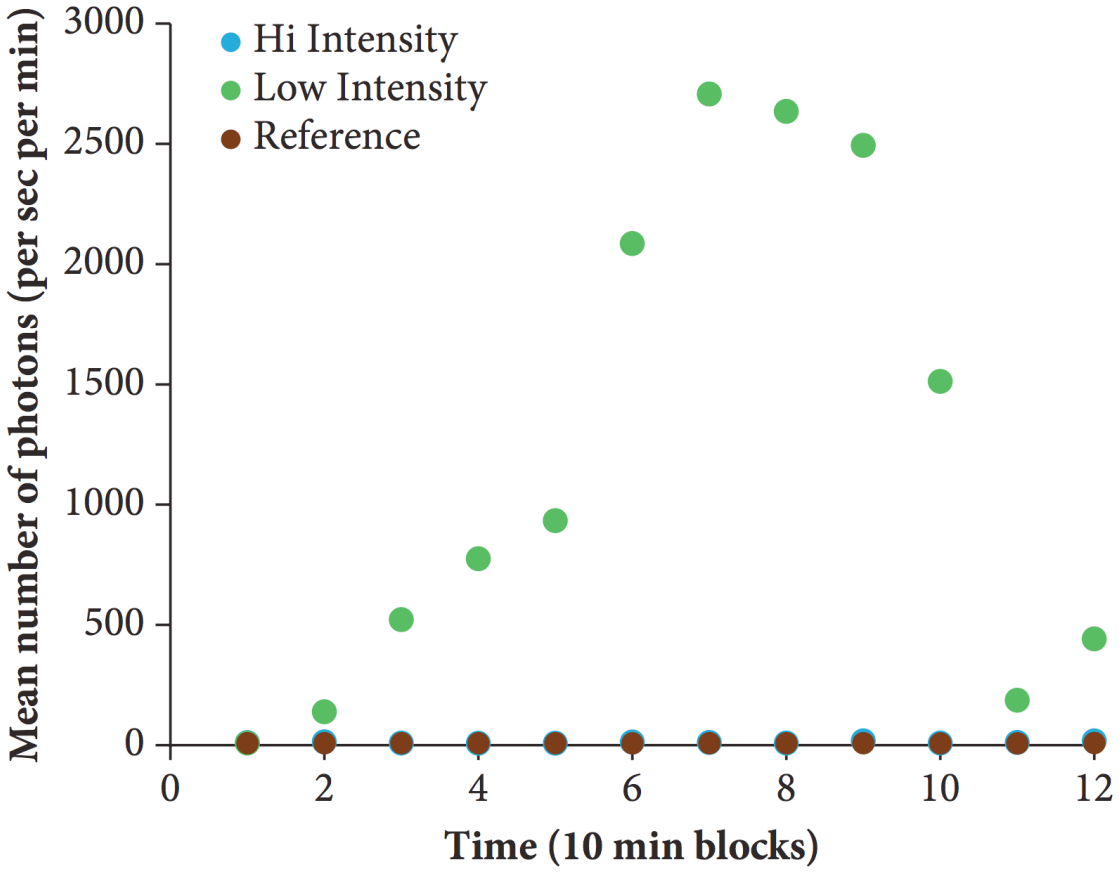

Figure 7. The mean numbers of photon emissions per s per min for successive 10 minute block after 60 min exposure to the low intensity, 1 ms point durations, geomagnetic patterned field plus light (green). In comparison the high intensity treatment (blue) did not differ from a random average of all other conditions including sham field exposures which at this scale overlapped.

Figure 8 shows the distribution over the 10 serial 10 min blocks of the photon emissions for each trial so that the individual variability can be appreciated. On average the re-emissions did not begin until about 30 to 40 minutes after the exposures had been stopped. Although for most trials the photon emissions were declining after 80 min, photon "re-emissions" were still increasing in one of the trials.

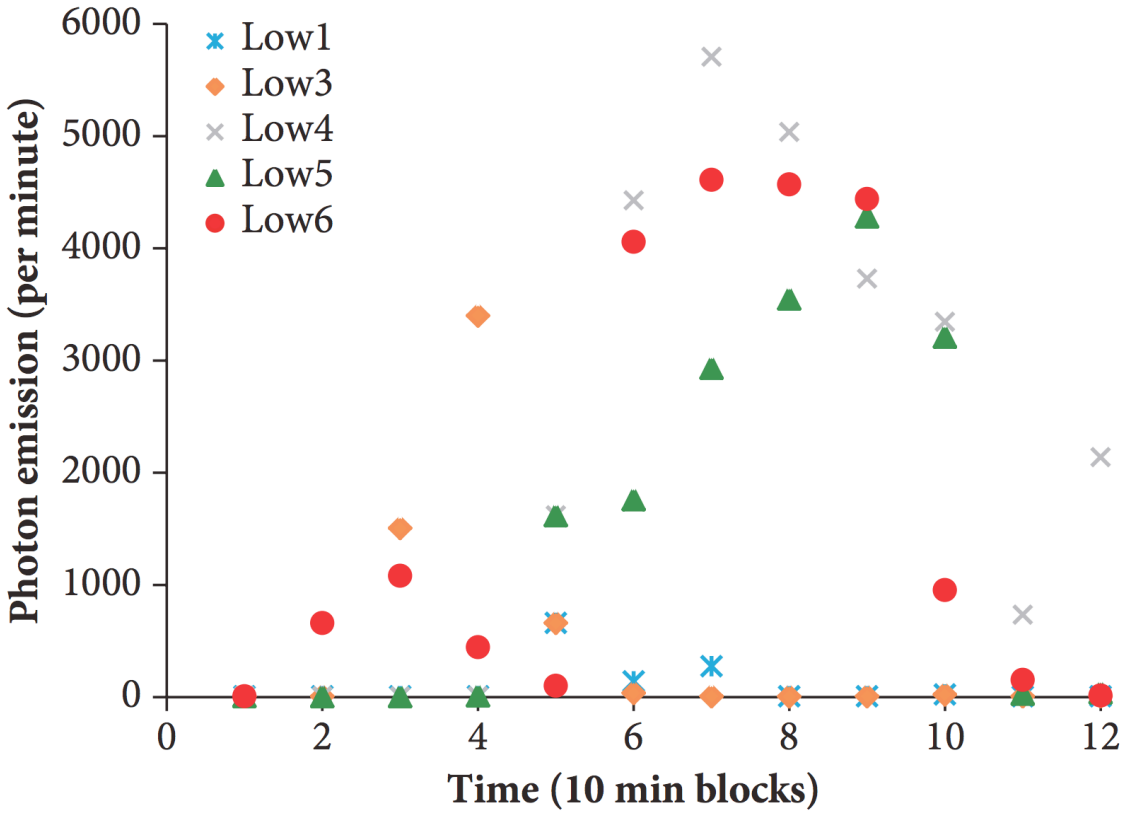

Figure 8. Emission values (photons per min) for 5 separate trials for the effective condition to demonstrate the variability within

the subsequent 120 min. By 120 min the numbers of photon emissions were approaching that of all other treatment groups.

Specificity of Light Emission

Fluorescence spectrometry confirmed and extended the results of the specific treatment. The fluorescence (raw photon) counts for the media only are shown in Figure 9. There was no specific "power peak" although 260 nm cannot be excluded if the criteria of z > +2.0 is applied for the individual points.

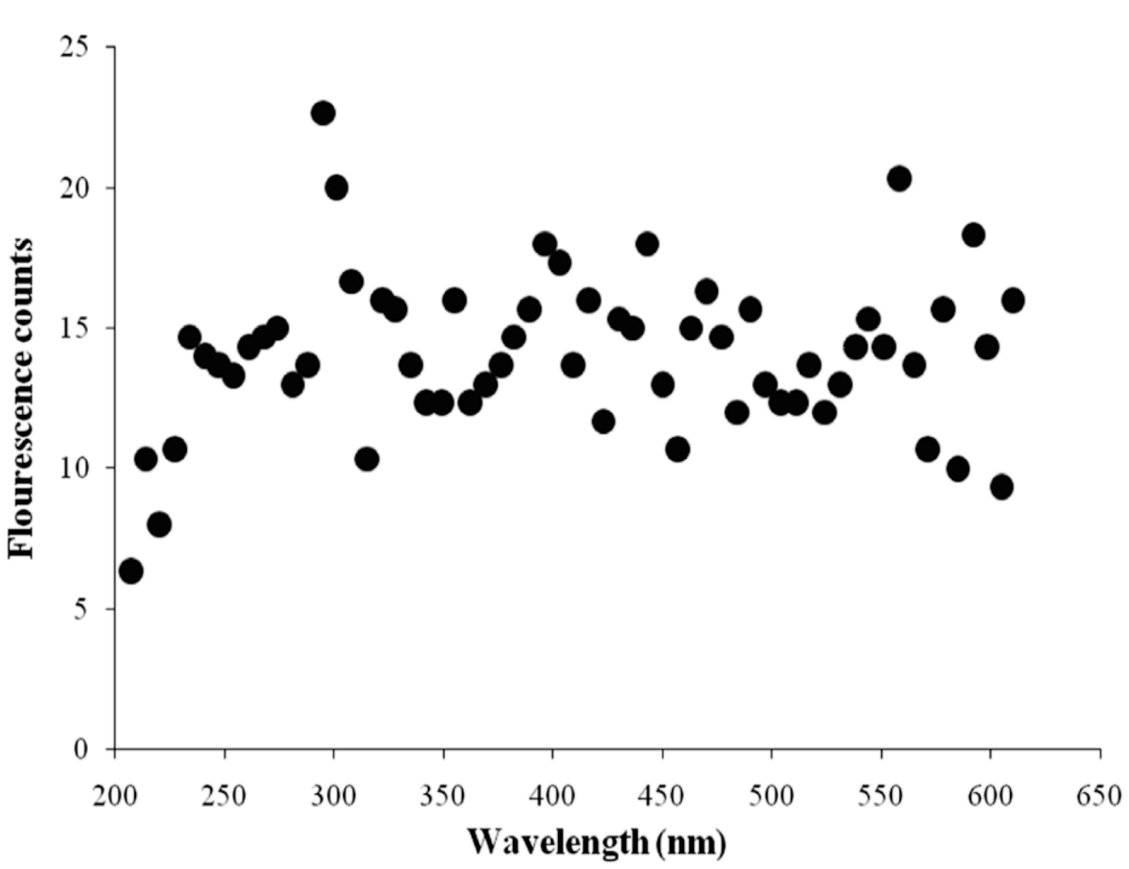

Figure 9. Vertical axis indicates the numbers of photon counts by fluorescent spectrometry measurements for the media only as a function of wavelength of emissions.

On the other hand the distribution of photon emissions from the cells that had been exposed to sham field conditions within the same media displayed a marked symmetrical maximum around 270 nm (Figure 10).

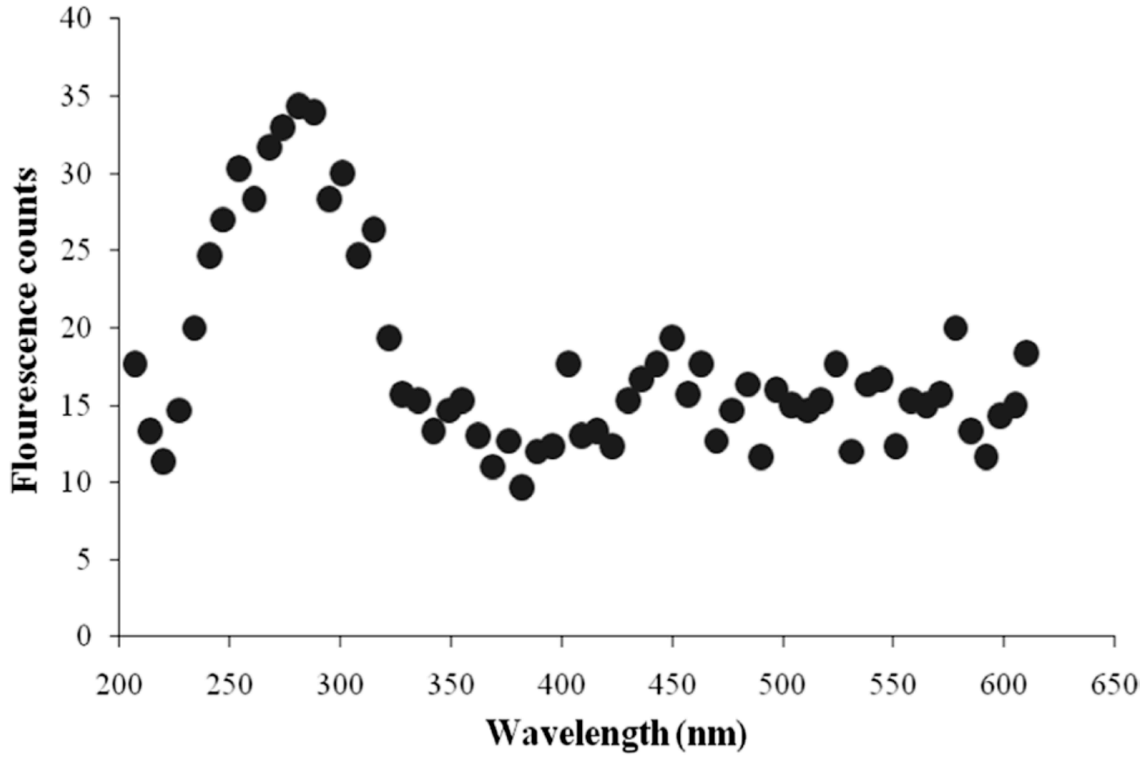

Figure 10. Vertical axis indicates the numbers of counts by fluorescence spectrometry for cells only (sham field) as a function of the wavelength of emissions.

Figure 11 shows the clear and reliable increase in "spontaneous" photon emissions occurred around 470 nm from the cells that had been exposed to paired geomagnetic field synchronized with 470 nm light flash about one hour previously.

In other words when the cells had been exposed to the combination of light and magnetic field there were still photon emissions from those cells at least 60 min after the exposures had been terminated. There was also a much smaller peak around 300 nm.

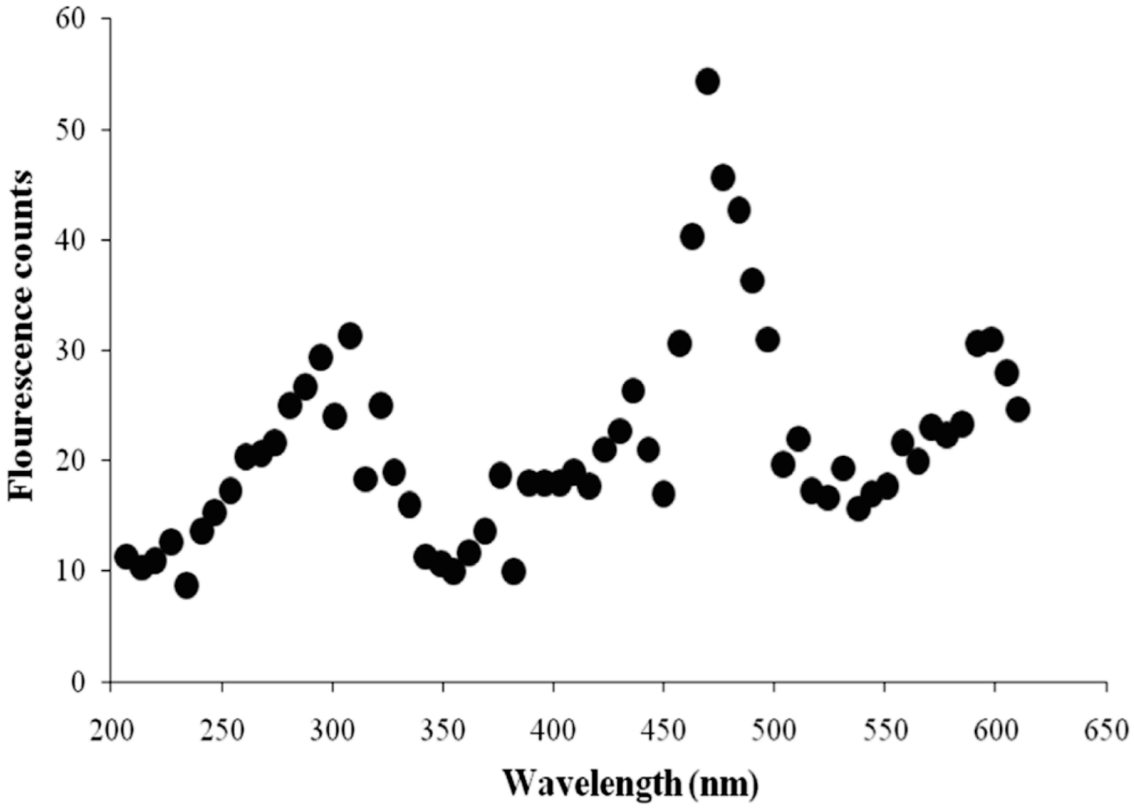

Figure 11. Vertical axis indicates the numbers of photon counts by fluorescence spectrometry as a function of wavelength of the emissions for the cells that had been exposed to the specific parameters of the low intensity magnetic field plus light (470 nm) condition. Note the peak of emission at 470 nm.

3.4 Discussion

The results of these experiments may be the first to demonstrate that the combination of the appropriate specific wavelength of light within the visible spectrum and complex patterned magnetic field induce the condition to maintain photon energies within cells. The specificity of the magnetic field pattern is indicated by the absence of any delay of photon emissions from the cells that were exposed to the frequency-modulated (Thomas) pattern or to the LTP pattern. The specificity of the timing of the point durations was indicated by the conspicuously different magnitude of photon emissions from the same "geomagnetic" pattern when it and the coupled 470 LED blue light were presented as 1 ms point durations but not at 3 ms point durations.

The narrow interval of the appropriate magnetic field intensity was clearly indicated by the presence of the effect around 2.8 μT fields but complete absence of the effect around 7 μT. The difference in amplitude of the photon emissions over protracted periods was approximately a factor of 100 to 1000. This is the largest effect we have ever measured in our biophoton research. Only the specific combination of the geomagnetic field pattern, the point durations of 1 ms, low intensity magnetic field (2.8 μT) and light (~60 Lux) produced this extraordinary effect.

The latency for the beginning of the "re-release" of the photons was about 30 min. This suggests that the condition that had "held" or "maintained" the photons (or more likely some process associated with the representation within the cells) and their aqueous environment began to dissociate after this period. The peak in the re-release of the photons was about 60 to 80 min after the termination of the 60 min exposure. By approximately 110 min after the termination of the exposures the photon emissions had declined to that of any of the other combinations that remained remarkable stable over the 120 min following removing from the different non-effective configurations of field patterns, intensities, and point durations. Consequently the phenomenon is not likely to have been related to artifact drift but to an actual quantity of energy that was maintained within the aggregate of cells and their aqueous solvent.

That the wavelength equivalent represented in some manner or "stored" within the aggregate of cells exposed to the optimal pattern of light and magnetic field was specific to the applied 470 nm was strongly suggested by this same peak emission wavelength as measured by the more precise fluorescence spectrometry. The photomultiplier units only measured the numbers of photons within the range of the sensors (near-ultraviolet through the visible boundary to near-infrared) and did not reflect the specific wavelength of the photons that were "re-

emitted". The validity of this emission is indicated by the shape of the distribution of the numbers of photons emitted at wavelengths around 470 nm for the cells that had been exposed to the light plus magnetic field.

Cells that had been exposed to sham conditions displayed peak photon emissions around 270 nm which is the value often reported for interfacial water by Pollack and his colleagues [12, 13]. Because the standardized power distribution over the range of wavelengths appeared to be displaced from the 270 nm emissions associated with interfacial water to those associated with the LED wavelength of 470 nm, we suggest that the intrinsic energy within the water and cell aggregate may have been recruited into the representation of the substrate by which the 470 nm energy was maintained as a quantity of energy. If this occurred then the 1 ms point durations of the geomagnetic field at the weak intensity could have created the coherent domains for this maintenance as hypothesized by Del Giudice and Preparata [3].

If the energy associated with the magnetic field was related to the energy of the total photon emissions their quantities should be similar. The median total numbers of photons emitted during the 120 min after the optimal exposure was $2 \cdot 10^5$ photons per average minute or $1.2 \cdot 10^7$ photons per s. If the cross-sectional area of the plate is accommodated with the area of the sensor for the photomultiplier unit the actual values would have

been around $1.2 \cdot 10^{8}$ photons per s. If the peak wavelength was around 470 nm the energy per photon would have been $4.2 \cdot 10^{-19}$ J and hence the total photon energy released per plate would have been $\sim 5 \cdot 10^{-11}$ J. In comparison the energy from the applied effective magnetic field of $2.8 \cdot 10^{-6}$ T within the 3 cc of the volume of the cells and surrounding fluid ($3 \cdot 10^{-6}$ m^3) would have been according to:

$$J = B^2 \, (2\mu)^{-1} \, m^3 \qquad (1),$$

where B is the field strength in Tesla, μ is magnetic permeability ($4\pi \cdot 10^{-7}$ $N \cdot A^{-2}$) and m^3 is volume, $\sim 1 \cdot 10^{-11}$ J. This is within the same order of magnitude as the photon energy release. Hence this is strong evidence that the amplitude of the 're-emission" photon effect was controlled by the intensity of the magnetic field.

If the total energy emitted during the subsequent 120 min was $5 \cdot 10^{-11}$ J and there were $\sim 5 \cdot 10^{5}$ cells (10^{5} to 10^{6} for 95% confluence), then there would have been $\sim 10^{-16}$ J per cell. However, the energy would have been distributed over the duration of the "release" which averaged about 80 min ($4.8 \cdot 10^{3}$ s). This would be equivalent to about $2 \cdot 10^{-20}$ J per second. This value is similar in coefficient and magnitude to estimated emissions from these cells when they were removed from incubation and placed in

room temperature for several hours [32]. During this time, shown by Dotta et al [6] there was a shift in predominant wavelengths across the near infrared to near ultraviolet boundaries as the cells responded to the ambient rather than incubation temperatures.

In comparison the cells that were exposed to the other combinations of fields, point durations and intensities emitted about 500 times fewer photons. The total numbers of photons emitted from these aggregates of cells were in the order of 900 to 1100 during the 120 min per. This would be equivalent to $0.4 \cdot 10^{-22}$ J per s per cell. The temperature equivalent according to the Boltzmann constant of $1.38 \cdot 10^{-23}$ $J \cdot K^{-1}$ would be about 2.8°K which is remarkably proximal to the cosmic microwave background temperature. This value has been shown to be a potential rate limiting value that maintains the small effect size for experimental demonstrations of excess correlation and entanglement [33, 34].

Clearly subsequent experiments must be completed to isolate the mechanisms for the specificity. However some rational possibilities can be discussed. The generation of the massive post-exposure photon emissions for the 1 ms point duration of the geomagnetic field configuration when the intensity of the field was 2.8 μT but not 7 μT indicates that magnetic energy available to the volume was not the critical variable. Persinger and

Lafrenie [35] have shown that the magnetic field strength equivalent to the approximately 27 mV resting membrane potential of cancer cells in general is about 2.7 to 2.8 μT. From their perspective such matching between field strength and resting membrane potential would facilitate the "cohesive" or "condensate" effects within all of the cells to behave as a single unit.

The fact that 1 ms point durations but not 3 ms point durations were associated with this powerful phenomenon may reveal the physical mechanisms. Koren and his colleagues [26, 27] had shown that 1 ms was the theoretical time required for an electron to expand one Planck's length on the bases of the present Hubble parameter. Experiments involving the measurement of photon flux densities from chemiluminescent reactions or LEDs between two loci sharing similar rotating magnetic fields with specific changing angular velocities have indicated that point durations of 1 ms may affect electrons while 3 ms point durations are more involved with protons [36]. If these measurements and inferences are correct then the 1000 fold increase in photon emissions noted in the present experiments would have primarily involved electrons or their movements within coherent domains.

There are several potential applications of these powerful effects to Biology and Medicine. First one experimental test of the Trushin [4] hypothesis is to discern if microorganisms or

cells displayed enhanced alterations in their interactive behavior within the present experimental condition which should elevate photon emissions. Second, the coupling of specific temporally patterned magnetic fields with “quantum well” like point durations and a “single” wavelength might be employed as a carrier upon which more specific information could be coded that then penetrates into the cells and remains within their boundaries for at least an hour. This may be sufficient time to directly affect the molecular mechanisms that control cell proliferation and aberrance. Third, if the energy of the total photon “storage” and release simply reflect the magnetic energy from the applied field within the target volume, then experimental or clinical manipulation of these amplitudes might be employed to titrate the treatment effects.

3.5 References

1. House CR (1974) Water transport in cells and tissues. Edward Arnold Publishers, London.
2. Cifra M, Fields JZ, Farhadi A (2011) Electromagnetic cellular interactions. Prog Biophys Molec Biol 105: 223-246.
3. Del Giudice E, Preparata G (1994) Coherent dynamics in water as a possible explanation of biological membranes formation. J Biol Phys 20: 105-116.
4. Trushin MV (2004) Light-mediated "conversation" among microorganisms. Microbiol Res 159: 1-10.
5. Cosic I (1994) Macromolecular bioactivity: is it resonant interaction between macromolecules? Theory and applications. IEEE Trans Biomed Eng 41: 1101-114.
6. Dotta BT, Murugan NJ, Karbowski LM, Lafrenie RM, Persinger MA (2014) Shifting wavelengths of ultra weak photon emissions from dying melanoma cells: their chemical enhancement and blocking are predicted by Cosic's theory of resonant recognition model for macromolecules. Naturwissenschaften 101: 87-94.
7. Karbowski LM, Murugan NJ, Persinger MA (2015) Novel Cosic resonance (standing wave) solutions for components of the JAK-STAT cellular signaling pathway: a convergence of spectral density profiles. FEBS Open Bio 5:245-250.

8. Persinger MA, Murugan NJ, Karbowski LM (2015) Combined spectral resonances of signaling proteins's amino acids in the ERK-MAP pathway reflect unique patterns that predict peak photon emissions and universal energies. Int Lett Chem Phys Astron 4: 10-25.

9. Persinger MA, St-Pierre LS (2015) The physical bases to consciousness: implications of convergent quantifications. J Sys Integrat Neurosci 1(2): 55-64.

10. Murgan NJ, Dotta BT, Karbowski LM, Persinger MA (2014) Conspicuous bursts of photon emissions in malignant cell cultures following injections of morphine: implications for cancer treatment. Int J Cur Res 6:10588-10592.

11. Dotta BT, Lafrenie RM, Karbowski LM, Persinger MA (2014) Photon emissions from melanoma cells during brief stimulation by patterned magnetic fields: is the source coupled to rotational diffusion within the membrane? Gen Physiol Biophys 33: 63-73.

12. Pollack GH (2001) Cells, gels and the engines of life. Ebner and Sons, Seattle (Wash).

13. Chai B, Yoo H, Pollack GH (2009) Effect of radiant energy on near-surface water. J Phys Chem 113: 13953-13958.

14. Persinger MA (2015) Thixotropic phenomena in water: quantitative indicators of Casimir-magnetic transformations from vacuum oscillations (virtual particles). Entropy 17: 6200-6212.

15. Murugan NJ, Karbowsk LM, Dotta DT, Persinger MA (2015) Delayed shifts in pH responses to weak acids in spring water exposed to circularly rotating magnetic fields: a narrow band intensity-dependence. Int Res J Pure and App Chem 5: 131-139.

16. Murugan NJ, Karbowski LM, Lafrenie RM, Persinger MA (2015) Maintained exposure to spring water but not double distilled water in darkness and thixotropic conditions to weak (1 μT) temporally patterned magnetic fields shift photon spectroscopic wavelengths: effects of different shielding materials. J Biophys Chem 6: 14-28.

17. Decoursey TE (2003) Voltage-gated proton channels and other proton transfer pathways. Physiol Rev 83: 475-579.

18. Murugan NJ, Karbowski LM, Persinger MA (2014) Serial pH increments (20 to 40 milliseconds) in water during exposures to weak, physiologically patterned magnetic fields: implications for consciousness. Water 6: 45-60.

19. Fels D (2009) Cellular communication through light. PLoS One 4: e5086

20. Popp FA (1979) Photon storage in biological systems. In Popp FA, Becker, G., Konig HL, Pescha, AM (eds) Electromagnetic bioinformation. Urban and Schwarzenger, Munich, 123-149.

21. Karbowski LM, Harribance SL, Buckner CA, Mulligan BP, Koren SA, Lafrenie RM, Persinger MA (2012) Digitized quantitative electroencephalographic patterns applied as magnetic fields

inhibit melanoma cell proliferation in culture. Neurosci Lett 523: 131-134.

22. Koren SA, Bosarge WE, Persinger MA (2015) Magnetic fields generated by optical coupler circuits may also be containment loci for entanglement of P-N junction-plasma cell membrane photons within exposed living systems. Int Lett Chem Phys Astron 3: 84-105.

23. Buckner CA, Buckner AL, Koren SA, Persinger MA, Lafrenie RM (2015) Inhibition of cancer cell growth by exposures to time-varying electromagnetic fields involves T-type calcium channels. PLoS One DOI: 10.1371/journal.pone 0124136 (April 14, 2015).

24. Martin LJ, Koren SA, Persinger MA (2004) Thermal analgesic effects from weak, complex magnetic fields and pharmacological interactions. Pharm Biochem Behav 78: 217-277.

25. Thomas AW, Kavaliers M, Prato FS, Ossenkopp KP (1998) Antinociceptive effects of pulsed magnetic fields in the land snail. Neurosci Lett 222: 107-100.

26. Persinger MA, Koren SA (2007) A theory of neurophysics and quantum neuroscience: implications for brain function and the limits of consciousness. Int J Neurosci 117: 417-420.

27. Koren SA, Dotta BT, Persinger MA (2014) Experimental photon doubling as a possible local inference of the Hubble Parameter. Open Astron J 7:1-6.

28. Persinger MA, Cook LL, Koren SA (2000) Suppression of experimental allergic encephalomyelitis in rats by brief, hourly pulses of nanoTesla complex magnetic fields that simulate geomagnetic activity. Int J Neurosci 100: 107-116.

29. Murugan NJ, Karbowski LM, Lafrenie RM, Persinger MA (2013) Temporally-patterned magnetic fields induce complete fragmentation in planaria. PLoS One, on line.

30. Rose GM, Diamond DM, Pang K, Dunwidde TV (1988) Primed burst potentiation: lasting synaptic plasticity invoked by physiologically patterned stimulation. In Haas HL, Buzsaki G (eds) Synaptic plasticity in the hippocampus. Springer: Germany, pp. 96-98.

31. Mach QH, Persinger MA (2009) Behavioral changes with brief exposures to weak magnetic fields patterned to simulate long-term potentiation. Brain Res 1261: 45-53.

32. Dotta BT, Buckner CA, Cameron D, Lafrenie RM, Persinger MA (2011) Biophoton emission from cell cultures: biochemical evidence for the plasma membrane as the primary source. Gen Physiol Biophys 30: 301-309.

33. Karbowski LM, Murugan NJ, Persinger MA (2015) Experimentally-induced inhibition of growth in melanoma cell cultures separated by 2 kilometers when both share excess correlation magnetic fields: macroscopic evidence of free-space quantum teleportation? J Sig Inf Process 6: 39-48.

34. Scott MA, Rouleau N, Lehman BS, Tessaro WE, Juden-Kelly LM, Saroka KS, Persinger MA (2015) Experimental production of excess correlation across the Atlantic Ocean of right hemispheric theta-gamma power between subject pairs sharing circumcerebral rotating magnetic fields. J Cons Explor Res 6: 658-684.

35. Persinger MA, Lafrenie RM (2014) The cancer cell plasma membrane potentials as energetic equivalents to astrophysical properties. Int Lett Chem Phys Astron 17: 67-77.

36. Dotta BT, Persinger MA (2012) "Doubling" of local photon emissions when two simultaneously spatially separated chemiluminescent reactions share the same magnetic field configurations. J Biophys Chem 3, 72-80.

3.6 Preamble to Chapter 4: Release of Specific Frequency Bands as Evidence for Specific Information Transfer within the Electromagnetic Spectrum

Having identified a capacity for cells to store and emit patterned light, we decided to tackle a serious problem, which remains largely unsolved or, rather, insufficiently addressed. That is, we wanted to know if we could apply our findings to detect malignancies within early stages of growth, which would otherwise go undetected by convention methods. Our approach, if successful, would represent a potential detection method capable of identifying early malignancies within largely healthy cell populations. Essentially, we cultured malignant and non-malignant cells together within the same media and exposed the mixed cultures to the photomultiplier tube. We then spectral analyzed the data to reveal intrinsic frequency-dependent fluctuations of photon emissions. If malignant cells and non-malignant cells absorb and emit alternative patterns, frequencies, and amplitudes of light, we should be able to discriminate between them. Even more interesting would be the prospect of an interaction between the two types of cells.

Chapter Four

Only 1% Melanoma Proportion in Non-Malignant Cells Exacerbates Photon Emissions: Implications for Tumor Growth and Metastases

Published in International Journal of Cancer Research and Molecular Mechanisms (2015) – Vol: 1.2. Pg. 1-3

Lukasz M. Karbowski, Nirosha J. Murugan, Blake T. Dotta and Michael A. Persinger

Abstract

Aim: Discern if there is a specific proportion of mixture of normal and malignant cells that increase photon emissions from cell cultures.

Method: Different proportions of B16-B6 mouse melanoma cells and Hek 293T cells were mixed and allowed to proliferate. Photon emissions were measured from the different mixtures of cells by digital photomultiplier units and then analyzed for Spectral Power Density (SPD).

Results: Mixtures of the malignant and non-malignant cells that were more than 10% of one component displayed photon emission flux densities that were significantly less than the photon emissions for either cell type when measured as pure samples. Only 1% proportion of the malignant cell in 99% of non-malignant cells produced the strongest photon emissions. Spectral density profiles of power flux density variations indicated elevated power around 22 Hz that was even greater than this signature for malignant cells only.

Conclusion: Only 1% of malignant cells in a normal aggregate, representative of the early stages of cancer development, resulted in conspicuously increased numbers of photon emissions and spectral power spectra that often reflect a total malignant cell population. This combination of photon flux density and spectra power profiles may be a potentially useful

(nanotechnology) tool to detect the minute changes in cell activities relevant to oncology.

4.1 Introduction

All living organisms emit photons [1,2]. Several authors [1,3,4] have shown that the emissions of ultraweak photons from basic biological units such as cells and bacteria may convey the essential "information" or "communication" patterns between these units. The temporal patterns within amplitude fluctuations of photon emissions may serve as the "code" or "key", involving very little energy, that determines the activation of the massive molecular components which progress through pathways that contain their own energies. From this perspective the ultraweak photon patterns between cells would initiate intracellular process but likely not affect them once they have been activated unless the light patterns are coherent with more energetic sources such as pattern-synchronized magnetic fields [5].

That the molecular pathways themselves are strongly correlated with dominant frequencies between the ultraviolet through the visible to the near infrared range has been shown by Dotta et al [6]. They found that during the ~ 20 hr after melanoma cells had been removed from incubation the peak wavelengths of emitted photons changed from infrared to ultraviolet which reflected the shifts from the initial activation of signaling molecules (near-IR) to growth and protein-structure factors (near-UV). The specific wavelength that was emitted from the corresponding molecular pathways was

predicted by Cosic's Molecular Resonance Recognition equation [7,8]. Filters with narrow transparencies of about 10 nm increments for photon emissions over the PMT aperture were employed to verify Cosic's model. Photon emissions within predicted wavelengths were either blocked or enhanced by the addition of pharmacological compounds that either inhibited or facilitated specific pathways.

Although there have been recent concerns about intrinsic contamination of cell lines [9], most cell culture experiments focus upon a single cell line. Within the organism and its organs there are multiple cell types existing simultaneously and proximally. The intrusion of malignant cells into a population would begin with one or a few cells. Here we present experimental results that when malignant and non-malignant cell lines are mixed in different proportions markedly elevated photon emissions occurred when the malignant cell was only 1% of the other cell line's population but not when the ratios were higher.

4.2 Methods

Mouse melanoma cells (B16-B6) and HEKs cells were split from confluent populations according to our usual procedures [10]. They were combined into volumes of 10 mL in 50 mL centrifuge tubes according to the following proportions: 100% B16; 100% HEK; 90% B16, 10% HEK; 50% B16, 50% HEK; 95% B16, 5% HEK; 90% B16, 10%

HEK; 90% HEK, 10% B16; 95% HEK, 5% B16; 99% HEK, 1% B16. There were 6 replications per group for a total of 48 preparations (and measurements).

The cells were re-suspended with 5 cc of additional media; 2.5 mL from a given source were placed on tissue dishes (55 mm diameter) and allowed to adhere for 24 hr to achieve 90% confluence. The plate was then placed over the aperture of digital photomultiplier unit (PMT). The PMT was a SENS-TECH, Ltd, DM0089C model (370 to 680 nm band) with dark counts of less than < 40 photons per second. The numbers of photon counts per 20 ms were obtained for 100 s (5000 samples). All measurements with the PMT were completed within the incubators that were hyper-dark and at standard temperature (37° C). We employed the same sampling and measurement procedure utilized for measuring photon emissions from whole mice with and without tumors or from homogeneous malignant or non-malignant cells lines [11].

Spectral Power Densities (SPD) were obtained by SPSS-16 PC software using methods described previously [12]. The sampling rate was 50 Hz (20 ms bins) due to the limits of the software and the sampling time was 100 s. The Nyquist limit was 25 Hz, that is, this sampling procedure allowed discernment of amplitude variation frequencies > 0 Hz to 25.0 Hz.

4.3 Results

Figure 1 shows the means and standard deviations for the numbers of photons per 20 ms from the various mixtures of cell cultures. The values are based upon 6 replications per condition. The B represents the B16 cells and the H refers to HEK cells. The number refers to the proportion or percentage of each type of cell. When the proportions of malignant and non-malignant cells were equal or there were 10% malignant cells in 90% normal cells or 10% normal cells in 90% malignant cells the photon emissions were lowest. These photon emissions were significantly less than the values when only B16 or HEK cells were homogenous (100%). The strongest photon emissions occurred when the non-malignant (99%) line contained only 1% of malignant cells.

The results of the spectral analyses are shown in Figure 2. The critical spectral power density (SPD) is the 22 Hz amplitude band. This peak has discriminated between different strains of human and animal malignant cell lines and non-malignant cells. It was significantly elevated for the mixed populations within the highest disproportions of cells. Although the elevation of the 22 Hz band SPD for 100% B16 cells compared to 100% HEK cells was expected, the power density was more than doubled in the mixtures where the B16 cells were composed 1% to 10% of the population. When the proportions of the two cell lines were equal or if 10% of the population was composed of HEK cells (90% melanoma) the

density values did not differ significantly from a homogeneous population of normal cells.

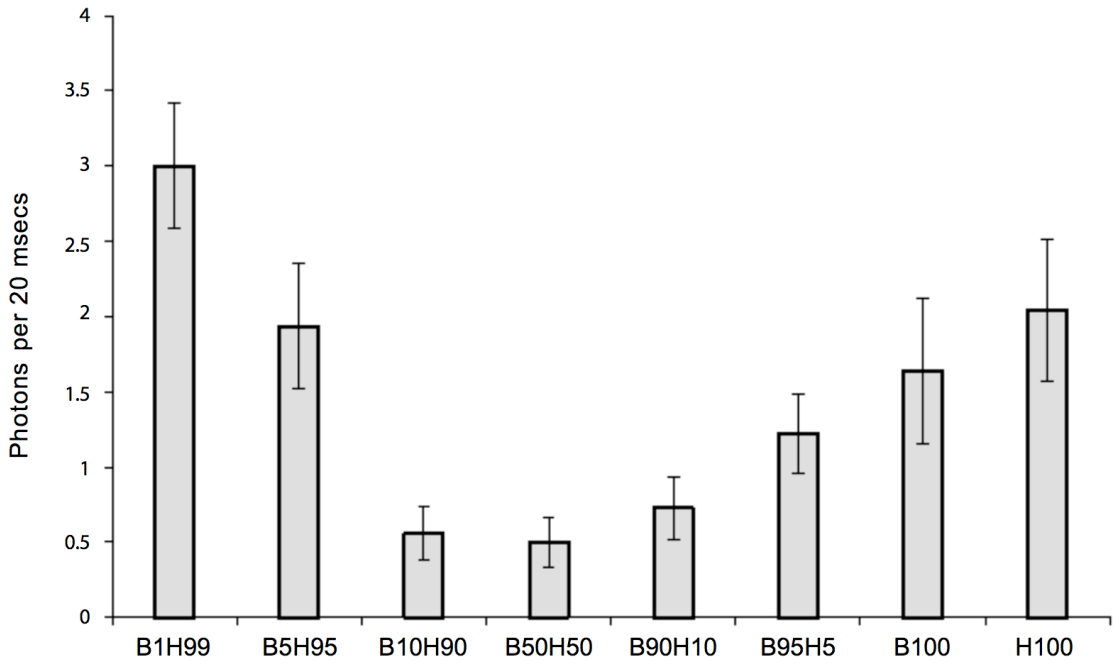

Figure 1. Numbers of photons per 20 ms as a function of the proportion of cell line mixtures were B is B16 (malignant) cells and H is HEK (non-malignant) cells. B100 and H100 refer to homogeneous populations of each type of cell. Vertical lines indicate standard deviations.

4.4 Discussion

To our knowledge this is the first experimental demonstration that different proportions of mixtures of cells, more typical of tissue, produce different radiant flux densities of photon emissions. Equal proportions of two lines, one

malignant, one not-malignant, or mixtures when there was 10%:90% proportions emitted about one-third of the photon power density from dishes that contained

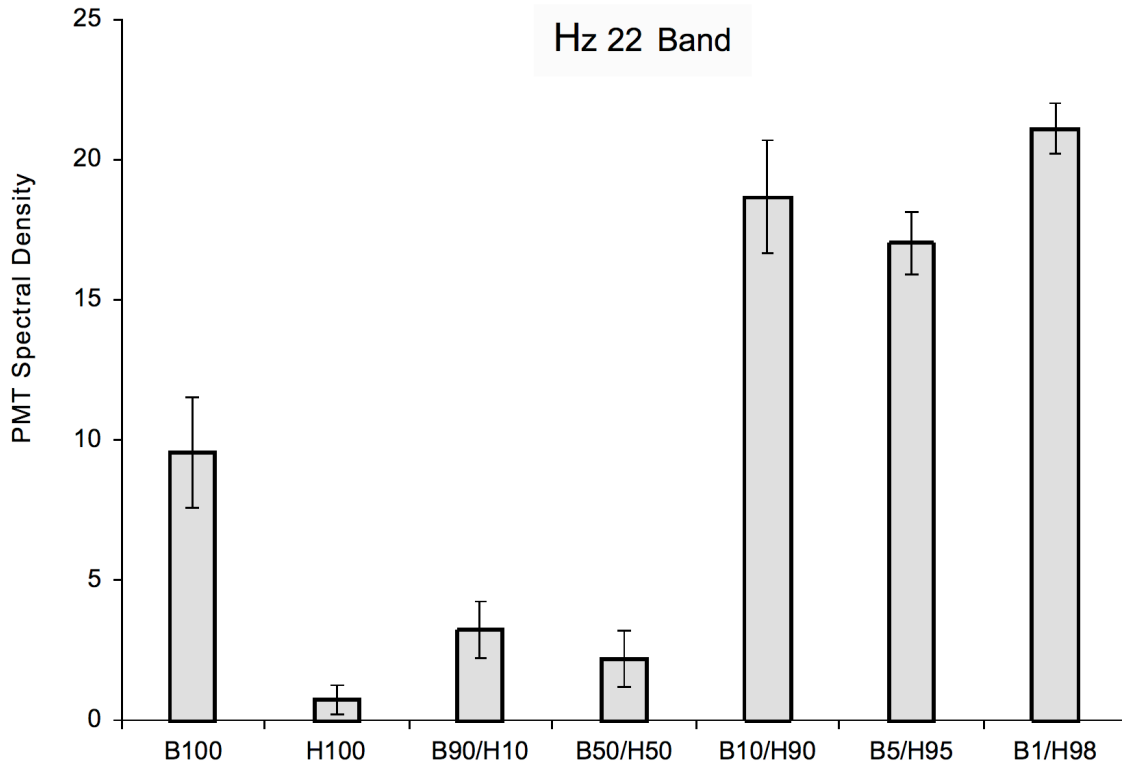

Figure 2. Relative units of Spectral Power Density (vertical axis) for photon emissions for the amplitude enhanced at the 22 Hz band as a function of the various combinations of malignant and non-malignant cells. Vertical lines refer to standard deviations.

100% of either of the cells. This suggests that once the proportion of one cell line is 10% or more within the aggregate

the photon emissions diminish significantly. In other experiments involving adjacent plates of microtubule preparations [13] such decreases in photon emissions have strongly suggested enhanced exchange of photons between the two preparations of microtubules. If this process was occurring here, then once the proportion of the other cell exceeds 10% the numbers of photons emitted into the general environment decreases and more of the photon emissions would remain intercellular. This would be consistent with intra-unit "communication" roles of photons proposed by Fels [3] and Trushin [4]. However it may also indicate a non-specific decrease of the processes that generate the intercellular photon emissions.

By far the most novel and potentially important result from the perspective of "metastasis" processes was the marked elevation of photon emissions when only 1% of the non-malignant cell population contained malignant cells. This enhanced photon density was about double the values of the homogeneous populations and 6 times the power for different proportions of the cells. The functional power flux density from the 1% contamination would be equivalent to (assuming $5 \cdot 10^{-19}$ J per photon and 50, 20 ms increments per s) $7.5 \cdot 10^{-17}$ W. Because the aperture was about 2 cm^2, the power density would be about $0.4 \cdot 10^{-12}$ $W \cdot m^{-2}$. If the spherical radiation of the photons is accommodated the actual power density would be around $2.5 \cdot 10^{-12}$

$W \cdot m^{-2}$. This is within the range of power density emitted by malignant cells lines that have been "distressed" by removal from 37°C incubation and maintained at room temperature [11]. On the other hand the typical background would be close to $2.5 \cdot 10^{-13}$ $W \cdot m^{-2}$ which is within the range of background cosmic radiation at sea level.

This increase in photon emission from the 1% "contamination" would also be within the range of the spikes of photon emissions recorded from melanoma cells following injections of therapeutic dosages of morphine [14]. Morphine compounds have been associated with metastases [15]. One interpretation of our results is that the initial intrusion of the malignant cell into a normal cell environment is associated with marked increases in photon emissions that could serve as stimuli for other cells to respond, like an "alarm". Alternatively the photon emissions may reflect information that would contribute to the migration of other malignant cells into the location or to the transformation of parenchymal cells into malignant forms. De-differentiation of cell types into those with malignant potential may be more frequent than suspected. If photons are involved with the mediation of "information" one would expect subsets or classes of "communications" that could facilitate a range of functions that include (metaphorically) "alarm", "cooperation" or even "submission" to the cellular context.

From a diagnostic perspective the spectral power densities are revealing. Although the amounts of photons have been considered the essential measurement for discerning the presence of tumors [16], our analyses here and in others contexts [12] indicate that the spectral power density within the extremely low frequency range has greater differentiating potential. In the present study the classic power fluctuation frequency (22 Hz) in cancer cell lines we have noted frequently during photon measurements was doubled in the normal cells with 1%, 5% and 10% mixtures of melanoma cells. When the value reached 50%-50%, this "abnormal" pattern was not observed. The source of the 22 Hz enhancement must still be isolated. For example, as suggested by reviewers, comparisons of the results from an immunocytochemical stain for S-100 protein Ab for the co-culture of 1% B16 cells mixed with 99% HEK cells and the 50%-50% combination at the 24-hr point after passage could discern relative plating of B16 cells. Consequently the association between viable (plating) of B16 cells and the SPD amplitudes of the 22 Hz peak could be determined. However even without such differentiation, the results support our suggestion that these profiles of photons might be developed to discern *very early* tumor growth or malignancy before it is even apparent by more traditional methods of imagining and identification when the tumor is very large and more difficult to treat.

4.5 Summary at a Glance

Different proportions of mixtures of cell lines, in this case a malignant and non-malignant cell type, emitted statistically significant different numbers of photons. Only 1% "contamination" of the normal cell line by the malignant cell generated marked increase in photon emissions from the aggregate of cells. The Spectral Power Density (SPD) profiles were similar but stronger than those from aggregates of homogeneous (100%) malignant cells. Photon (irradiant) flux density and SPDs in combination might be employed to discern the first stages of infiltration or development of malignancy into healthy organs.

4.6 References

1. Popp FA (1979) Photon storage in biological systems. In Popp FA, Becker G, Konig HL, Pescha (eds) Electromagnetic bioinformation. Urban and Schwarzenger, Munich, pp. 123-149.

2. Gurwitsch AA (1988) A historical review of the problem of mitogenetic radiation. Experientia 44: 545-549.

3. Fels D (2009) Cellular communication through light. PLOS ONE 4(4): e5086.

4. Trushin MV (2004) Light-mediated 'conversation' among microorganisms. Microbiol Res 159: 1-10.

5. Murugan NJ, Karbowski LM, Persinger MA (2015) Synergistic interactions between temporal coupling of complex light and magnetic pulses upon melanoma cell proliferation and planarian regeneration (in submission).

6. Dotta BT, Murugan NJ, Karbowski LM, Lafrenie RM, Persinger MA (2014) Shifting wavelengths of ultraweak photon emissions from dying melanoma cells: their chemical enhancement and blocking are predicted by Cosic' theory of resonant recognition model for macromolecules. Naturwissechaften 101: 87-94.

7. Cosic I (1994) Macromolecular bioactivity: is it resonant interaction between macromolecules? Theory and applications. IEEE Trans Biomed Engin 41: 1101-1114.

8. Karbowski LM, Murugan NJ, Persinger MA (2015) Novel Cosic resonance (standing wave) solutions for components of the JAK-STAT cellular signaling pathway: convergence of spectral density profiles. FEBS Open 5: 245-250.

9. Neimark J (2015) Line of attack. Science 347: 938-939.

10. Murugan NM, Karbowski LM, Persinger MA (2014) Weak burst-firing magnetic fields that produce analgesia equivalent to morphine do not initiate activation of proliferation pathways in human breast cells in culture. Integ Can Sci Theapeautics 1(3): 47-50.

11. Dotta BT, Buckner CA, Cameron D, Lafrenie RM, Persinger MA (2011) Biophoton emissions from cell cultures: biochemical evidence for the plasma membrane as the primary source. Gen Physiol Biophys 30: 301-309.

12. Dotta BT, Vares DEA, Buckner CA, Lafrenie RM, Persinger MA (2014) Magnetic field configurations that evoke long term potentiation shift power spectra of light emissions from microtubules from non-neural cells. Open J Biophys 4, 112-118.

13. Vares DAE, Dotta BT, Persinger MA (2015) Experimental demonstration of "communication" of magnetic field exposure from photon exchanges between two plates of microtubule preparations (in submission).

14. Murugan NJ, Dotta BT, Karbowski LM, Persinger MA (2014) Conspicuous bursts of photon emissions in malignant cell cultures following injections of morphine: implications for cancer treatment. Int J Cur Res 6: 10588-10592.

15. Ishikawa M, Tanno K, Kamo A, Takayanagi Y, Sasaki K (1993) Enhancement of tumor growth by morphine and its possible mechanism in mice. Biol Pharm Bull 16: 726-766.

16. Takeda M, Tanno Y, Kobayashi M, Usa M, Ohuchi N, Satomi S, Inaba H (1998) A novel method of assessing carcinoma cell proliferation by biophoton emission. Can Let 127: 155-160.

4.7 Preamble to Chapter 5: Theoretical Approaches for Discerning Information as Electromagnetic Energy

That photon emission frequencies display biologically relevant information content, differentiating malignant and non-malignant cell types as well as interactions between mixed cultures, suggests a molecular basis or epiphenomenon. Just as signals within molecular pathways can be traced from some starting point to some end point, so too should their intrinsic photonic representations be associated with analogous pathways of equivalent complexity. We employed Cosic's resonant recognition model to predict the resonant energy between interacting molecules. Our approach served to validate the concept that proteins and their associated polypeptide chains, composed of sequences of molecules some of which express intrinsic charges, are associated with intrinsic resonant frequencies which can be targeted by applications of light or electromagnetic fields – circumventing the requirement that a particular signalling molecule be present at a particular point in the pathway. Before experimentally applying light or electromagnetic fields, the aim was to quantify the resonant frequencies of the common JAK-STAT pathway according to Cosic's algorithm and determine if these theoretical values overlap with empirical measurements.

Chapter Five

Novel Cosic Resonance ("Standing Wave") Solutions for Components of the JAK-STAT Cellular Signaling Pathway: A Convergence of Spectral Density Profiles

Published in FEBS OpenBio (2015) – Vol: 5. Pg. 245-250

Lukasz M. Karbowski, Nirosha J. Murugan and Michael A. Persinger

Abstract

Cosic discovered that spectral analyses of a protein sequence after each constituent amino acid had been transformed into an appropriate pseudopotential predicted a resonant energy between interacting molecules. Several experimental studies have verified the predicted peak wavelength of photons within the visible or near-visible light band for specific molecules. This concept was applied to a classic signaling pathway, JAK-STAT, traditionally composed of nine sequential protein interactions. The weighted linear average of the spectral power density (SPD) profiles of each of the eight "precursor" proteins displayed remarkable congruence with the SPD profile of the terminal molecule (CASP-9) in the pathway. These results suggest that classic and complex signaling pathways in cells can also be expressed as combinations of resonance energies.

5.1 Letter

In contemporary cellular chemistry the mechanisms by which changes within an outer boundary (the plasma cell membrane) and an inner boundary (the nucleus) intercalate have been based upon a serial causality [1]. The operational model is that in order to satisfy the conditions for locality successive activations of different proteins mediate the changes along the surface of the plasma cell membrane to the nucleus that then initiates and effectively controls the ultimate structures and functions of the cell. The fundamental presumption is that the structural or spatial patterns of the molecule determine its interactions and its functions. This approach is a classic example of the particulate or matter-based description of cell function. However there may be an equally valid energy-based process [2] involving the correlative spatial resonance [3] and resulting spectral power density (SPD) of the specific properties of the units of molecules. The approach allows the potential inclusion of energy-based processes that are dependent upon the sequential units of molecular structure. The comparison would be analogous to de Broglie's matter waves which assumed that a sequence of particles could also be expressed as a pattern of waves. Here we present evidence that the JAK (Janus Kinase)-STAT (Signal Transducer and Activator of Transcription) pathway, one of the classic signaling pathways within the cell whose final component affects the

nucleus, can be described as a resonance pattern that is composed of the spectral characteristics of the pathway that converge at the nuclear interface as CASP-9. The protein interactions can be considered a transfer of resonant energy between interacting molecules through an oscillating physical field that could be expressed within the domain of classic photons.

While investigating a persistent anomaly that some complex molecular structures with quite different geometries displayed similar functional characteristics Irena Cosic [3,4] developed the Resonance Recognition Model (RRM). Spectral analyses (Fast Fourier Transform) are usually applied to temporal phenomena in order to discern the power densities of specific intervals of frequencies or periodicities. Cosic applied the concept to spatial sequences. She equated each amino acid with a value that was employed as an inference of the pseudopotential of the de-localized electrons. They are electrons whose orbits exceed distances of the individual atom (over several adjacent atoms) or molecule that define the unit entity of a composite structure. De-localized electrons from a particular amino acid were assumed to determine the major component of the electronic distribution of the entire protein. The energy of the delocalized electrons had been calculated as the pseudopotential of electron-ion interaction (EIIP) of each amino acid residue. These serial numerical values for each amino acid represented the distribution

of free electron energies along the protein molecule. When spectral analyzed the intrinsic spatial frequency with the most power was employed to predict the molecule's primary photon emissions. Cosic's concept is that "each specific biological function within the protein or DNA is characterized by one frequency".

Several of our experiments and quantifications [5,6,7,8] have supported Cosic's concept. We had demonstrated that during the hours after melanoma cells were removed from standard incubation temperatures and remained at room temperature (21°C-23°C) reliable and conspicuous shifts in the dominant frequency of the visible photon emissions were measured by digital photomultiplier units. The power density shifts between 400 and 800 nm were discerned by employing appropriate filters. The potential coupling between Cosic's predictions of photon frequencies based upon the spectral analysis of the delocalized electron values for the serial amino acids composing a protein were verified to a resolution of 10 nm (the limits of a filter). Compounds which are known to inhibit components of cell signaling and proliferation for a specific photon emission frequency as predicted by Cosic diminished the radiant flux density photon emissions while compounds that facilitate the specific components increased the radiant flux density of photon emissions.

The validity of the Cosic model can also be seen with molecules defined by simpler structures. For example bovine albumin is a protein that contains 607 amino acids. The calculated wavelength from the Cosic Resonant Recognition Model for this molecule is ~380 nm. The average of a triplicate of experiments where 4 g of albumin had been placed in 50 mL of PBS (phosphate buffered saline) and measured for photon emissions confirmed this prediction. This was completed by placing 1.5 cc of this solution in a quartz cuvette and then measuring fluorescent counts by a RSM-OLIS spectroflourometer. Figure 1 shows the fluorescent counts for the solvent only and the counts for the same solvent containing the albumin. The major peak of spectral power displayed by the albumin (red arrow) was about 385 nm. This is well within measurement error of the peak predicted by the RRM. The Cosic procedure assumes a linear sequence of amino acids. One would expect smaller modulating contribution from higher order, non-linear spatial configurations. The sources of the smaller peaks have not been established clearly. However our preliminary experiments and quantitative analyses suggested they could indeed reflect the second and higher order conformational features of the molecule’s geometry.

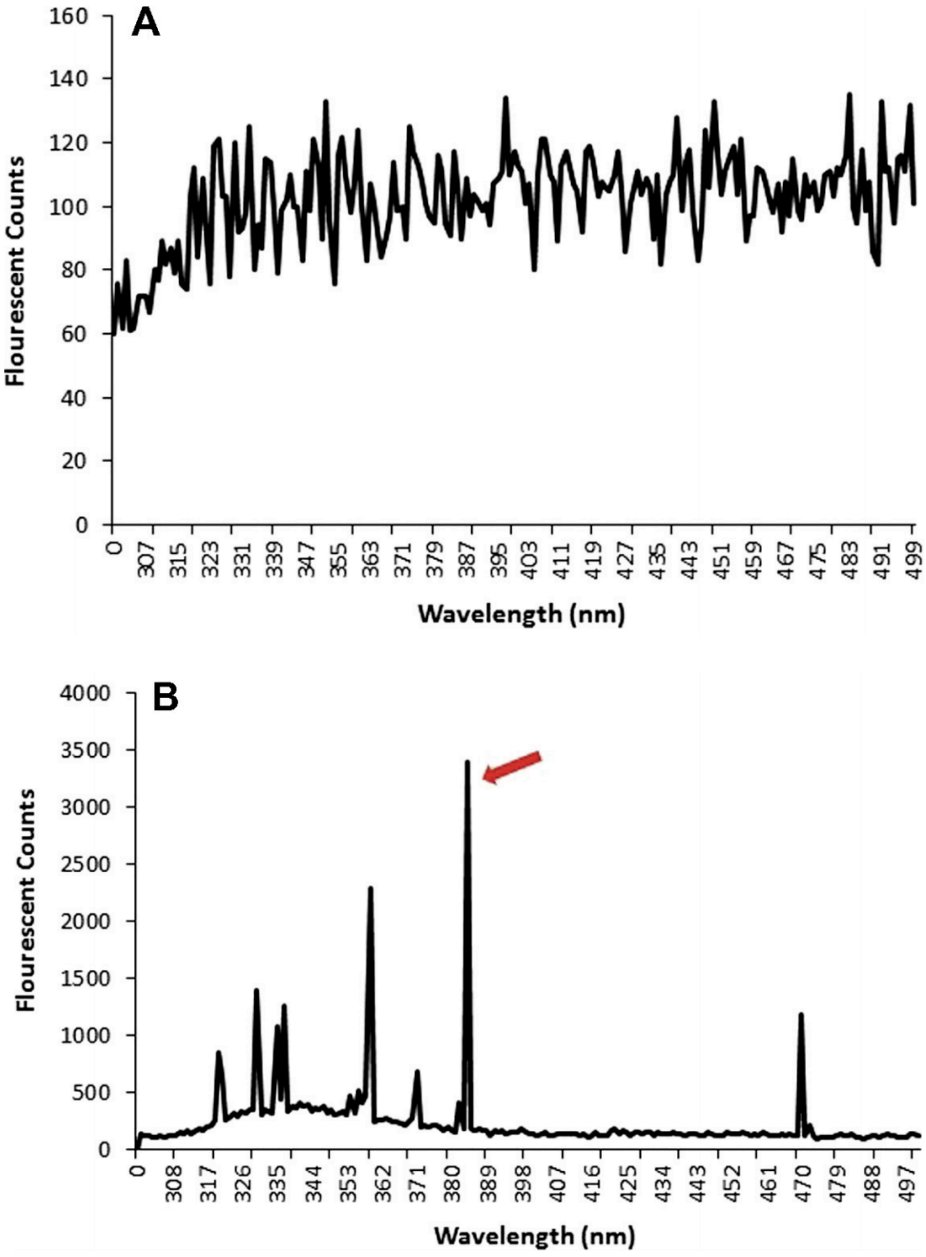

Figure 1. Fluorescence (photon) counts for the medium (left) and the medium containing bovine albumin (right). The red arrow refers to the peak wavelength in nm predicted by Cosic's Recognition Resonance Model.

The question we then addressed is whether or not the RRM would reveal new relationships that are represented as periodicities of spatial power densities in different molecular structures that have been shown to be intercalated by serial interactions that define a "pathway". In other words could an entire "signaling" pathway be characterized by a "single spectral pattern" in a manner similar to Cosic's concept that *each biological function of a protein is characterized by one frequency*. To date the RRM has been applied to single unit phenomenon such as a specific molecule. Although a traditional particulate approach to bioorganic chemistry would first invoke the successive transmission of minute structural changes mediated by a particular quantity of energy in different molecules, the operation of resonance predicts that the spatial spectral densities of the de-localized electrons of the components of a pathway should converge at the final "step".

The JAK (Janus kinase) –STAT (Signal Transducer and Activator of Transcription) signaling pathway has been considered a primary source of "information" from chemical stimuli external to the cell boundary to the promoters of gene expression from the DNA within the nucleus. The sequential steps presently understood for this pathway include: Il2, Il6, Jak1, Tyk2, cSRC, STAT3, STAT5, BCLxl and CASP-9. The full names of these acronyms can be found elsewhere [1]. The JAK-STAT pathway has remained

relatively stable as inferred by evolutionary analysis from the original persistent life forms (green algae) that first emerged about 3 billion years ago to present day mammals. Disruption of this pathway has been correlated with various malignant cell disorders and disrupted immune functions.

To test the hypothesis that the combined spectral power densities of the delocalized electron values for each of the mediating proteins between the cell surface and nuclear interface in the JAK-STAT pathway would converge to reflect the SPD profile of the molecule (CASP-9) directly influencing the nucleus, the Cosic procedure was applied to each molecule. This was completed by substituting each amino acid in the molecule by the appropriate pseudopotential calculated by Cosic. Because simultaneous spectral analysis for the program we employed (Spectra, SPSS-16) required equal length of cases, the pseudopotential values for each protein that was shorter than the longest protein were continued so that all molecules displayed equal cases.

To discern an optimal range for the numerical frequency associated with the spectral analyses the estimated width of amino acid was assumed to be 0.35 nm. It was divided by the numerical frequency. We selected ≤ 0.80 nm for this "functional" wavelength for convenience and for aesthetic reasons. It would be approximately πd of the average of width (d) of the median width

of critical bond distances such as covalent and ionic bonds that constitute hydrogen bonds. Although perhaps spurious, this cutoff value demonstrated the most robust effect. It included the actual range (numerical frequency) from the spectral analysis of between 0.438 and 0.500. If one assumed Cosic's value for a residual amino acid width of 0.38 nm, the numerical frequency would not change.

The results are shown in Figure 2. The spectral power density values (n=73, Δf=0.001) between 0.70 and 0.80 nm (numerical frequency 0.500 to 0.438) for each of the 9 components of the JAK-STAT pathway reflect the differences of the resonance characteristics of these molecules. Expanding inclusion of numerical frequencies up to and including the entire range of SPDs (n=584) did not demonstrate this powerful relationship. In fact the effect size diminished progressively. The degree of convergence between the first molecule, Interleukin 2, within the outer boundary (the plasma cell membrane) and the nucleus (CASP-9) is not obvious. Even serially adjacent proteins in the pathway do not appear to share any similarity of spectral power densities.

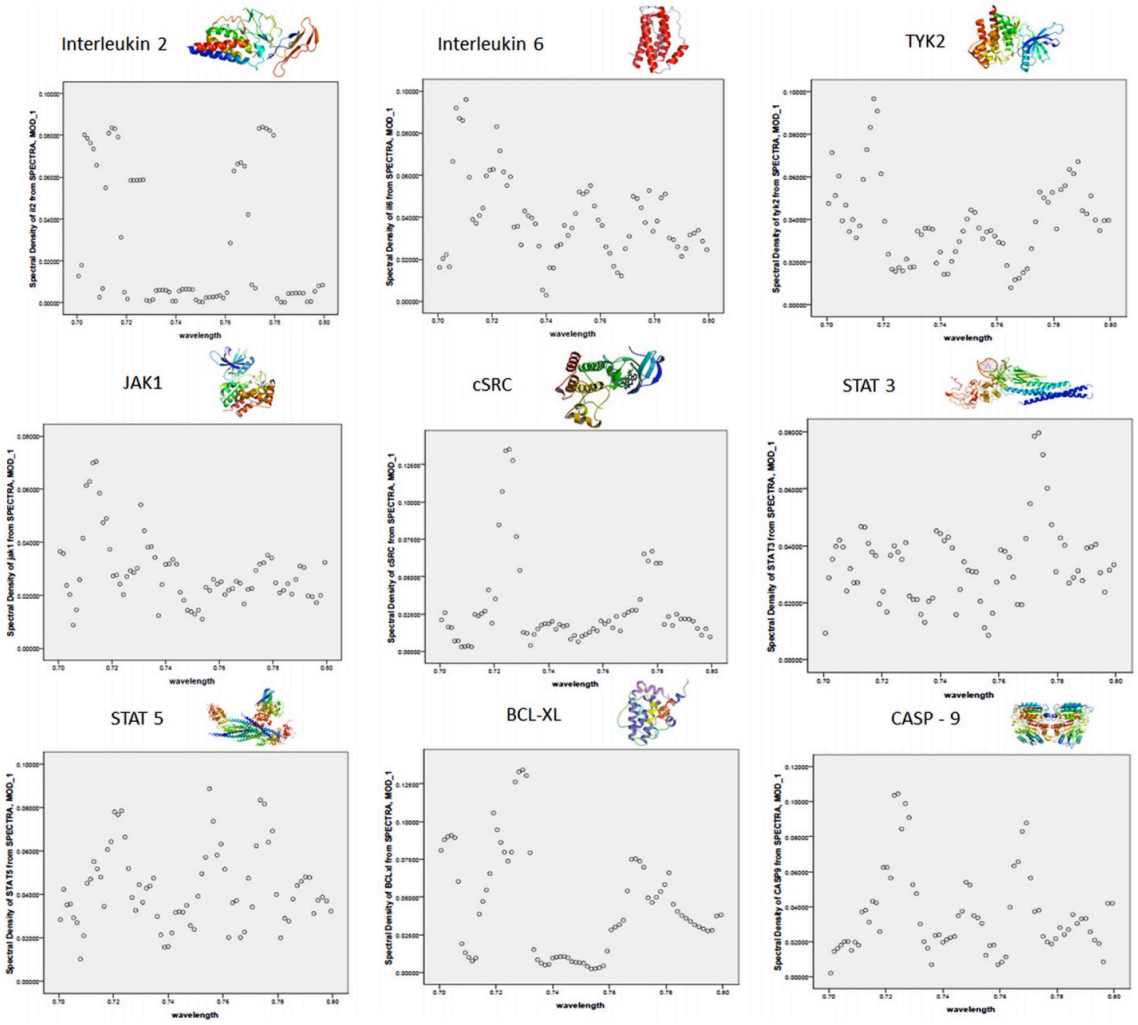

Figure 2. Stylized shapes and descriptions of the proteins composing the JAK-STAT pathway (on top) and the distribution of Spectral Power Densities predicted by the Cosic Method for each protein between interleukin 2 (on the receptor) and CASP-9 at the end of the pathway.

However when the spectral profiles of the 8 precursor proteins before CASP-9 were averaged, the results were more compelling. Multiple regression analyses, which removed redundant variance indicated that 50% of the variance in the spectral profile of CASP-9 [$F(3,69)=23.71$, $p < .001$] could be predicted by the linear combination of the spectral densities (unstandardized partial regression coefficients or slopes in parentheses) of cSRC (0.347), tyk2 (-0.350), and BCLxl (0.18) with a constant of 0.3. Figure 3 shows the distribution of the predicted values over the base frequency units that were employed by Cosic for single molelcules. These units, which are required for the calculation of potential photon wavelength, are the raw spectral frequency values form the Fast-Fourier Transform without correction for absolute values of the units.

The conspicuous congruence between the values predicted by the equation from the weighted linear combination of the spectral densities of the three precursors and the raw spectral density for CASP-9 is shown in Figure 4. The blue dots refer to the raw CASP-9 values and the green dots refer to the predicted values. Lag/lead analyses of the 73 cases (Δfs) for $\leq$0.8 nm (or numerical frequency $\geq$ 0.438) for the SPDs for each molecule, that is, including the unit shifts in SPD in the regression equation for the 8 precursor variables to a maximum of ±3 spectral units (Δfs) with maximum steps=7 (to accommodate sample size), increased the

strength of the association to 0.90 [F(7,65)=39.58, p <.001]. All precursors except Interleukin 6 and Tyk2 entered the equation. Only cSRC entered the equation twice (no lag/lead and a lead by 3 units). The overlaps between the actual SPD profile for CASP-9 and the predicted SPD profile based upon the weighted averages of the spectral densities approached an identity (Figure 5) if one assumes the classic statistical measurement error of ~10%.

The results indicated that the linear combination (or "weighted" average) of the SPD profiles based upon the serial values of the pseudopotential of each amino acid in each protein in the pathway reflect the SPD profile of the final molecule in the pathway. In other words the combination of the constituents along the pathway "averages" or "combines" to produce the final pattern that presumably would affect the nucleus. These results suggest that a specific signaling pathway could be described by their combined spectral patterns such that an aggregate pattern would reflect the entire pathway.

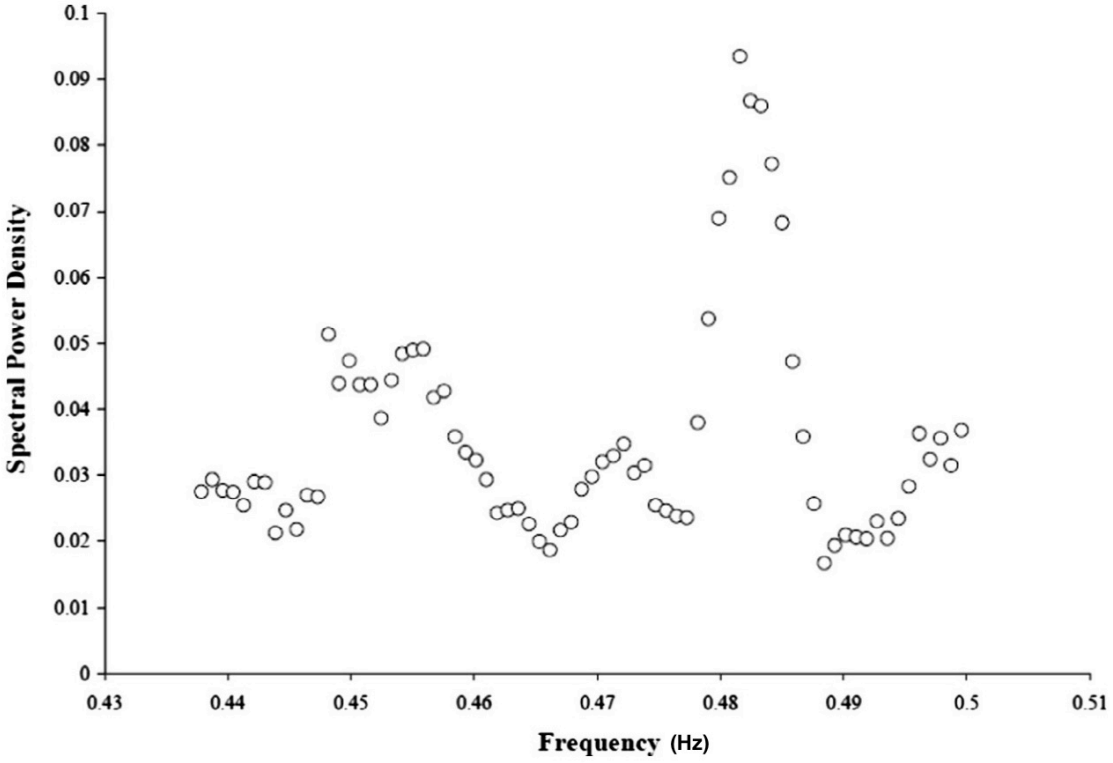

Figure 3. Predicted Spectral Density Profile for CASP-9 based upon the optimal combination of SPDs as a function of numerical frequency according to multiple regression analyses of the antecedent proteins in the JAK-STAT pathway.

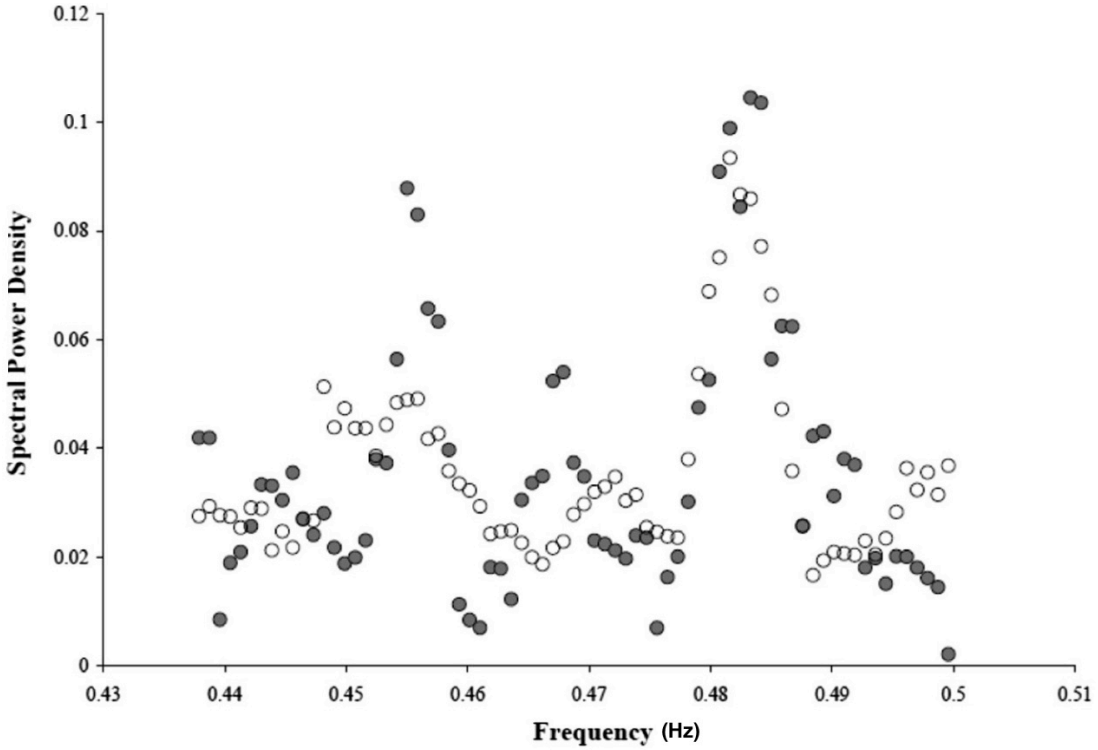

Figure 4. Congruence of distribution of Spectral Power Densities profiles for pseudopotentials for composite amino acids as a function of numerical frequency for CASP-9 (closed circles) and that predicted (open circles) by the composite SPDs of precursor proteins in the pathway.

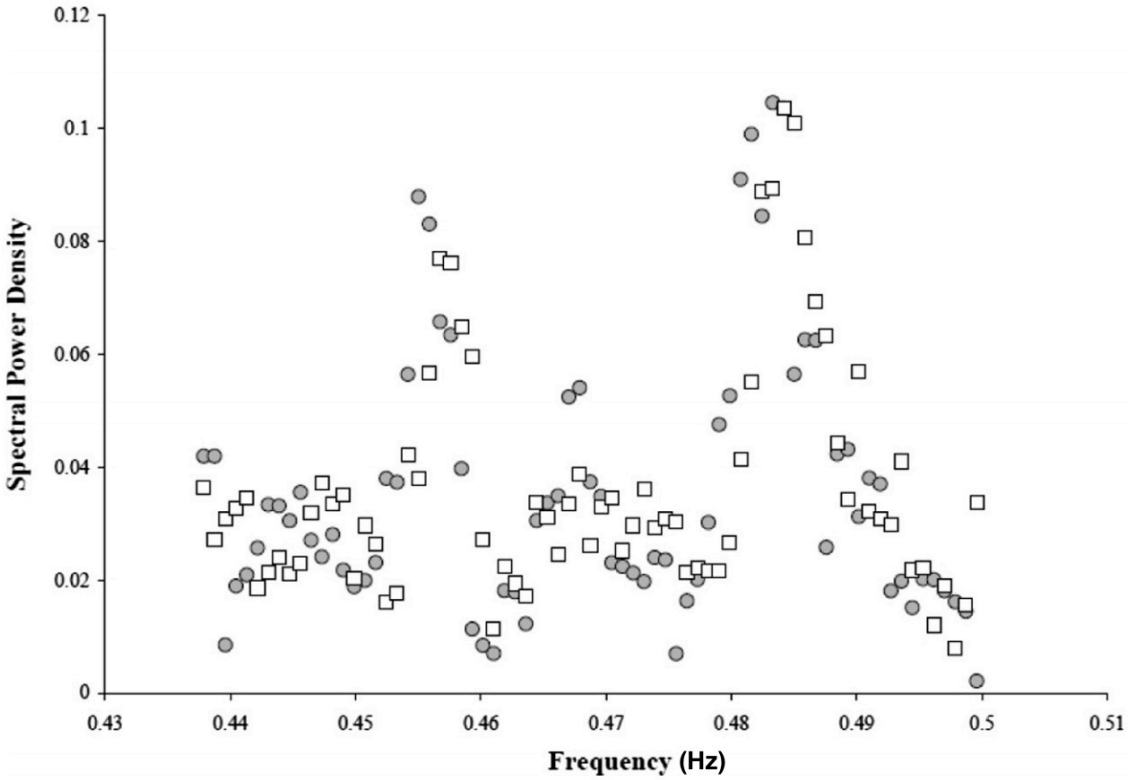

Figure 5. Maximum congruence of SPD profiles for CASP-9 (closed circles) and that predicted (open squares) by the most optimal combination of ±3 Δf shifts in numerical frequency of SPDs for precursor proteins in the JAK-STAT pathway.

There are several potentially important implications of these results. First, what may be equally as important as molecular structure in the mediation of information from location A (the external boundary) to location B (the nucleus, an inner boundary) is the resonant pattern of the molecule. Second, the importance of the resonant pattern of SPD of the amino acid sequence of the protein indicates that there could be potential substitution of "carrier" molecules. From this perspective the persistence of the "same" and reliable protein in a pathway might only reflect the *prominence* (molarity or activity) of that molecular species in the typical cell rather than the uniqueness of a particular molecule. The critical feature may the correlative quantity of energy [2]. This approach would mean that in other cell systems, such as malignant lines and cancers where different molecules might be dominant because of a different metabolism, other proteins with similar resonance patterns could mediate the serial reactions. Such "stimulus substitution" would be relevant to pharmacological or chemical strategies that target the molecular component of these pathways. This traditional approach attempts to simulate structural similarities at the interface of molecular interactions rather than the similarities of the system's resonance.

Perhaps the most significant result of these analyses is the suggestion of three peaks (two major) of SPDs that could define

or at least alternatively represent the resonance pattern of the pathway. According to Cosic's solution, which divides the constant 201 by the peak numerical frequencies in Figure 5, the maxima for photon flux densities should cluster around the wavelengths of 441, 430 and 416 nm. When the frequencies for these wavelengths were calculated and multiplied by Planck's constant ($6.626 \cdot 10^{-34}$ J·s) the differences between the first two was $1 \cdot 10^{-20}$ J and between the second and third wavelength was $1.6 \cdot 10^{-20}$ J. This is within the range of the energies associated with hydrogen bonds (0.04 to 0.3 eV, 0.7 to $2.2 \cdot 10^{-20}$ J). It may not be spurious that the equivalent wavelength for this increment of energy is 10 µm, the typical width of the prototypical cell which is also the median solution for the wavelength at physiological temperatures according to Wein's law (0.29 cm·deg/°K) [2].

This particular quantity of energy may be a fundamental "unit" [2] for a variety of cellular mechanisms that include the action potential of axons, the binding of ligands to receptors and the energy per molecule for intracellular processes. It is also the energy produced by electric forces over the average distance between potassium ions forming the single layer of ions that have been attributed historically to the source of the resting membrane potential for the classical cell plasma membrane [2]. The importance of this increment of energy in cell processes

has been shown by direct experimentation with cells [9] and human brain activity [10,11].

This value is also within the range of the protons in the second shell hydrogen bonds, according to Decoursey [11], and is consistent with empirical measurement of the mobility of protons. The role of protons within the hydronium ions of water, which determines pH and hence the rate and even occurrence of many enzymatic and proteinacious reactions, may have been underestimated in many conceptions of signaling pathways. Proton channels are copiously represented within plasma membranes and may be essential for accommodating the proton accumulation associated with normal metabolism.

5.2 References

[1] Albert, B., Johnson, A., Lewis, J., Raff, M., Roberts, K. and Walter, P. (2002) Molecular Biology of the Cell Garland Science, N.Y.

[2] Persinger, M.A. (2010) 10^{-20} Joules as a neuromolecular quantum in medicinal chemistry: an alternative approach to myriad molecular pathways?. Curr. Med. Chem. 17, 3094-3098.

[3] Cosic, I. (1994) Macromolecular bioactivity: is it resonant interaction between macromolecules?-theory and applications. IEEE Trans. Biomed. Engin. 41, 1101-1114.

[4] Cosic, I., Lazar, K. and Cosic, D. (2014) Prediction of Tubulin resonant frequencies using the Resonant Recognition Model (RRM). IEEE Trans. NanoBiosci. 10, 1109.

[5] Dotta, B., Murugan, N., Karbowski, L., Lafrenie, R. and Persinger, M. (2014) Shifting wavelengths of ultraweak photon emissions from dying melanoma cells: their chemical enhancement and blocking are predicted by Cosic's theory of resonant recognition model for macromolecules. Naturwissenschaften. 101, 87-94.

[6] Dotta, B., Lafrenie, R., Karbowski, L. and Persinger, M. (2014) Photon emission from melanoma cells during brief stimulation by patterned magnetic fields: Is the source coupled to rotational diffusion within the membrane?. Gen. Physiol. Biophys. 33, 63-73.

[7] Persinger, M., Murugan, N. and Karbowski, L. (2015) Combined Spectral Resonances of Signaling Proteins' Amino Acids in the ERK-MAP Pathway Reflect Unique Patterns That Predict Peak Photon Emissions and Universal Energies. Int. Lett. Chem. Phys. Astron. 4, 10-25.

[8] Dotta, B., Buckner, C., Cameron, D., Lafrenie, R. and Persinger, M. (2011) Biophoton emissions from cell cultures: biochemical evidence for the plasma membrane as the primary source. Gen. Physiol. Biophys. 30, 301-309.

[9] Dotta, B., Saroka, K. and Persinger, M. (2012) Increased photon emission from the head while imagining light in the dark is correlated with changes in electroencephalographic power: Support for Bókkon's Biophoton Hypothesis. Neurosci. Lett. 513, 151-154.

[10] Dotta, B., Buckner, C., Lafrenie, R. and Persinger, M. (2011) Photon emissions from human brain and cell culture exposed to distally rotating magnetic fields shared by separate light-stimulated brains and cells. Brain Res. 1388, 77-88.

[11] Decoursey, T. (2002) Voltage-Gated Proton Channels and Other Proton Transfer Pathways. Physiol. Rev. 83, 475-579.

5.3 Preamble to Chapter 6: Patterned Low-level Electromagnetic Energy and Malignant Growth Interference

Investigating applications in cancer, our work suggested that certain patterned electromagnetic fields could induce complete dissolution of malignant cells while healthy cells remained unaffected. Given our findings with water, malignant cells, and Cosic's resonant recognition model, we understood that the electromagnetic field applications were likely interfering with some intrinsic communication process operating between cells. We endeavoured to investigate the specificity of the field application including the order of presentation and the spatial planes of space within which the cells are exposed. If communication was central to the phenomenon, these factors should be relevant considering amplitude variations and the temporal presentation of certain frequency bands.

Chapter Six

Seeking the Source of Transience for a Unique Magnetic Field Pattern That Completely Dissolves Cancer Cells *in Vitro*

Published in Journal of Biomedical Science and Engineering (2015) – Vol: 8 (8). Pg. 531-543

Reproduced with Permission from Scientific Research

Lukasz M. Karbowski, Nirosha J. Murugan, Stanley A. Koren and Michael A. Persinger

Abstract

Purpose: Exposure to a particular pattern of weak (~3 to 5 μT) magnetic fields produced by computer-generated point durations within three-dimensions completely dissolved malignant cancer cells but not healthy cells. Biomolecular analyses and confocal microscopy indicated excessive expansion followed by contraction of the cell contributed to the "explosion" of the cell. However after months of replicable effects the phenomenon slowly ceased. Objective: Considering the potency of the complete dissolution of cancer cell lines after 5 days of 6.5 hour daily exposures and the implications for human treatment, the potential source of the disappearance of the effect was pursued by summarizing all of the 50 experiments and assessing the likely etiologies. Materials and Methods: B16-BL6, MDA MB 231 and MCF7 malignant cells and HSG, a non-malignant cell line, were exposed to a sham-field condition or to a specific pattern of computer-generated magnetic fields produced from converting different voltages each with point durations of 3 ms to 3-D magnetic fields. Conclusion: The specific serial presentation of the two field patterns (one frequency modulated; the other amplitude and frequency modulated) completely dissolved malignant cells but not normal cells within a "zone" within the exposure volume at the conjunction of the three planes of the applied magnetic fields. The affected cells underwent massive melanin production, expansion, contraction and

"beading" of submembrane actin structures before fragmentation within this zone. However this powerful all-or-none phenomenon may have been disrupted by moving the cells, excess mechanical agitation during exposure, or non-optimal point durations of the field parameters. Indirect effects from communication signals (WIFI) through line currents that operated the incubators could not be excluded.

6.1 Introduction

The classic Greek Philosopher Heraclitus is credited with stating that "one can never step into the same river twice". The operation if it were homogeneously valid would eliminate the potential for replication, the most essential property of knowledge derived from experimentation. Most models of physics depend upon the assumption of constancy for parameters that determine interactions between matter and energy superimposed within space. However the earth has not been in the same space during human history as the solar system orbits the galactic center approximately once every 250 million years. If even a subset of terrestrial phenomena is influenced by the intrinsic changes in spatial structural, then the ephemeral reliability of multiple observations in a relatively narrow temporal band might originate from processes other than random or spurious variation. The unique features of biological systems with respect to electromagnetic field-energetic interactions have been reviewed by Cifra et al [7]. The quantifiable relationships between chemical dynamics of cell-relevant systems and the specificity of the applied fields have been reiterated by many researchers [3, 4, 29].

Within the domain of cancer research there have been multiple claims over the century that appeared to be very efficacious within the specific laboratory or historical period that

ultimately or "suddenly" lost their potency. The most typical attributions have involved experimenter incompetence, changes in quality of reagents and equipment, or anomalous cell lines. Although all of these factors are likely to have been present in many of the failures to replicate, they are still *post hoc* explanations and attributions rather than experimental proofs. The actual combination of causal variables that result in elimination or attenuation of malignant cell growth without necessarily adversely affecting normal cells may not be identified in our lifetimes. However a tradition of systematically reporting the most powerful, although transient, treatment effects in the scientific literature may ultimately contribute to the solution.

There are several studies that have demonstrated a moderate slowing of cell growth of malignant cells when they are exposed for one hour to a few hours per day to patterned magnetic fields with intensities within the microTesla to milliTesla range [1,8,12]. Murugan et al [20] had found that exposing planaria for 6.5 hr per day for 5 days to one frequency-modulated pattern that also produced analgesia in invertebrates and vertebrates produced no conspicuous effects. However on the fifth day when the worms were exposed for an additional 6.5 hours to a very complex magnetic pattern that was an accelerated amplitude

modulated form, there was complete dissolution of the worms within about two hours [20].

The effect did not occur if this accelerated pattern was presented first for five days and then the frequency-modulated pattern was presented. The proportion of dissolution of the planaria was also a function of the duration of the antecedent exposure to the fields on the last day as well as field intensity. Such directionality, similar to the variable efficacy of L and R stereoisomers, has been found for a specific pattern that produces analgesia, cell growth, and infusion of calcium into cells [6,16]. Presentation of the same pattern but in reverse sequence resulted in no effect. When we exposed mouse melanoma cells to this protocol we measured complete elimination of cells on the fourth and fifth days after the treatment began. The effect was conspicuous and displayed an intensity threshold. This was manifested as an area at the interface of the three-planes of magnetic field application with cell absence surrounded by relatively normal cells. Despite dozens of replications over several months, this powerful and potentially clinically applicable effect slowly attenuated over a period of about two months. Here we present the general conditions and characteristics of this phenomenon.

6.2 MATERIALS AND METHODS

6.2.1 General Experimental Protocol

For all 50 experiments the preparation, extraction and handling of cells were as similar as possible and involved at least three different experimenters. The primary cell line was a mouse melanoma (B16-BL6). Because of the initial success other lines such as MDA MB 231, MCF 7 and HSG cells were tested. As shown in Table 1 there were a total of 50 experiments completed over a period spanning three years (2012, 2013, 2015).

The B16-BL6 murine melanoma cells were cultured *in vitro* in DMEM that contained 10% fetal bovine serum and antibiotics in a carbon dioxide environment at 37° C in standard incubators. Plates of cells were exposed to the "Thomas pulse" magnetic field pattern within the incubators for 6.5 hr per day for 5 days unless specified otherwise. On the fifth day an additional 6.5 hr exposure to the second ("geomagnetic" pulse) occurred. Four experiments involved 1 day and 3 days to discern "duration" dependence. Each day, after the exposure, one of the plates was harvested to observe the effects. Cells were harvested following incubation with trypsin and collection by centrifugation at 400 x g for 10 min. The pellets of cells were re-suspended in PBS containing 0.1% trypan blue. Quantification was completed using a hematocytometer. For each sampled plate eight separate counts were obtained and averaged.

6.2.2 Biochemical Measures

Acridine-Orange Confocal Microscopy (Detection of Apoptosis)

B16-BL6 cells were cultured on glass coverslips and allowed to adhere for 24 hour at 37°C. The cells were exposed to sham or MuKarb-EMF for 6.5 hr per day with the geomagnetic component of the tandem field sequence presented only on the 5th day. After treatment, the cells were collected 6 hours post-treatment on days 1, 2, 3, 4, or 5. B16-BL6 cells were also treated with 6 µg/ml of camptothecin and collected 6 hours post-treatment. This procedure was employed as a positive control for apoptosis. The cells were stained with 100 mg/ml acridine orange (Sigma Aldrich) for 5 min and then stained with 100 mg/ml of ethidium bromide (Sigma Aldrich) for 5 min. The coverslips were washed in PBS, gently mounted onto a glass slide, and sealed with clear nail polish. Fluorescence was visualized by a LSM510 microscope using the 488 nm laser for activation and Fset 17 (detection 515-585nm) for acridine orange and Fset 28 (detection 617 nm) for ethidium bromide (acridine orange excitation at 502 nm and emission at 526 nm and ethidium bromide excitation 510 nm and emission 595 nm).

Phalloidin Confocal Microscopy (Actin Detection)

B16-BL6 cells were cultured on glass coverslips and allowed to adhere for 24 hour at 37°C. The cells were exposed to sham or MuKarb-EMF with the geomagnetic component of the tandem field sequence presented only on the 5th day. After treatment, the cells

were collected 6 hours post-treatment on days 1, 2, 3, 4, or 5. Cells were washed in PBS and fixed using formaldehyde (3.7%) for 10 minutes at room temperature. The coverslips were washed with acetone at -20°C for 5 minutes and stained with 5uL Alexa Fluor® 488 Phalloidin (Life Technologies) for 5 min. Fluorescence was visualized using a LSM510 microscope.

6.2.3 Equipment

The equipment was similar to previous experiments. The exposure volume was a 10 cm x 10 cm x 10 cm plastic box (Figure 1C). Six (3 pairs) of solenoids that were modified reed relays (Radio Shack 275-0232 SPST 5VDC, Contact rating: 0.5 A, 125 VAC, nominal current: 20 mA). Each solenoid was 50 Ω within which a small nail was inserted to enhance flux density and was contained within a plastic canister. Each canister containing the solenoid was placed at the midpoint of each wall of the box. The circuit was connected such that at any given time the two solenoids on opposite sides of the same plane were activated and the field was generated between these solenoids across the cells (Figure 2).

(A) (B) (C)

Figure 1. The three main components of the system from top to bottom: A) the source computer containing the code (pattern) numerical sequence, B) the DAC (digital to analogue converter) that transformers the numbers to voltages, and, C) the three orthogonal pairs of solenoids generating the magnetic field fields within which plates of cells are exposed.

The plates were stacked 6 high in the middle of the box so that the cells were exposed to the interface of the three planes of the continuously generated magnetic fields. The average intensity of the magnetic fields in the center of the box as measured by a power meter was 26 mG (range 26-29 mG) for both types of fields. For the Thomas pattern the field strength increased quasi-exponentially to 150 mG (range 140 to 160 mG) adjacent to the solenoids as shown in Figure 2. The peak exposure in the plates along the edges was ~50 mG. However the Geomagnetic pattern produced an unusual gradient. Starting with the 26 mG value in the center the strength *diminished* towards the solenoids to about 18 mG and then rapidly escalated to the increasing intensities as any given solenoid was approached. The perimeter for this sudden shift was about 4 cm from the center. Sham-field exposures involved placing the plates of cells in the same boxes except there was no field generation. The background power frequency magnetic fields (60 Hz) within the incubators were about 1.5 mG.

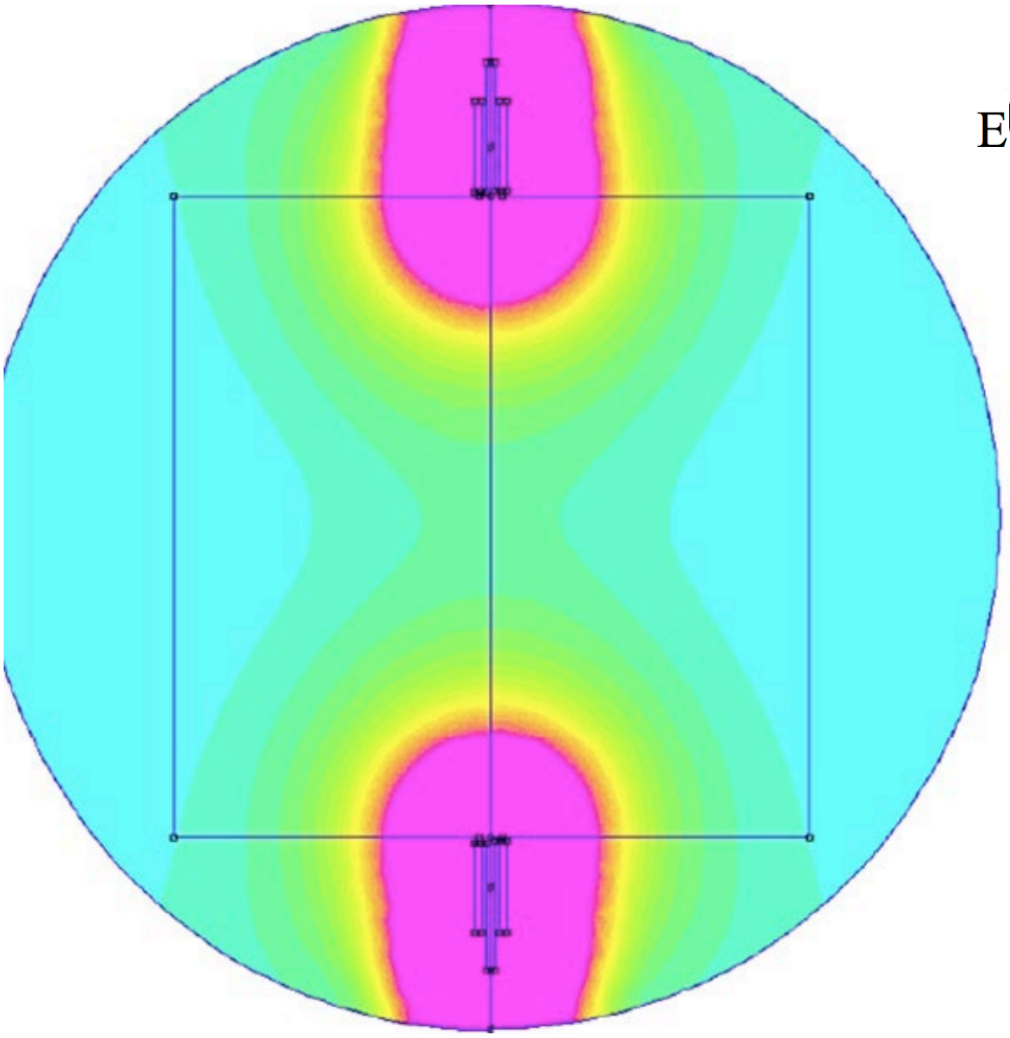

Figure 2. Colorized measurement of the strength of the Thomas pattern magnetic field generated between any two pairs of solenoids within the exposure area (thin line blue square). The cell dropout zone was approximately from the yellow corona one solenoid to the other in all three dimensions.

The magnetic fields were generated by software and equipment developed by Koren and Persinger (U.S. Patent 6,312,376 B1: November 6, 2001; Canadian Patent No. 2214296). Essentially a series of numbers (in a column) from 1 through 256 were converted to voltages between -5 and +5 V (127=0 V) through a custom-constructed digital-to-analogue-converter (DAC). The Complex software was developed by third author (Stanley A. Koren) and was organized such that any column of numbers could be transformed to specific voltages from a computer (Figure 1A). This allowed unlimited flexibility for the type of patterns that could be generated including those digitized from natural recordings of cell activity. The output of the DAC (Figure 1B) was delivered to the successive pairs of solenoids of the exposure boxes (Figure 1C).

The software was designed to control the point duration of each voltage. The value is the time allocated to generating a specific voltage (based upon the number between 0 and 257 being transformed) to the exposure device. The software also allowed programmable times between the presentations of patterns, that is the interstimulus or interpattern interval. Multiple previous experiments have shown that 3 ms point durations are most effective for slowing growth of cancer cells *in vitro* as well as

in mice and for producing analgesia in rats that is equivalent to 4 mg/kg of morphine following only 30 min of exposure.

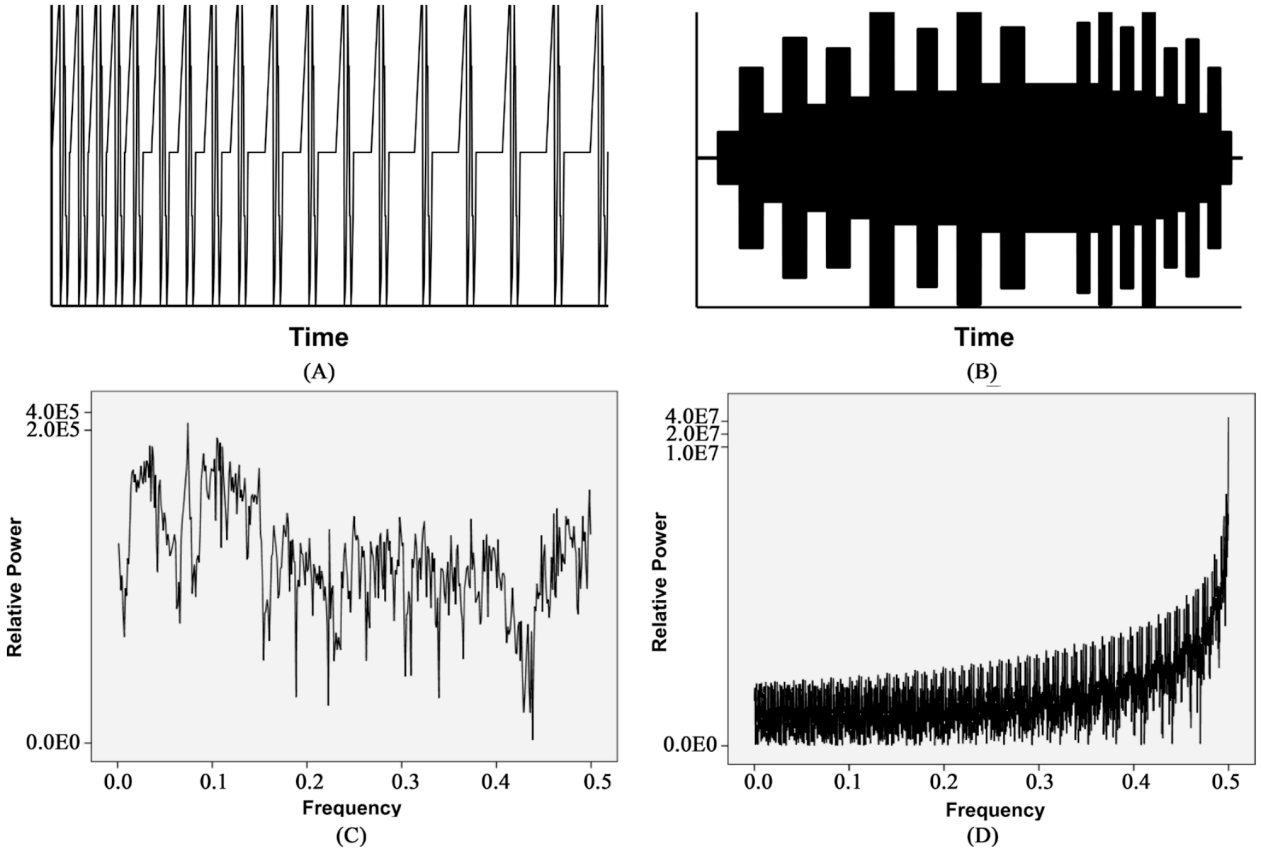

Figure 3. A: "Thomas" or frequency-modulated pattern; B: the geomagnetic pattern; C: relative spectral power density for A as a function of spectral frequency; D: relative spectral powr density for B as a function of spectral frequency. Real frequencies are obtained by multiplying base frequency by 333 Hz.

The “MUKARB” (Murugan-Karbowski) sequence is composed of two patterns. The first pattern, a frequency modulated field often described as the “Thomas pulse”, has been shown to produce slowing of cancer cell growth rates and analgesia in vertebrates and invertebrates. It is composed of 849 points (i.e., numbers between 0 and 257) and is shown in Figure 3A. The second pattern (composed of 9,999 points) is shown in Figure 3B. It was initially designed to imitate a sudden geomagnetic storm commencement by employing point durations of 69 ms such that a fundamental 7 Hz field was amplitude-modulated as well as (sub-harmonic) frequency-modulated over an approximately 6 min period. The spectral power densities are shown Figure 3C, 3D. To obtain real frequency multiply the spectral frequency by 333 Hz (i.e., the Nyquist limit is ½ or 167 Hz for 3 ms point durations). These patterns indicated that most of the energy for the “Thomas pulse” was between 8 and 25 Hz while the geomagnetic pulse was densely distributed across the low frequency band with a marked exponential increase approaching the Nyquist limit. When this pattern’s point duration was set to 3 ms and presented after the Thomas pattern exposures, Murugan et al [20] found that planarian dissolved within two hours after the presentation of the field. Presenting the fields in reversed order or for briefer than optimal periods did not produce this effect.

In the present series of experiments over three years the MUKARB sequence was presented to different cell batches and types by different experimenters. In some experiments the MUKARB was reversed. The "geomagnetic" component was presented first and then the Thomas pattern was presented second. For some experiments the durations of exposures were less than 5 successive days. Following the failure to produce this robust effect additional manipulations of the point durations (year 2015) were completed to discern timing effects because precision has been shown to be critical.

6.3 Results

The summary of all of the results for the 50 experiments are shown in Table 1. Between 14 February and 22 July 2012 the dropout rate from the MUKARB exposure was 100% for the B16 and MDA MB 231 cells and about 65% for the MCF 7 cells. On the other hand HSG cells which are considered "non-malignant" showed no or minimal dropout during this period. This reiterated previous experiments that these patterned magnetic fields specifically affect cancer cells but not normal cells.

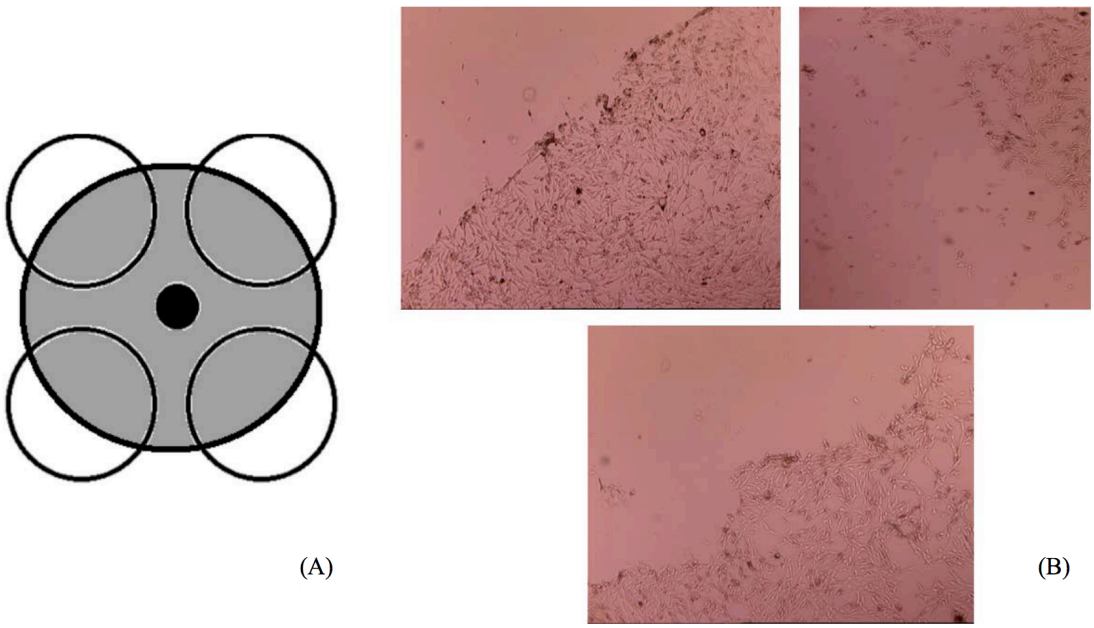

Figure 4. A shows the position of the plates (6 stacked plates per quadrant) with respect to the central intersection of the magnetic fields generated across the three planes. The grey area (which extend about 4 cm from the center) indicates the zone where no cells were found. B displays the drop out pattern that was evident in the plates. Note the discrete boundaries for the difference between decimated cells and typical cell densities

Table 1A. Results of all of the experiments that include the dates, parameters, cell type and effect (% dropout) of malignant cells for this specific magnetic field configuration.

MuKarb *in Vitro* Experiments					
Start Date	**End Date**	**Experiment**	**Cell**	**Effect**	**Point Duration**
Year: 2012					
14-Feb	18-Feb	5 day mukarb	B16	100% drop	3/3msec
21-Feb	25-Feb	5 day mukarb	B16	100% drop	3/3msec
04-Mar	09-Mar	5 day mukarb	B16	100% drop	3/3msec
11-Mar	16-Mar	5 day mukarb	B16	100% drop	3/3msec
19-Mar	24-Mar	5 day mukarb	B16	100% drop	3/3msec
26-Mar	30-Mar	5 day mukarb	B16	100% drop	3/3msec
03-Apr	07-Apr	5 day mukarb	B16	100% drop	3/3msec
23-Apr	28-Apr	5 day mukarb	B16	100% drop	3/3msec
13-May	14-May	1 day mukarb	B16	15% drop	3/3msec
04-Jun	06-Jun	3 day mukarb	B16	40% drop	3/3msec
11-Jun	15-Jun	reverse mukarb	B16	0% drop	3/3msec
05-Jul	09-Jul	reverse mukarb	B16	0% drop	3/3msec
29-Jun	03-Jul	5 day mukarb	B16	100% drop	3/3msec
12-Jul	16-Jul	5 day mukarb - 1 hr	B16	0% drop	3/3msec
12-Jul	16-Jul	5 day mukarb	B16	100% drop	3/3msec
19-Jul	20-Jul	1 day mukarb	B16	15% drop	3/3msec
24-Jul	26-Jul	3 day mukarb	B16	40% drop	3/3msec
11-Apr	15-Apr	5 day mukarb	MDA MB 231	100% drop	3/3msec
18-Apr	22-Apr	5 day mukarb	MDA MB 231	100% drop	3/3msec
28-Jul	01-Aug	5 day mukarb	MDA MB 231	100% drop	3/3msec
03-Aug	08-Aug	5 day mukarb	MDA MB 231	100% drop	3/3msec
30-Apr	04-May	5 day mukarb	MCF 7	67% drop	3/3msec
07-May	11-May	5 day mukarb	MCF7	59% drop	3/3msec
18-May	22-May	5 day mukarb	MCF7	60% drop	3/3msec
25-May	29-May	5 day mukarb	B16	100% drop	3/3msec
12-Jul	16-Jul	5 day mukarb	B16	100% drop	3/3msec
18-Jul	22-Jul	5 day mukarb	B16	100% drop	3/3msec
19-Mar	24-Mar	5 day mukarb	HSG	0% drop	3/3msec
26-Mar	30-Mar	5 day mukarb	HSG	0% drop	3/3msec
03-Apr	07-Apr	5 day mukarb	HSG	5% drop	3/3msec
12-Aug	16-Aug	5 day mukarb	B16	35% drop	3/3msec
20-Aug	24-Aug	5 day mukarb	B16	35% drop	3/3msec
26-Aug	30-Aug	5 day mukarb	B16	20% drop	3/3msec
04-Sep	08-Sep	5 day mukarb	B16	25% drop	3/3msec
09-Sep	13-Sep	5 day mukarb	B16	0% drop	3/3msec
25-Sep	29-Sep	5 day mukarb	B16	0% drop	3/3msec
11-Nov	15-Nov	5 day mukarb	B16	0% drop	3/3msec
19-Nov	23-Nov	5 day mukarb	B16	0% drop	3/3msec
10-Dec	14-Dec	5 day mukarb	B16	0% drop	3/3msec

By 100% dropout, we mean there were no cells visible within this portion of the dishes. This is similar to the complete dissolution of the planarian we published previously [20]. Reversing the direction of the pattern ("reverse MUKARB") produced no dropout. Abbreviated exposures also produced less effect. After 22 July the effect began to diminish (August and September). During the remaining months of 2012 and the first part of 2013 the MUKARB sequence was no longer effective and was similar to sham-field treatments.

That the effect was geometric-intensity dependent is indicated in Figure 4. During the period of the optimal effect from the MUKARB sequence the initial dropout of the cells began in the areas of the dishes that were exposed to the central portion of the experimental field where all three planes intersected. The width of the "dissolution zone" was about 3.8 cm. This width would overlap with the perimeter where the geomagnetic pattern shifts from its declining intensity from the center and suddenly increases (following the typical exponential curve) towards the solenoids.

Table 1B. Continuation of summary of results from Table 1A.

Year: 2013					
14-Jan	18-Jan	5 day mukarb	B16	0% drop	3/3 msec
17-Mar	22-Mar	5 day mukarb	B16	0% drop	3/3 msec
24-Mar	28-Mar	5 day mukarb	B16	0% drop	3/3 msec
Year: 2015					
20-Apr	24-Apr	5 day mukarb	B16	35% drop	3/3 msec
27-Apr	01-May	5 day mukarb	B16	20% drop	3.25 msec
04-May	08-May	5 day mukarb	B16	30% drop	0.1/0.1 msec
04-May	08-May	5 day mukarb	B16	25% drop	3.38 msec/3.38 msec
Biomolecular Analysis: 2012					
27-Feb		confocal	B16	equal to camptothecin	3/3 msec
28-Mar		phalloidin	B16	positive actin staining	3/3 msec
17-Mar		trypan blue test/morphology	B16	enlargement and shrinking	3/3 msec

Biochemical measures

Melanin production in the cells exposed to the MUKARB when it was effective was visibly evident as shown in Figure 5. There was a clear duration dependent increase in melanin production following exposure on the fifth day to the MUKARB sequence compared to the sham-exposed, camptothecin (the positive control for DNA damage) or either only the Thomas component or geomagnetic component of the MUKARB pattern. In other words the specific MUKARB sequence was required to produce the massive melanin production.

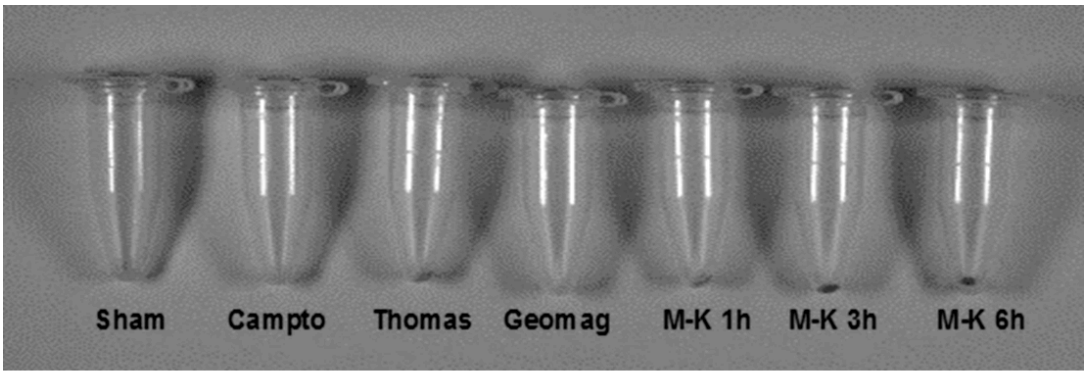

Figure 5. Presence of conspicuous melanin formation from precipitants of melanoma cells after exposure to various treatments including sham field, camptothecin, the Thomas only pattern, the geomagnetic pattern only and the combination (MUKARB or M-K) for 1 hr, 3 hr or 6 hr. Note the time duration increase in melanin precipitant in the pellet.

There was a clear time-dependence in the accumulation of melanin in the actual cells that was discernable after 15 min and maximized after 60 min as shown in Figure 6. It occurred only after the onset of the second (geomagnetic) field. Measurements were completed during the first hour because by the end of the 6.5 hr exposure there were no cells remaining. Trypan blue measurement of the morphology indicated that enlargement of the cell by about 50% followed by rebound contraction by about 50% occurred within a period of about 2 hours. Note the marked

melanin precipitant from cells 1 hr after exposure to the final component of the MUKARB pattern.

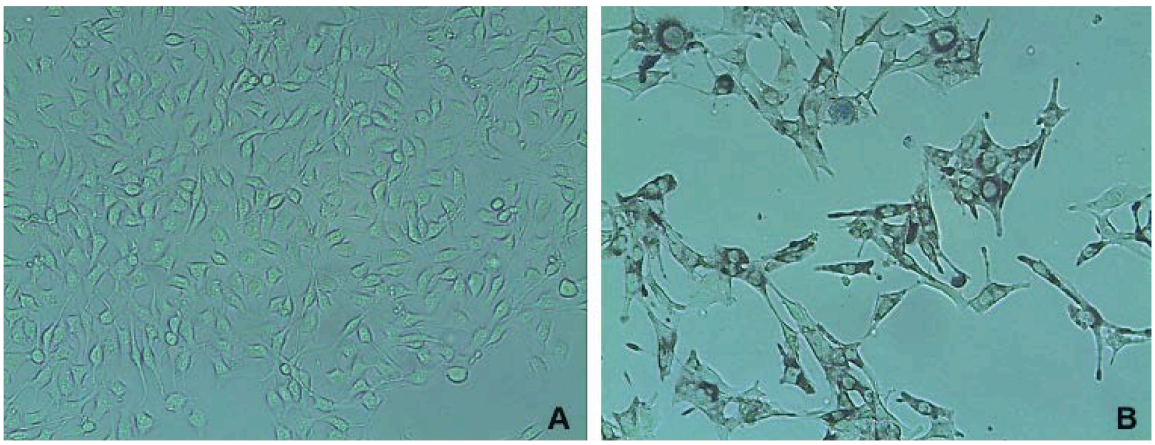

Figure 6. The appearance of melanin in melanoma cell increased as a function of time of exposure to the MUKARB magnetic pattern (100 X). Above A) sham field exposed; B) 60 min after exposure to the final component of MUKARB.

The phalloidin stain (Figure 7) revealed a positive actin staining within the cells that was evident along the insides of the plasma membranes as revealed by CONFOCAL microscopy. However unlike normal cells or sham-field exposed cells the indicator of actin staining revealed enhanced heterogeneity of density along the internal perimeter. The "smooth" distribution observed for normal cells was replaced with successive increments of short "widening" of the "ring" as if coalescence was beginning. This beading is most obvious with the acridine orange stain shown in Figure 8 as well as at low magnifications.

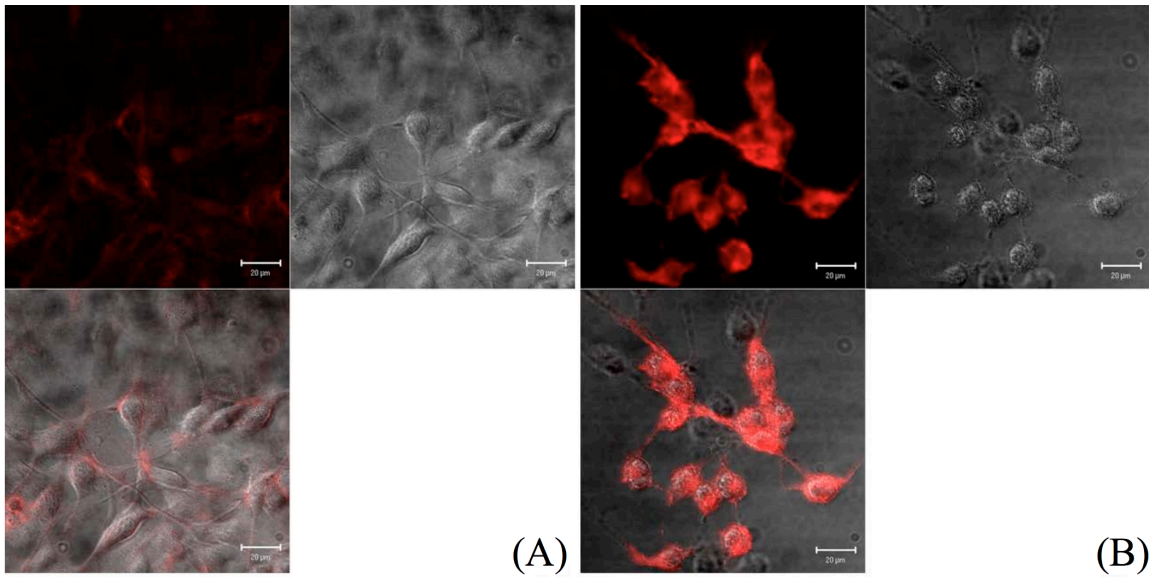

Figure 7. Fluorescence visualized for phalloidin using a LSM510 microscope for cells that have been exposed to the sham field (A: left 3 panels) or to the MUKARB pattern (B: right 3 panels). Red indicates marked actin staining. Horizontal line indicates 10 µm.

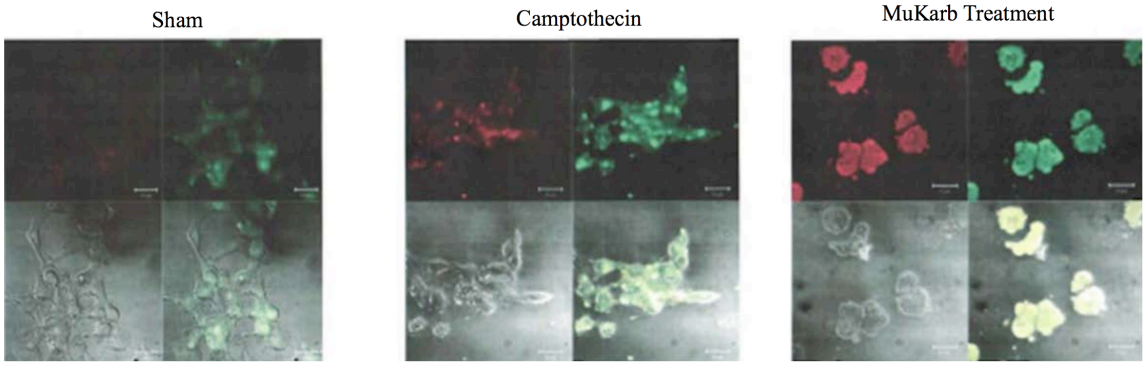

Figure 8. Acridine orange stain results for cells exposed to the sham field, the camptothecin treatment, or the MuKarb treatment. The "beading" of likely actin of the peripheral cytoskeleton is evident in the latter.

6.4 Discussion

We [12, 16, 20, 31] have been examining the effects of various patterns, phases, intensities, frequencies, and origins of magnetic fields upon biological systems for decades. The development of the personal computer and the specialized software by S. A. Koren that allowed the generation of innumerable sequences of voltages (and magnetic fields) each with specific point durations significantly changed the flexibility for producing applicable electromagnetic patterns that could imitate those generated by natural processes. Our original research with relatively short duration patterns (about 1 to 2 s) repeated over periods of 30 min to 60 min produced analgesia in rats [16, 18] that was equivalent to 4 mg/kg of morphine and was blocked by pharmacological agents known to antagonize mu receptors [16] and the nitric oxide correlates [18]. Similar effects were found with invertebrates during the same period of exploration by Alex Thomas, Frank Prato, Klaus-Peter Ossenkopp and their colleagues [33].

The progress from single pattern exposures to tandem sequences of different patterns was a logical extension that produced powerful effects. Prenatal exposure of rats to a complex pattern composed of about 20 patterns (some repeated) resulted in conspicuous morphological changes in hippocampuses in adult brains [31]. When adult mice were exposed to this same pattern for several days

micro-array analyses indicated significant shifts in genes associated with the pathways involved with membrane and myelin integrity and formation. When a protocol, involving the same two patterns employed in the present experiments, was applied to planarian for several hours per day over 5 days a conspicuous and complete dissolution of these worms occurred within hours of the initiation of the second pattern [20].

In a manner similar to the elicitation of powerful limbic seizures and brain damage in rats injected systemically with therapeutic concentrations of lithium followed 4 hours later by pilocarpine but not if the order of drug injection was reversed [23], reversing the Thomas-Geomagnetic order produced no dissolution of the worms [20]. When the treatment was effective over several months we found similar massive disruptions of cell integrity in cultures exposed daily for briefer durations. Subsequent biochemical analyses revealed potential intracellular changes that would be consistent with the decimation of the entire cell within a defined perimeter at which the three planes of the applied magnetic fields intersected. When the order of the pattern was reversed the cell morphology and biochemistry did not differ from sham field controls.

6.4.1 Potential Mechanisms

The results of the phalloidin stain following exposure to the MUKARB sequence were conspicuous. The typical thin "layer" of actin that we presume reflects the internal cytoskeleton often seen in normal and non-exposed cells was replaced with an emerging "beady" texture as if a series of discontinuities had been introduced into this layers' continuity. It appeared similar to what we [15] and others [27] have seen with traditional histological stains by light microscopy in the myelin in the long tracts in brains of patients and rats who have sustained massive impacts of mechanical energy to their skulls. This "beading" is called "retraction balls" and has been attributed to the result of the sudden contraction and expansion of the cerebral volume during the mechanical impact. Along the path of the pressure wave there were discrete clusters of shrunken, darkly stained neuronal cell bodies containing marked "granulated" structures visible at 1000 X.

The trypan blue indicators were consistent with relatively quick enlargement and shrinkage of the cells following the onset of the second component of the MUKARB. We suggest that the "bead-like" nature of the phalloidin perimeter might reflect the analogue of "retraction balls" found in myelin and would support the microscopic observation that the cells underwent distention/contractions beyond the elastic limit of the actin-

containing cytoskeleton. The phenomenon might be considered analogous to the long-term consequences of excessive extension of actin-myosin molecules in muscle fibers that result in anomalous changes in Z-lines that subsequently affect the tissue's capacity to display maximum displacement in response to interactions with ATP. This condition is often associated with the deposition of fine particles of calcium salts. In the cellular instance the distention appears to have exceeded the tensile strength of these proteins resulting in micro-fragmentation or "bursting" of the cells.

6.4.2 Potential Sources for Inconsistency of Effects

The reasons for the "slow" diminishment of this conspicuous effect are not clear. We consider at least four possibilities. The first involved the introduction of pervasive and dense wireless communication within the facility. Although one would expect that the incubators would behave as simulated "electrically shielded" Faraday cages, this may not be correct. Many facilities, including the one in which our experiments were conducted, superimpose (unknowingly or by design) the wireless signals within the peripheral shielding of the cables delivering the line current. We have measured these microwaves signatures through the protective covering of the lines from the power supplies (although they are grounded) that power the DAC systems.

It may be useful to remember that with a background of 10 $mW \cdot m^{-2}$ from microwave appliances (which we measured in the laboratory where the experiments were completed) the energy across a cell with a cross-sectional area of $\sim 10^{-10}$ m^2 is about a picoJoule per s. This is within the range of the energy per second utilized by the cell from glucose metabolism. Whether or not these energy sources would be interactive must still be discerned.

The second source is the role of thixotropic phenomenon as described by Verdel and Bukovec [35] Thixotrophy refers to the slow increase in gel-like behavior of water, that is increased viscosity of a volume of water, when it is remains stable in the same place and usually in the dark. Mechanical processing such as movement of the plate or intrinsic vibrations from the environment diminishes this additional viscosity. Thixotrophy develops spontaneously over time and is likely to involve the formation of structured networks of hydrogen bonds between ions in aqueous solution and the water molecules. The width of these networks ranges between 30 to 500 nm with a median of about 100 nm. In other experiments Murugan et al [21] found that exposure of spring water (but not double distilled water) sitting undisturbed in the dark for more than a week to the Thomas pattern resulted in marked increases (100 photons or about 20% more than sham field exposed) in photon emissions as measured by fluorescent spectrophotometry within the visible wavelength. The

shift from about 390 to 409 nm involved a difference of about 10^{-20} J. Spectral analyses of the enhanced photon counts across the 1 nm frequency band revealed a spatial periodicity of 10 nm, the width of a membrane. Excessive mechanical agitation of the samples during transport to the laboratory eliminated the effect. The third possible explanation is that the fidelity of the components of the DAC system, which transforms the columns of numbers to voltages and hence ultimately to the current that generates the magnetic fields within the solenoids, may be limited. The unique feature of this method of generating magnetic fields involves an optocoupler that if our assumptions are valid [14] results in superimposition of photons within the magnetic field within which the cells are exposed. There is accumulating evidence the "information" within patterns of ultraweak ($\sim 10^{-12}$ $W \cdot m^{-2}$) biogenic photon emissions from living cells may actually be the control stimuli that determine the integrity, dynamics and perhaps mortality of the cell [9, 10, 34]. We have noted that the optocoupler is particularly vulnerable to the rapid reversals from maximum-to-minimum values which would have been encountered with the geomagnetic signal because of the rapid alterations in maximum polarities. In other experiments replacement of optocouplers with the appropriate load capacity has resulted in the increased efficacy of slowing

malignant cells growth when previously the diminishment was less or not different from sham field controls.

The fourth possibility, which is less palatable to many scientists and in many respects a challenge to the scientific tradition of maintained replicability, is the possibility there has been a change in the inertial frame or intrinsic space through which the earth as a component of the solar system is moving as it orbits the galaxy. Although potentially coincidental the disappearance of the MUKARB effect occurred at approximately the time the background radiant flux densities of photons that we measure continually by analogue photomultiplier tubes began to increase from the values of ~10^{-12} to 10^{-11} $W \cdot m^{-2}$. Transient increases of the photon flux density by a factor of 10 about two weeks before very intense (>8.0 M) seismic events anywhere on the planet have been measured [25]. However the PMT values always returned to baseline within a day or two after the seismic event. Since about July, 2012 we have measured a persistent rise in background photon power density from unknown sources [26].

That subtle changes associated with the solar cycle can affect chemical reactions has been known for more than a century. Takata [32] measured extensively the “flocculation index” in blood and discerned sunrise/sunset effects as well as latitude and solar rotational components. The famous Piccardi effect [28] whereby the precipitation measures for bismuth compounds followed

the solar cycle is particularly relevant because these colloidal-like suspensions share many of the physical parameters such as viscosity with the cytoplasm and its interface with surface boundaries. Calculations indicate that the cell membrane's energy is predicted by mass interactions with the earth [22] and has the potential to be modulated by the subtle shifts in the energy across the membrane generated by the time-dependent changes in force as a function of lunar distance [25]. This relationship at a behavioural level was demonstrated repeatedly by Frank Brown, Jr and his colleagues decades ago [5]. Recently the global effects [2] of such "subtle forces and energies" were measured for photon emissions from seedlings that are similar over the surface of the planet [19].

Although cells contain intricately connected organelles the interfacial water properties along the inside and outside of the plasma membrane is also a special condition that exhibits unique properties [13]. As shown repeatedly by Pollack and his colleagues [30], the viscosity of the water within the boundary interface (interfacial water) is increased by a factor of 10 compared to bulk water. The potential difference (voltage) from the resulting sheet of protons becomes equivalent to the traditional membrane potential attributed to extracellular-intracellular discrepancies of ion concentrations such as potassium [24]. Solutes remain excluded for protracted periods.

This allows for a potential "condensate" like state where application of the appropriate temporally complex magnetic fields that simulate this resonance can be trapped within cohesive domains of water. Like a crystal state the convergence of temporal patterns towards the natural frequency could disintegrate the supportive structure.

6.5 General Conclusion

We suggest the specific temporal-spatial configurations of these sequential magnetic fields promote the coherence required for the "trapping" of the magnetic fields within the domains occupied by intrinsic cytoskeleton that promotes its dissolution much like the superimposition of applied oscillations to the "natural frequency" of a suspension bridge can produce its collapse. However any physical mechanism that disrupts the required conditions, such as mechanical perturbation, competitive EM fields, or alterations in precise timing can prevent the effect. When this occurs the cancer cells are not affected by the applied field. The phenomenon is analogous to the requirement for structural congruence between an exogenous ligand and the extracellular head group of a transmembrane protein for response to occur. If the temporal "structure" of the applied field is not resonant with the malignant cells' cytostructural because of obscuring sources there is no effect.

6.6 References

[1] A. Barbault, F. P. Costa, B. Bottger, R. F. Munden, F. Bomholt, N. Kuster and B. Pasche (2009) Amplitude-modulated electromagnetic fields for the treatment of cancer: discovery of tumor-specific frequencies and assessment of a novel therapeutic approach. J Exp Clin Cancer Res, **28**, 1-10.

[2] L. Yu. Berzhanskaya, V. N. Berzhanskii, O. Yu. Beloptovota, T. G. Pil'nikova and T. N. Metlyayev (1995) Bacterial bioluminescent activity as a pointer to geomagnetic disturbances. Biophys, **40**, 761-764.

[3] M. Blank and R. Goodman (1997) Do electromagnetic fields interact directly interact with DNA? Bioelectromagnetics **18**, 111-115.

[4] M. Blank and L. Soo (2001) Electromagnetic acceleration of transfer reactions, J. Cell Biochem, **81**. 278-283.

[5] F. A. Brown, Jr. and C. S. Chow (1973) Interorganismic and environmental influences through extremely weak electromagnetic fields. Biol Bul, **144**, 437-461.

[6] C. A. Buckner, A. L. Buckner, S A. Koren, M. A. Persinger and R. M. Lafrenie (2015) Inhibition of cancer cell growth by exposure to a specific time-varying electromagnetic field involves T-type calcium channels. PLOS ONE, DOI: 10:1371/journal.pone.0124136.

[7] M. Cifra, J. Z. Fields and A. Farhadi (2011) Electromagnetic cellular interactions. Prog Biophys Molec Biol **105**, 223-246.

[8] S. Crocetti, C. Beyer, G. Schade, M. Egli, J. Froehlich and A Franco-Obregon (2013) Low intensity and frequency pulsed electromagnetic fields selectively impair breast cancer cell viability. PLOS ONE, **8**, Issue 9 e72944.

[9] B. T. Dotta, N. J. Murugan, L. M. Karbowski, R. M. Lafrenie and M. A. Persinger (2014) Shifting wavelengths of ultraweak photon emissions from dying melanoma cells: their chemical enhancement and blocking are predicted by Cosic's theory resonant recognition model for macromolecules. Naturwissenschaften, **101**, 87-94.

[10] D. Fels (2009) Cellular communication through light. Plos ONE, **4** (4): e5086.

[11] E. Del Giudice, P. S. Spinetti and A. Tedeschi (2010) Water dynamics at the root of metamorphosis in living organisms. Water, **2**, 566-586.

[12] J. H . Hu, L. S. St-Pierre, L. S. Buckner, R. M. Lafreniere and M. A. Persinger (2010) Suppression of growth of injected melanoma cells by whole body exposure to specific spatial-temporal configurations of weak intensity magnetic fields. Int J Rad Biol, **86**, 79-88.

[13] L. M. Karbowski and M. A. Persinger (2015) Variable viscosity of water as the controlling factor in energetic quantities that control living systems: physicochemical and astronomical interactions. Int Lett Chem Phys Astron, **4**, 1-9.

[14] S. A. Koren, W. E. Bosarge, M. A. Persinger (2015) Magnetic fields generated by optical coupler circuits may also be containment loci for entanglement of P-N junction-plasma cell membrane photons within exposed living systems. Int Lett Chem Phys Astron, **3**, 84-105.

[15] W. E. Lado and M. A. Persinger (2012) Spatial memory deficits and their correlations with clusters of shrunken neuronal soma in the cortices and limbic system following a

"mild" mechanical impact to the dorsal skull in female rats. J Behav Brain Sci, **2**, 333-342.

[16] L. J. Martin, S. A. Koren, and M. A. Persinger (2004) Thermal analgesic effects from weak, complex magnetic fields and pharmacological interactions. Pharm Biochem Behav, **78**, 217-227.

[17] L. J. Martin and M. A. Persinger (2004) Thermal analgesia induced by 30-min exposure to 1 microTesla burst-firing magnetic fields is strongly enhanced in a dose-dependent manner by the alpha-2 agonist clonidine in rats. Neurosci Lett, **366**, 226-229.

[18] B. E. McKay and M. A. Persinger (2003) Complex magnetic fields potentiate agmatine-mediate contextual fear learning deficits in rats. Life Sci, **72**, 2489-2498.

[19] T. A. Moraes, P. W. Barlow, E. Kingele and C. M. Gallep (2012) Spontaneous ultra-weak light emissions from wheat seedlings are rhythmic and synchronized with the time profile of the local gravimetric tide. Naturwissenschafen, **99**, 465-472.

[20] N. J. Murugan, L. M. Karbowsk, R. M. Lafrenie and M. A. Persinger (2013) Temporally-patterned magnetic fields induce complete fragmentation in planaria. PLOS ONE, 8(4);e61714.

[21] N. J. Murugan, L. M. Karbowski, R. M. Lafrenie and M. A. Persinger (2015) Maintained exposure to spring water but not double distilled water in darkness and thixotropic conditions to weak (1 uT) temporally patterned magnetic fields shift photon spectroscopic wavelengths: effects of different shielding materials. J Biophys Chem, **6**, 14-28.

[22] M. A. Persinger (2014) Terrestrial and lunar gravitational forces upon the mass of a cell: relevance to cell function. Int Lett Chem Phys Astron, **2**, 15-21.

[23] M. A. Persinger, Y. R. J. Bureau, M. Kostaskos, O. Peredery and H. Falter (1993) Behaviors of rats with insidious multifocal brain damage induced by seizures following single peripheral injections of lithium and pilocarpine. Physiol Behav, **53**, 849-866.

[24] M. A. Persinger and R. M. Lafrenie (2014) The cancer cell plasma membrane potentials as energetic equivalents to astrophysical properties. Int Lett Chem Phys Astron, **17**, 67-77.

[25] M. A. Persinger, G. F. Lafreniere and B. T. Dotta (2012) Marked increases in background photon emissions in Sudbury,

Ontario more than two weeks before the magnitude > 8.0 earthquakes in Japan and Chile. Int J Geosci, **3**, 627-629.

[26] M. A. Persinger, B. Lehman, B. T. Dotta and G. F. Lafreniere (2015), Four years of daily photon emissions that have predicted major earthquakes: raw data, spectral power density analyses and implications for geosciences. Int J Geosci, **6**, 311-316.

[27] J. T. Povlishock and T. H. Coburn (1989) Morphopathological change associated with mild head injury. In H. S. Levin, H. M. Eisenberg and A. L. Benton (eds) Mild head injury, Oxford University Press, N.Y., pp. 37-53.

[28] G. Piccardi (1962) Chemical basis of medical climatology. C C. Thomas, Springfield (Ill).

[29] A. A. Pilla, D. J. Muehsam, M. S. Markov and B. F. Sisken (1999) EMF signals and ion/ligand binding kinetics: prediction of bioeffective waveform parameters. Bioelectrochem. Bioenergetics, **48**, 27-34.

[30] G. H. Pollack, X. Figuerora and Q Zhao (2009) Molecules, water, and radiant energy: new clues for the origin of life. Int J Mol Sci, **10**. 1419-1429.

[31] Linda S St-Pierre, A. Mazzuchin and M. A. Persinger (2008), Behavioral, blood chemical, and hippocampal histomorphological differences in adult rats exposed prenatally to physiologically-patterned weak magnetic fields. Int J Rad Biol, **84**, 325-335.

[32] M. Takata (1951) Uber eine neue biologisch wirksame Komponente de Sonnenstrahlung: Beitrag zu einer experimentellen Grundlage der Heliobiologe. Arch Meteor Geophys Bioklim Series B, **2**, 486-508.

[33] W. Thomas, M. Kavaliers, F. S. Prato and K-P. Ossenkopp (1997) Antinoceptive effects of a pulsed magnetic field in the land snail, Cepaea nemoralis. Neurosci Lett **222**, 107-110.

[34] M. V. Trushin (2004) Light-mediated "conversation" among microorganisms. Microbiol Res, **159**, 1-10.

[35] N. Verdel and P. Bukovec (2014) Possible further evidence for the thixotropic phenomenon of water. Entropy **16**, 2146-2160.

6.7 Preamble to Chapter 7: Specificity in Information of Low-Level Electromagnetic Effects on Biological Organisms

Having identified some parameters, which were necessary in order to induce malignant cell dissolution upon the presentation of electromagnetic fields, we undertook a detailed analysis of other factors, which could be tuned to increase or decrease the effects systematically. Previous theoretical and experimental works suggested that point duration, an increment of field presentation, would be important. We also considered the role of some of the circuitry involved in the exposure devices, which were used to process signals from digital computers or produce the electromagnetic fields. We expected to see highly specific and pronounced responses to particular parameters with moderate responses associated with parameters whose values approximated those which were optimal. That is, just as molecular interactions can be characterized by their effects with regard to molar concentration and other relevant chemical factors, we predicted that point durations would center upon some central, optimal value which optimally "activated" biological processes.

Chapter Seven

Temporal Precision and Instrumental Complexity Determine the Efficacy of Cancer Treatment by Weak, Complex Patterned Magnetic Fields.

In Preparation for Submission

Lukasz M. Karbowski, Nirosha J. Murugan, John A. Carscallen, Stanley A. Koren and Michael A. Persinger

Abstract

The application of advanced principles of physics to specific application geometries may open novel avenues to solve biological dilemmas such as cancer treatment. We have found that weak magnetic fields generated by serial fluctuations of approximately 3 ms point durations can penetrate tissue, elicit powerful analgesia and reduce the growth of malignant cell lines (but not normal lines) and tumors in mice. We designed systematic experiments to discern the precision of the point durations as well as the specific circuitry required for the maximum effect. The results of 175 experiments with the cell cultures (melanoma, B16-BL7) and 20 with groups of mice involving 18 different configurations of exposure, combinations of computers, and variations of the digital-to-analogue (DAC) opto-couplers indicated that the circuitry that generated the most consistent effect produced 3.2 ms point durations for the same temporally-structured magnetic field pattern. "Tuning" of the DAC, solenoids that generated the field and the circuit by appropriately varying the circuit resistance determined the range of the growth-inhibiting effect. The importance of precision in molecular structure for receptor-sequestering is an established principle. Whereas spatial patterns determined pharmacological effects, temporal patterns appear to determine magnetic field effects. What appears to be "the same" equipment may not

generate the precision of point durations, which may be in the order of a fraction of a millisecond, that are required for maximum inhibitory effects of malignant cell growth.

7.1 Introduction

Matter, be it expressed as de Broglie "matter waves" or aggregates of particle-mediated electromagnetic fields, is the primary constituent of living systems. For the last 10 years we have been pursuing the equivalence between the spatial organization of molecules that constitute matter and its particulate expressions such as molecules and the temporal ordering of energy that is often described as electromagnetic patterns [1,2]. There have been several recent reports that appropriately patterned amplitude- modulated electromagnetic fields may delay or attenuate the growth of malignancies [3]. Extremely low frequency, physiologically patterned magnetic fields have the potential to penetrate the volume [4] of the exposed person or test animal such that any "effect", unlike most chemotherapies, is not dependent completely upon vascular boundaries or distributions. Recently Murugan et al [5] found that exposure of human breast cell lines to a microTesla, physiologically-patterned magnetic field that produces analgesia equivalent to an injection of 4 mg/kg of morphine in rats [6] and planarian [7] did not (unlike morphine) initiate activation of proliferation pathways.

If the metaphor employed by Martin et al [8] is applicable whereby spatial (molecular) structure determines the functions of molecules and the configuration of temporal patterns (complex

frequencies) determines the functions of electromagnetic fields, then one would expect inordinate numbers of "patterns" to exist with specific temporal parameters that, if optimally selected, could directly affect specific types of cancer as indicated by Barbault et al [9]. The specification of such temporal precision may accommodate the variability of effects from historical attempts to treat cancer cells with applied magnetic fields. Here we present evidence that suggests the precision of timing is required to reduce the growth *in vitro* and *in vivo* of one type of malignant cell. The results emphasize the importance of precision engineering and calibration according to non-traditional theories.

There are several murine studies indicating the appropriately patterned rather than sinusoidal, symmetrical magnetic fields can reduce tumor growth. Yamaguchi et al [10] showed the mice injected with B16-BL6 melanoma cells and exposed to a 0.25 T, 25 Hz (238 μs) pulses for 17 days displayed reduction of tumor growth. Crocetti et al [11] showed that 20 Hz, 3 mT pulsed magnetic fields were toxic to MCF-7 breast cancer cells but not to normal MCF-10 cells. In contrast Babincova [12] found that two-dimensional C6 rat glioma tumors exposed to 10 mT, 10 to 50 Hz fields increased growth. Hu et al [13] exposed mice in which melanoma cells had been injected to a variety of classical application geometries for 2 to 5 μT-intensity magnetic fields

and found profound reduction in tumor growth (to about $1/5^{th}$ that of controls) in one particular pattern that was rotated systematically in each of the three spatial planes within the volume where the mice were exposed. The reduction of tumors was more effective than the Yamaguchi et al procedure [14] that involved intensities 100,000 times more intense. The effect was precisely coupled to the timing of the pulses. In a manner similar to high and to low affinity receptor types optimal magnetic field treatments may be finely tuned to temporal structure rather than intensity, *per se*. Recently Buckner et al [15] found that the same magnetic field temporal structure (μT) that inhibited tumor growth in the Hu et al [16] study involved T-Type calcium channels at the same intensities. Blocking the T-channels eliminated the magnetic field attenuating effect on cell proliferation.

We have generated these effective fields through programmable computer software that operated through custom-constructed, digital-to analogue converters to the specific application geometry such as different shaped coils or arrays of solenoids. Subsequent extraordinarily detailed work by Buckner [17] who examined different point durations of the voltages that contributed to the specific pattern for a variety of cell cultures indicated that 3 ms per point for a frequency modulated field composed of 849 points reduced growth in several human and

mouse malignant cell lines for different tissues but *did not affect* the growth of non-malignant cells. The same pattern presented with shorter, e. g., 2 ms or 1 ms, or longer 4 ms, 5 ms, point durations produced minimal effects. A similar maximum effect from 3 ms point durations for this frequency-amplitude modulated magnetic field was clearly apparent for fluorescent calcium influx into melanoma cells as measured by confocal microscopy during the optimal field exposures was evident after 15 min, conspicuous after 30 min of exposure, and achieved asymptote around 1 hr.

The selection of the 3 ms point duration was derived from a large-scale physics theory that related Planck's Length to the Hubble's Constant (H) with respect to the time require for a particular length (d) to expand one Planck's Length (P_L) [26]. This was expressed as: $[(H \cdot d) \cdot P_L^{-1}]$. Assuming a Hubble's parameter of 74.8 $km \cdot s^{-1} \cdot$MParsec , the time would be solve for 3.2 ms for a proton and 1.1 ms for an electron based upon contemporary assumptions about the linear extent (diameter) of those "particles". Several experiments involving excess correlation [13, 24] strongly suggested that point durations associated with 3 ms of appropriately patterned rotating magnetic fields with dissociation between the group and phase velocity was

associated with the proton while 1 ms was associated with the electron.

Exposure systems that have been most effective involve primarily IBM 286 computers and Complex (© Stanley A. Koren) software which operates the digital to analogue converter through optic couplers [18]. This array provides the most stable timing is intrinsic to the system. More advanced computers that do not operate by DOS or that employ WINDOWS display variable timing and inconsistent point durations. Even computers with the same specifications contain different components that can affect temporal precision. In non-carcinogenic settings, the precision of the point durations determine the efficacy of analgesia. For example 30 min whole body exposures of rats to 3 ms point durations of the patterned fields (that slow tumor growth) produce analgesia [15,16] to thermal or electric stimuli. The alteration in nociceptive thresholds is equivalent to an injection of 4 mg/kg of morphine. Similarly complete dissolution of planarian occurred after only five days of 3 hr daily exposures to a specific tandem sequence of two different patterned fields if these precise point durations composed the sequences [18]. However there have been inconsistencies of the inhibition of growth of the malignant cells that is typical of hardware operations. Here we present the summary of efficacies for one malignant cell line (B16, mouse melanoma) and their

growth in mice and show the importance of *precision* for the point duration. The solution appears to require the integration and application of physics, engineering and the appreciation for quantitative (mathematical) precision.

7.2 Method

7.2.1 Cells

We employed the same method in an exact manner for a total of 175 experiments involving B16-BL6 murine melanoma cells. They were cultured *in vitro* in DMEM containing 10% fetal bovine serum and antibiotics in a CO_2 incubator (copper jacketed) at 37° C. Plated cells were exposed in the same manner for all experiments. The plates containing the cells were Starstedt 60 x 14 mm. They were placed within the same position (in the middle) within a 10 cm x 10 cm x 10 cm plastic box to which six (3 pairs) of solenoids (modified reed relays) were affixed midway along each plane. The solenoids were connected so that the applied field, which was always the same pattern, was generated in each of the three planes simultaneously. Each solenoid was 50 Ω, embedded with a small nail (to enhance the field) and contained within a plastic (film) canister. The strength of the field within the plate exposure area ranged from 3 to 5 μT during the presentation of the pattern and was measured by several different types of power meters. Immediately proximal to the solenoids on the wall

of the exposure area the intensities are 14 to 16 μT. The strength of the field was based upon the theoretical calculations by Persinger and Lafrenie [28] which considered the equivalent energies for the typical hypopolarization of plasma membranes of most cancer cells relative to non-malignant cells as summarized by Levin [9] and others.

The plates were exposed to the magnetic field pattern for 1 hr per day for 5 successive days. Cell cultures in the sham condition, accompanying each field condition for each experiment, were placed in the exposure apparatus except the fields were not activated. Each day, after exposure, one of the plates from each condition (field, sham) was harvested to observe the effects of the specific pattern upon cell proliferation. Cells were harvested following incubation in trypsin and collected by centrifugation at 400 x g for 10 min. The cell pellets were re-suspended in PBS containing 0.1% trypan blue. A hemocytometer was used for quantification. For each sampled plate eight separate counts of live cells were obtained and averaged. The percentage inhibition of cell growth in the magnetic fields for each experiment was obtained by dividing the average numbers of cells for the field exposed plate to its sham field control and subtracting that value from 100.

7.2.2 Mouse Exposures

All mouse exposures (19 different experiments) were completed over three years as similarly as possible. After habituation to standard colony conditions for at least two weeks, male C57 mice, between 60 days and 160 days (similar age for a given experiment) and maintained 4 per cage were injected subcutaneously with 100 µL of B16 cells over the right flank. There were approximately $5 \cdot 10^5$ cells injected. Over the subsequent 20 days mice from the same cage were exposed to the same magnetic field pattern as the one employed for the cells or to the same sized plastic box with no field presentation. The exposure box, which was the same one employed in the Hu et al [8] study that produced the largest effects, was 30 cm by 30 cm by 30 cm. However because of the increased volume, different solenoids (50 ohm, 28-I-24VDC, Guardian Electric Manufacturing, Woodstock, IL, USA) that were affixed midway on each wall and were inserted with a 20 x 0.75 cm iron rod to enhance the field intensity. The experimental magnetic field strength in the middle of the box was 2.5 µT and about 5 µT along the periphery.

The computers that operated the mouse exposure box rotated the activation of the pairs of solenoids every 0.5 s such that the field was presented in each spatial plane sequentially and then in all 3 planes simultaneously. Hence each cycle was 2 s (0.5 Hz spatial rotation frequency). The mice were exposed during the

scotophase (after 8 P.M.) in the dark (or red light) for 3 hr every night for 20 days. When the tumor growth was sufficient to met Animal Care Guidelines in any given mouse the entire experiment was terminated by barbiturate injection, carbon dioxide exposure or decapitation. The melanomas were excised carefully and weighed to the nearest 0.01 gm. The percentage suppression of tumor growth was obtained by dividing the average mass of the tumors of the mice exposed to the field by those exposed to the sham fields and subtracting that value from 100.

7.2.3 Equipment Design and Specifications

The accessibility to the broad capacity of the personal computer and the Complex Software developed by Professor S. A. Koren allowed flexibility that could not be derived from function generators that generated only square, sine or saw-tooth waves. The software and equipment were created by Koren and Persinger (U.S. Patent 6,312,376 B1: November, 2001; Canadian Patent No. 2214296). Any pattern that can be digitized, mathematically derived or imagined can be transformed to real time temporal configurations by converting a column of numbers from 1 through 256 to -5 to + 5 V where 127=0 volts.

The base software allows programmable values (as integers) in ms for the following parameters. The first is the point duration. This is the time each number (from 1 through 256) is converted to

its appropriate voltage. Although point durations have been tested as integers between 1 ms and 69 ms, the optimal point durations for diminishing growth of malignant cells without affecting "normal" cells remained around 3 ms. Subsequent experiments indicate the precision involves at least the first decimal point. Consequently additions to the circuitry allowed selection of point durations with decimal points. Different computers (even the same model) have different port times, i.e., the latency between generating the DAC voltage with each change in number that can alter temporal precision. The second parameter is the time between the presentation of a pattern, or the inter-stimulus interval. This determines the progressive continuity of the pattern and, in light of the "temporal sensing" capacity for cells, is an important feature for discerning mechanisms.

The files (columns of numbers between 0 and 257) from which the exposure patterns are generated have typically ranged from 239 to 9,999 points. One sequence, composed of 849 points, traditionally labeled as the "Thomas pattern" [16,31] has been particularly effective in slowing the growth of only tumor cells (human and animal) *in vitro* and diminishing the size of tumor weights in mice injected with melanoma cells. This pattern is shown in Figure 1. Spectral analyses of the Thomas pulse at 3 ms point durations have indicated most of the power for the amplitude fluctuations is between about 6 and 25 Hz.

When the point duration is programmed to be 3 ms the software reads each successive number (1-256) and transfers this information to a digital-to-analogue (DAC), custom-constructed converter. This device, whose central component components involve an optocoupler, Tyristor, Triac Switch and light emitting diodes (LEDs) within the complex electronic circuit [14], transforms the voltage into current that is then delivered to the three pairs of solenoids oriented in the three spatial planes. At any given time the magnetic field is generated between the two opposite solenoids in the same plane. The field can be rotated through each plane singly (X, then Y, then Z) and then in all planes (X,Y,Z) simultaneously, or, presented in all three planes continually. Our experimental work indicated that for (effectively) two dimensional cell plates rotation of the magnetic pattern through the planes is not required. For three-dimensional and moving mice the optimal effect is enhanced by rotation of the field pattern through the 3 planes.

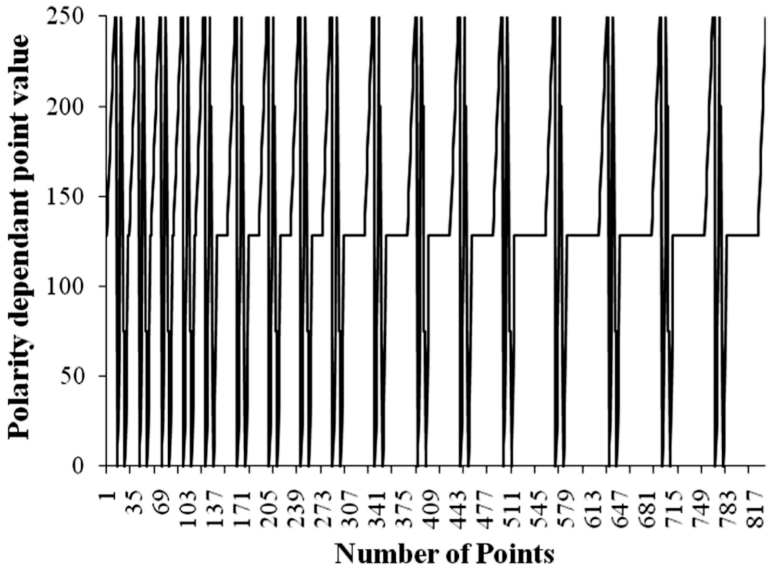

Figure 1. The shape of the frequency shifting magnetic field. The horizontal axis was composed of 839 points each with a duration of 3 ms. The vertical axis refers to the amplitude which was an expression between -5 V and +5 V from the conversion of numbers from 0 through 256 with 127=0 V. The functional frequency was about 28 Hz to 6 Hz.

The application or field generating devices are similar for cell and for mouse exposures and differ primarily in volume and type of solenoid in order to maintain more or less similar intensities. We have found that an average magnetic field strength in the exposure area should be about 25 to 30 mG which matches theoretical and empirical [28] predictions and results. An example of the cell exposure units are shown in Figure 2. For the present studies the mice were removed from their home cage for the exposures. More recently a large mouse exposure unit has been developed where the entire home cage is inserted. Standard exposure times for the cells were 1 hr per day for 5 days. To reiterate, the standard exposure times for the mice were 3 hr per night for 15 or 20 nights (usually in red light or dark conditions to minimize disruptions of melatonin) until tumor size criteria were obtained.

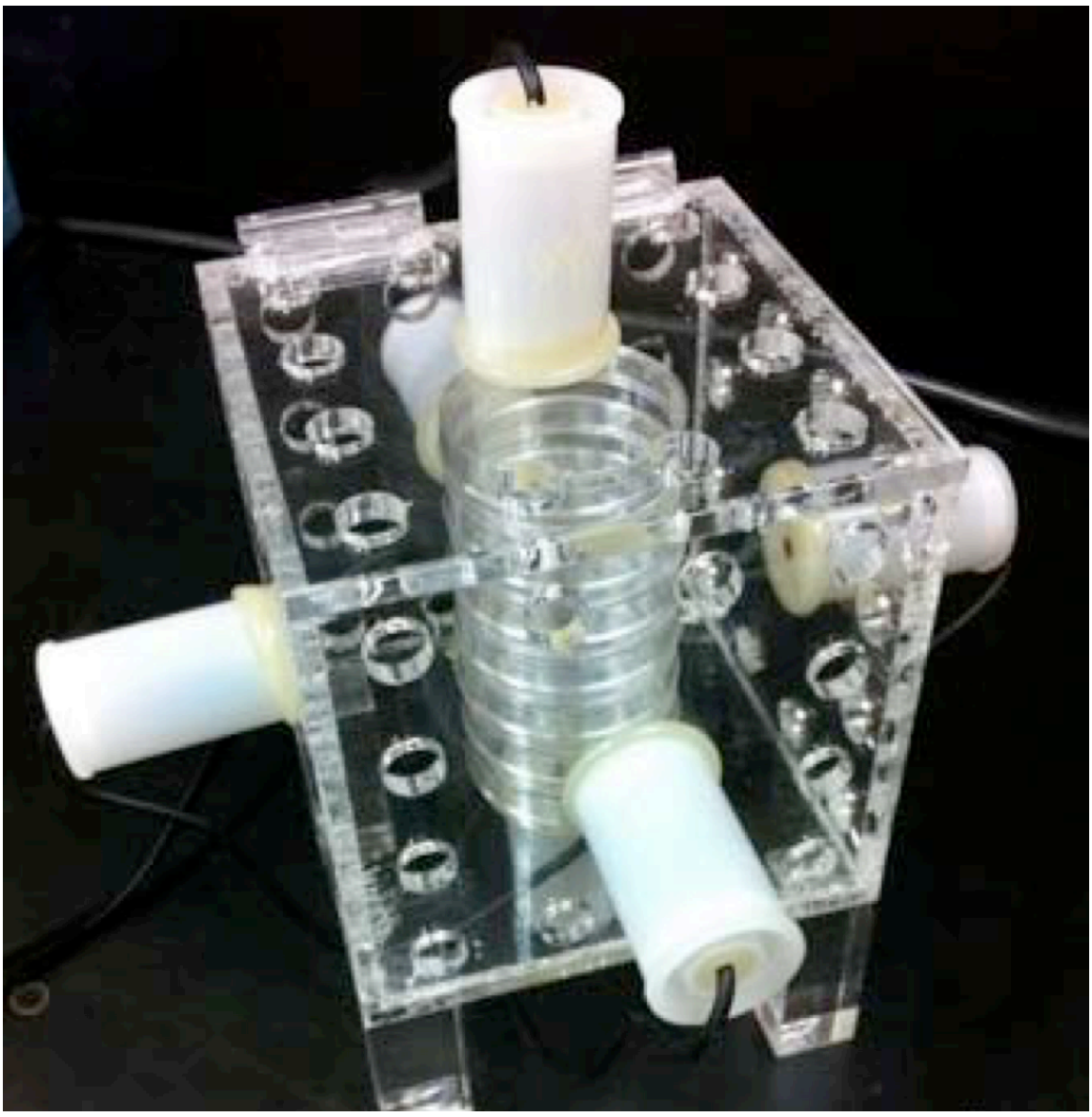

Figure 2. An example of the acrylic 10 cm x 10 cm x 10 cm box through which pairs of solenoids generated the pattern in Figure 1 in each plane simultaneously. The stacks of cell dishes can be seen in the middle of the box.

In the following experiments a variety of DAC units built from the original specifications of the patent with various substitutions for components were explored for their efficacy to generate magnetic fields through application geometries and to slow cancer cells *in vitro* or reduce the masses of the tumors in mice for B16 cells. This exploration was necessary because of the precision that is required for the timing of the point durations that compose the magnetic fields. Because manufacturers terminate or change specifications of production of components and the actual geometry of the relationship within the DAC units contributed to efficacy, we explored all of the major iterations until a reliable system was obtained that should be able to be reproduced by any experimental or clinical researcher who adheres to the specifications.

7.3 Results

The results of all of the 175 experiments involving 5 daily, 1 hr exposures to the same patterned magnetic field produced by the same software but from different computer-DAC-exposure box interfaces for the B16 cell lines and groups of mice injected subcutaneously within these cells are shown in Table 1. Each value for the *in vitro* effect is a different experiment. A brief description of the idiosyncratic nomenclature for the different systems is contained in Appendix I. The percentage is the degree

of diminishment of growth compared to sham field reference cultures. The first obvious pattern is that some configurations of equipment produced no significant changes in cell growth compared to controls. Other configurations with the same cells and procedures were inconsistent.

Some configurations were consistent for both the diminishment of cell growth in culture and reduction in tumor size of the exposed mice. For example DAC Box 5, once a specific amplifier and opto-coupler (MC3010) was installed, delivered reliable effects. The replication of this circuit in a self-contained design without the interfacing computer, indicated by DAC Box 12 (PP) showed how the effect could be controlled by direct manipulation of the point duration between 2 Table 1. Descriptions of the various units that generated the magnetic fields, their effectiveness (relative change in cells counts compared to sham treatments) for cells and the effect on tumor weights for mouse studies (website).

Table 1. List and brief descriptions of the various types of Digital to Analogue converters employed within the 175 experiments, the in vitro effect on cell growth in terms of relative change in cell counts. Percentages indicate the proportion of cell growth suppression compared to shame field controls. In vivo effects on tumor weights in mice that exposed

to a larger equivalent of the box in Figure 2. refers to the proportional diminishment of the tumor weight as well.

Equipment (DAC)		*In vitro* Effect Relative change in cell counts (%)	*In vivo* Effect Relative change of tumor weights (%)
DAC Box 1	DAC Box 1 Orignial 1.1 (amp 1)	0% ; 0%; 0%	0%
	DAC Box 1 Orignial 1.2 (amp 2)	0% ; 0%; 0%	-
	DAC Box 1 Orignial 1.3 (amp 3)	0% ; 0%; 0%	-
	DAC Box 1 Orignial 1.4 (amp 4)	21% ; 25%; 15%, 20%	0%
	DAC Box 1 Orignial 1.5 (amp 4 + opto 1- MC 3010)	20%; 20%; 24%; 20%; 15%; 22%	20%
	DAC Box 1 Orignial 1.6 (amp 4 + opto 2- MC 3011)	0% ; 0%; 0%	-
	DAC Box 1 Orignial 1.7 (amp 4 + opto 3- MC 3012)	0% ; 0%; 0%	-
DAC Box 2	DAC Box 2 MK-4-1	0% ; 0%; 0%	-
DAC Box 3	DAC Box 3 MK-3-2 1.1 (amp 1)	0%; 5%; 0%; 0%	-
	DAC Box 3 MK-3-2 1.2 (amp 2)	25%; 30%; 27%; 25%; 25%	-
DAC Box 4	DAC Box 4 Black 1.1 (amp 1)	5%; 10%; 6%; 5%	-
	DAC Box 4 Black 1.2 (amp 2)	0%; 0%; 0%; 0%	-
	DAC Box 4 Black 1.3 (amp 3)	30%; 31%; 20%; 25%; 32%	-
DAC Box 5	DAC Box 5 S-DAC 1.1 (amp 1)	0% ; 0%	-
	DAC Box 5 S-DAC 1.2 (amp 2)	0% ; 5%	-
	DAC Box 5 S-DAC 1.3 (amp 3)	0% ; 0%	-
	DAC Box 5 S-DAC 1.4 (amp 4)	35%, 36%, 30%, 25%, 30%, 29%, 25%, 30%	25%, 30%, 30%, 22%
	DAC Box 5 S-DAC 1.5 (amp 4 + opto MC3010)	30%, 30%, 34%, 33%, 30%, 29%, 37%, 25%, 31%, 35%	25%, 18%

	DAC Box 5 S-DAC 1.6 (amp 4 + opto MC3011)	10%; 11%; 7%; 10%	-
	DAC Box 5 S-DAC 1.7 (amp 4 + opto MC3012)	5%; 7%; 0%	-
DAC Box 6	DAC Box 6 C Thru 1.1	0%; 0% ; 0%	-
DAC Box 7	DAC Box 7 StanA 1.1 (amp1)	0%; 0% ; 0%	-
	DAC Box 7 StanA 1.2 (amp2)	0%; 0% ; 0%	-
	DAC Box 7 StanA 1.3 (amp2 + opto MC3010)	0%; 0% ; 0%	-
DAC Box 8	DAC Box 8 Sandwich 1.1 (amp1)	0%; 0% ; 0%	-
	DAC Box 8 Sandwich 1.2 (amp2)	0%; 0% ; 0%	-
	DAC Box 8 Sandwich 1.3 (amp3)	0%; 0% ; 0%	
	DAC Box 8 Sandwich 1.4 (amp4)	15%; 17%; 14%; 22%; 13%	11%
	DAC Box 8 Sandwich 1.5 (amp5)	31%, 25%, 27%, 30%	22%; 18%; 24%
DAC Box 9	DAC Box 9 Blue 1.1.	0%; 0%	4%
DAC Box 10 (PP)	DAC Box 10 MK-3-3 1.1	25%, 27%, 29%	-
DAC Box 12 (PP)	DAC Box 12 MK-3-4 1.1 (2ms)	0%; 2%, 0%	-
	DAC Box 12 MK-3-4 1.2 (2.5ms)	0%; 0% ; 0%	-
	DAC Box 12 MK-3-4 1.3 (2.9ms)	5%; 7%; 3%	-
	DAC Box 12 MK-3-4 1.4 (3ms)	10%; 11%; 7%	-
	DAC Box 12 MK-3-4 1.5 (3.1ms)	12%; 10%; 14%	-
	DAC Box 12 MK-3-4 1.6 (3.2ms)	25%; 22%; 19%	-
	DAC Box 12 MK-3-4 1.7 (3.25ms)	30%; 26%; 30%; 27%; 25%; 26%; 29%; 29%; 30%; 25%; 28%; 23%; 34%; 31%	30%, 25%, **

	DAC Box 12 MK-3-4 1.8 (3.5ms)	7%; 4%; 0%	-
	DAC Box 12 MK-3-4 1.9 (4ms)	0%; 0% ; 3%	-
DAC Box 13	DAC Box 13 RandomRockRoom 1.1	0%; 0% ; 0%	-
DAC Box 14	DAC Box 14 Original Animal Colony	0%, 3%, 0%	7%, 5%
DAC Box 15 (Hybrid PP)	DAC Box 15 BlkReverse 1.1 (3ms)	10%; 7%; 11%; 4%	-
	DAC Box 15 BlkReverse 1.2 (3.25ms)	40%; 38%	-
DAC Box 16	DAC Box 16 Water	5%; 0%; 4%	7%
DAC Box 17	DAC Box 17 A227 Burst	0%; 0%; 0%	-
DAC Box 18 (PP)	DAC Box 18 1PP3.25 1.1	27%	-
DAC Box 19 (PP)	DAC Box 19 0PP3.25 1.1	24%	-

2 ms and 4 ms with the peak effect around 3.2 ms. The coefficient of variation of diminishment of cell growth after 5 days in vitro was remarkably small and was also evident in the tumor growth suppression in the whole mouse exposures.

To emphasize the precision that is required to produce a reliable diminishment of cell growth *in vitro*, these values as a function of the point durations of the same pattern generated from the self-contained unit are shown in Figure 3. Each point involved between 2 and 10 replicates. The precision is within 0.1 ms around the 3.2 ms.

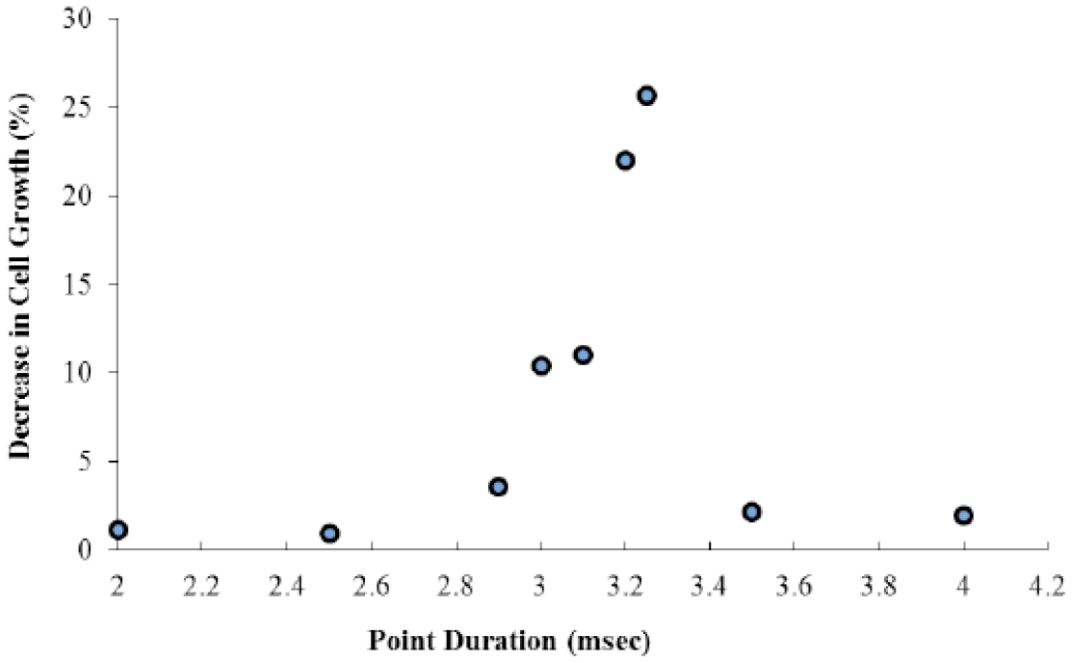

Figure 3. Percentage suppression of growth of melanoma cells as a function of the point duration (in msec) of the same magnetic field pattern.

Because all DACs (the circuits that generate the fields) possess two potentiometers the resistance could be modified. We selected the most effective PP DAC which produced 28% cell dropout. The resistance in one of the potentiometers was manipulated. This allowed the current flowing into the amplifiers and optocouplers to be increased or decreased. As shown in Figure 2, compared to the regular resistance of the system, increasing the resistance to an optimal level reduced the numbers by almost 50%. On the other hand decreasing the resistance attenuated the efficacy of this temporally patterned magnetic field to slow

cancer cell rate of growth. Control refers to cells that were not exposed to any manipulation. The data support the assumption that there is a tuning component that strongly influences the efficacy of the DAC for producing the type of magnetic field that maximally retards malignant cells growth.

7.4 Discussion

The advantage of employing physiologically-patterned, optimal intensity magnetic fields with specific point ("pulse") durations according to our results is that the fields *slow the growth of only malignant cells* but not normal (non-malignant) cells. Buckner et al [2] measured the growth rates of about six different malignant cell lines involving both human and mouse sources and found that only the cancer cells were affected. Growth of different lines of normal cells did not differ from those exposed to sham-field reference conditions. This may have an advantage over traditional treatments such as radiation and chemotherapy which tend to adversely affect all cells even with titration of intensities and dosages. From that perspective the frustrations and challenges of pursuing this new technology are warranted.

There is a general principle in science and medicine that structure dictates function. From a biochemical and pharmacological context this involves the spatial precision of the molecular structures with respect to the molecules within

which they are sequestered. From the perspective of electromagnetic fields the efficacy can be considered to be a function of their temporal precision. Although there is no clear "Rosetta Stone" that allows systematic equivalence between specific molecular structures and precise temporal patterns of electromagnetic fields or energies its ultimate discovery could illuminate the relationship between the particle (molecular) and wave (energetic) expressions.

Irena Cosic's Resonance Recognition Model [3] that relates energy to the spectral density of spatial periodicity of amino acid sequence in proteins may be a first step to this unification. Dotta et al [6,7] have found that specific wavelengths of photons within the visible range emitted from B16 cells that correspond to particular molecular pathways are increased or decreased by specific agonists and antagonists to within the band of about 10 nm. The wavelength of the specific component of the pathway was exactly predicted by Cosic's equation. These experiments indicated proof of principle that specific molecular structures exhibited parallel, specific patterns of electromagnetic energies.

If the complex but specific patterned magnetic field can simulate the cellular function of specific pharmacological treatments or even indigenous molecular pathways then the difficulties concerning vascular distributions and permeability

(diffusion) may be minimized. We have shown that these patterned magnetic fields within the μT range exhibit very effective penetration [27]. The issue that "pervasive penetration" implies a limited ability to "focus" the beam may not be an issue if the applied field is designed to overlap only within specific targets defined by their intrinsic resonance, Cosic solution, or electromagnetic activity.

For comparisons hypophyseal peptides are release into the entire blood and are "distributed profusely". However their effect is dependent upon the "congruence" of structure with specific receptors contained within specific locations. Finally the effects of the fields are likely to involve quantities of energies typical of those found at the level of ligand-receptor sequestering and resting membrane potentials, i.e., 10^{-20} J [25] rather than or in addition to the usual Faradic inductions. As shown by Karbowski and Persinger [11] the ratio of the magnetic moment of a proton to the unit charge multiplied by viscosity of water produces a force that when applied across the distance of O-H bonds results in 10^{-20} J. All of the reactions within cells occur within water. Our calculations and measurements indicate that the intensities employed in our experiments produce energies sufficient to enhance the release of photons [7]. We have considered ultraweak biophoton emissions [23] as the ultimate source of "communication" and "information" from cells that

initiate or terminate the massive cellular machinery that ultimately becomes the cancer cell [22].

The unique properties of physiological (ion containing) water with its capacity to "store" photonic energy [12] or to entrap specific resonant magnetic fields may be central to the malignant cell inhibiting effects of weak, physiologically-patterned magnetic fields as well as a source of variability. The brilliant work of Pollack [30] has emphasized the colloidal or gel state of water within living systems particular at the interfaces with surface. This interfacial water displays increases in viscosity by a factor of 10 compared to bulk water. The accompanying sheets of free protons are sufficient to accommodate the potential difference that defines plasma membrane potentials. We suggest that the future technology may require extremely fine tuning of the spatial and temporal parameters of the magnetic fields required to stop or even eliminate malignant cell growth without adversely affecting normal cells.

We had initially selected the Koren Complex software to generate the magnetic fields through custom constructed digital-to-analogue because of the remarkable flexibility for manipulating timing variables. They involve the point durations that each voltage generated by each of the numbers that compose the pattern, the complexity of the pattern and the time between the patterns. This produces the flexibility and capacity to copy

and to digitize natural patterns that could be then re-applied to target cell populations. The research involving human [29], rat [16] and cell [10] exposures indicated that point durations of about 3 ms were optimal for producing the maximum physiological endpoint. Point durations that were less or more, e.g., 2 ms or 4 ms, were shown to be less or not effective to influence the criterion measure.

What we learned from the present study is that all computers even with the same specifications by the manufacturer and electronic components that are considered "equivalent" are not the same. Although our original design of programmable parameters through the software adjusted to different computer types (e.g., IBM 286, 486, Pentiums, etc) through additional software was an admirable goal, the introduction of Microsoft software with its potential for simultaneously processing a myriad operations in the background to produce the "same" output for the human operator, produced fluctuating timing. This can modify or eliminate the slowing of cancer cell growth by these fields. This reiterates the concept that adding variables may allow consistency at the level of a larger increment of temporal observation but occurs at the expense of greater variability within the much smaller multiple increments of time that produce this stability.

Once the consistency of the base timing of 3.25 ms (from which the effective field patterns were generated) was obtained through a fixed electronic network with quantitative specification of each of the components (particularly the optocouplers) within the system the effects of diminished cell growth for B16 cells became reliable in magnitude. As noted in Table 1, the coefficient of variation was less than 5% which suggests that the contributions for Gaussian factors, where the coefficient of variation (for a normal distribution) is about 30%, has been minimized. This is characteristic of a robust effect.

One of the frequent frustrations in cancer research is the translation from cell line effects to organism effects. We found that the 3.25 ms point duration was optimal to produce the shift in melanoma cells and slow their rate of growth over 5 days. This reflects two levels of discourse: ionic (and presumably membrane) and cellular. The comparable magnitude reduction in the mass growth of tumors in C57 mice when the optimal point durations were applied suggests the effect from the precision of the timing of the magnetic fields generalizes to the entire organism. Thus far our method has not been applied to human patients. However the success of Brabault et al [1] indicates the feasibility of this application.

7.5 References

[1] Barbault, A., Costa, F. P., Bottger, B., Munden, R. F., Bohmolt, F., Kuster, N., Pasche, B. Amplitude-modulated electromagnetic fields for the treatment of cancer: discovery of tumor-specific frequencies and assessment of a novel therapeautic effect. J. Exper. Clin. Cancer Res. 28 (2009) 51(1-10).

[2] Buckner, C. A., Buckner, A. L., Koren, S. A., Persinger, M. A., Lafrenie, R. M. Inhibition of cancer cell growth by exposure to a specific time-varying electromagnetic field involves T-type calcium channels. PLOS One, 2015: DOI: 10.1371/journal.pone.0124136.

[3] Cosic, I. Macromolecular bioactivity: is it resonant interaction between macromolecules? Theory and applications. IEEE Trans. Biomed. Eng. 41 (1994) 1101-1114.

[4] Costa, F. P., de Oliveira, A. C., Meirelles, R., Machado, M. C., Zanesco, T., Surhan, R., Chammas, M. C., de Souza Rocha, M., Morgan, D., Canter, A., Zimmerman, J., Brezovich, I., Kuster, N., Barbault, A., Pasche, B. Treatment of advanced hepatocellular carcinoma with very low levels of amplitude-modulated electromagnetic fields. Brit. J. Can. 105 (2011) 640-648.

[5] Crocetti, S., Beyer, C., Schade, G., Egli, M., Frohlich, J., Franco-Obregon, A. Low intensity and frequency pulsed electromagnetic fields selectively impair breast cancer cell viability, PLOS One 8 (2013) Issue 9.

[6] Dotta, B. T., Lafrenie, R. M., Karbowski, L. M., Persinger, M. A. Shifting wavelengths of ultraweak photon emissions from dying melanoma cells: their chemical enhancement and blocking are predicted by Cosic's theory of resonant recognition model for molecules. Naturwissenchaften 101 (2014) 87-94.

[7] Dotta, B. T., Lafrenie, R. M., Karbowski, L. M., Persinger, M. A. (2014) Photon emission from melanoma cells during brief stimulation by patterned magnetic fields: is the source coupled to rotational diffusion within the membrane? Gen. Physiol. Biophys. 33 (2014) 63-73.

[8] Hu, J. H., St-Pierre, L. S., Buckner, C. A., Lafrenie, R. M., Persinger, M. A. Suppression of growth of injected melanoma cells by whole body exposure to specific spatial-temporal configurations of weak intensity magnetic fields. Int. J. Rad. Biol. 86 (2010) 79-88.

[9] Levin, M. Molecular bioelectricity in developmental biology: new tools and recent discoveries. Bioessays. (2012): DOI 10.1002/bies.201100136.

[10] Karbowski, L.M., Harribance, S. L., Buckner, C. A., Koren, S. A. et al. Digitized quantitative electroencephalographic patterns applied as magnetic fields inhibit melanoma cell proliferation in culture. Neurosci. Lett. 523 (2012) 131-134.

[11] Karbowski, L. M. and Persinger, M. A. Variable viscosity of water as the controlling factor in energetic quantities that control living systems: physiochemical and astronomical interactions. Int. Lett. Chem. Phys. Astron. 4 (2015) 1-9.

[12] Karbowski, L. M., Murugan, N. J., Persinger, M. A. Experimental evidence that specific photon energies are "stored" in malignant cells for an hour: the synergism of weak magnetic field-LED wavelength pulses. Biol. Med. 8 (2016):1 (BM-162-16).

[13] Koren, S. A., Dotta, B. T., Persinger, M. A. Experimental photon doubling as a possible local inference of the Hubble Parameter. Open Astron. J. 7 (2014) 1-6.

[14] Koren, S. A., Bosarge, W. E., Persinger, M. A. Magnetic fields generated by optical coupler circuits may also be containment loci for entanglement of P-N junction-plasma cell membrane photons within exposed living systems. Int. Lett. Chem. Phys. Astron. 3 (2015) 84-105.

[15] Martin, L. J., Koren, S. A., Persinger, M. A. Thermal analgesic effects from weak, complex magnetic fields and pharmacological interactions. Pharm. Biochem. Behav. 78 (2004) 217-277.

[16] Martin, L. J., Koren, S. A., Persinger, M. a. Influence of complex magnetic field application in rats upon thermal nociceptive thresholds: the importance of polarity and timing. Int. J. Neurosci. 114 (2004) 1259-1276.

[17] Michalak, K. P., Nawrocka-Bogusz, H. The changes of the frequency specific impedance of the human body due to the resonance in the kHz range in cancer diagnostics. J. Phys. 329 (2011) 012024.

[18] Murugan, N. J., Karbowski, L. M., Lafrenie, R. M., Persinger, M. A. Temporally patterned magnetic fields induce complete fragmentation in planaria. PLOS One, 2013.

[19] Murugan, N. J., Karbowski, L. M., Persinger, M. A. Serial pH increments (20 to 40 millisesconds) in water during exposures to weak, physiologically-patterned magnetic fields: implications for consciousness. Water 6 (2014) 45-60.

[20] Murugan, N. J., Persinger, M. A. Comparisons of responses by planarians to micromomolar to attomolar dosages of morphine or naloxone and/or weak pulsed magnetic fields: revealing receptor subtype affinities and non-specific effects. Int. J. Rad. Biol. 2014.

[21] Murugan, N. J., Karbowski, L. M., Persinger, M. A. Weak burst-firing magnetic fields that produce analgesia equivalent to morphine do not initiate activation and proliferation pathways in human breast cells in culture. Int. Can. Sci. Thereap. 1 (2014) 47-50.

[22] Murugan, N. J., Dotta, B. T., Karbowski, L. M., Persinger, M. A. Conspicuous bursts of photon emissions in malignant cells following injections of morphine: implications for cancer treatments. Int. J. Curr. Res. 6 (2014) 10588-10592.

[23] Murugan, N. J., Karbowski, L. M., Lafrenie, R. M., Persinger, M. A. Maintained exposure to spring water but not double distilled water in darkness and thixotropic conditions to weak (1 uT) temporally patterned magnetic fields shift photon spectroscopic wavelengths: effects of different shielding materials. J. Biophys. Chem. 6 (2015) 1-9.

[24] Persinger, M. A. Experimental evidence that Hubble's Parameter could be reflected in local physical and chemical reactions: support for Mach's principle of imminence of the universe. Int. Lett. Chem. Phys. Astron. 11 (2013) 86-92.

[25] Persinger, M. A. Thixotropic phenomena in water: quantitative indicators of Casimir-magnetic transformations from vacuum oscillations (virtual particles). Entropy 17 (2015) 6200-6212.

[26] Persinger, M. A., Koren, S. A. A theory of neurophysics and quantum neuroscience: implications for brain function and the limits of consciousness. Int. J. Neurosci. 117 (2007) 157-175.

[27] Persinger, M. A., Saroka, K. S. Minimum attenuation of physiologically-patterned, 1 microTesla magnetic fields through

simulated skull and space. J. Electromag. Analysis App. 5 (2013) 151-155.

[28] Persinger, M. A., Lafrenie, R. F. The cancer cell plasma membrane potentials as energetic equivalents to astrophysical properties. Int. Lett. Chem. Phys. Astron. 17 (2014) 67-77.

[29] Persinger, M. A., Murphy, T. Validating new technologies to treat depression, pain, and the feeling of Sentient Beings: a reply to "Neuroscience for the Soul". Neurosci. Med. 7 (2016) 27-44.

[30] Pollack, G. H. Cells, gels and the engines of life. Ebner and Sons: Seattle (2001).

[31] Thomas, A. W., Kavaliers, M., Prato, F. S., Ossenkopp, K.-P. Antinociceptive effects of pulsed magnetic fields in the land snail. Neurosci. Lett. 222 (1998) 107-110.

[32] Whissell, P. M., Persinger, M. A. Emerging synergisms between drugs and physiologically-patterned weak magnetic fields: implications for neuropharmacology and the human population in the 21st century. Cur. Neuropharm. 5 (2007) 278-288.

[33] Yamaguschi, S., Oguieu-Ikeda, A., Sekino, M., Ueno, SH. Effects of pulsed magnetic stimulation on tumor development and immune functions in mice. Bioelectromagnetics 27 (2006) 72-74.

7.6 Preamble to Chapter 8: Specificity of Circuit Structure Dictating the Importance of Proper Electromagnetic Field Propagation

Our experiments demonstrated that highly-specific point durations were central to our electromagnetic field effects which dissolved malignant cells without adversely affecting healthy cells. We wanted to know if we could tune the exposure devices with further increased precision. Based upon theoretical models, we suspected that phase shifts for the energy associated with proton movement could be involved with our effects. Therefore we decided to test our paradigm with alternative pre-optocoupler voltages to discern any relevant differences.

Chapter Eight

Experimental Demonstration That Aharanov-Bohm Phase Shift Voltages In Optical Coupler Circuits of Tuned Patterned Magnetic Fields Is Critical for Inhibition of Malignant Cell Growth

Published in Journal of Advances in Physics

(2016) – Vol: 11 (5). Pg. 1-8

Reproduced with Permission from CirWorld

Lukasz M. Karbowski, Nirosha J. Murugan, Robert M. Lafrenie and Michael A. Persinger

Abstract

The physical processes by which specific point duration magnetic fields affect aberrant expressions of living matter may involve non-classical mechanisms. The Aharanov-Bohm voltage for a quantum of energy that is convergent with the quotient of the proton's magnetic moment to its charge multiplied by the viscosity of water at homeostatic temperatures applied across the distance of O-H bonds in conjunction with its phase modulation is about ±4.3 V. Application of frequency shifting, temporally-patterned magnetic fields produced by 3 ms point durations at average intensities of ~28 mG (that are equivalent to Nernst thresholds for plasma membranes) generated through optocoupler light emitting diodes produced the strongest inhibition of malignant cells growth when the pre-coupler value for the circuit maintenance was ±4.3 V compared to increments of voltage below or above this value. Spatial expansion of the effective zone for growth diminishment also occurred with this pre-voltage level. These results indicate that phase modulation of the electrons mediating cellular molecular pathways may be central to the etiology and potential treatment of malignant cells but not to normal cells dynamics. Consideration of quantum effects rather than classical electromagnetic theory may be a more effective strategy for impeding the physical bases for the molecular pathways that define malignant cells.

8.1 Introduction

The theoretical bases for the marked efficacy of optocoupler systems to generate magnetic fields with point durations derived from universal constants, for example Hubble's parameter [1,2], to affect the activity of malignant but not normal cells at the level of the proton have been described by Koren et al [3]. The central role of quanta of $\sim 2 \cdot 10^{-20}$ J in the physical mechanisms [4] that mediate the information or digital patterns of activity within cells is evident within molecular pathways [5,6] and may originate from fundamental physical constants. For example the quotient of the magnetic moment of a proton ($1.41 \cdot 10^{-26}$ $A \cdot m^2$) and unit charge ($1.6 \cdot 10^{-19}$ $A \cdot s$) multiplied by the viscosity of water at Life temperatures ($8.94 \cdot 10^{-4}$ $kg \cdot m^{-1} \cdot s^{-2}$) results in a force that when applied across the distance of two O-H bonds ($1.92 \cdot 10^{-10}$ m) results in $\sim 2 \cdot 10^{-20}$ J [7]. This is the level of energy involved with the motion of protons manifested within hydronium ions [8]. The Aharanov-Bohm phase shift is an unusual but important quantum effect. As stated by Tonomura et al [9] "the predicted effect is the production of a relative phase shift between two electron beams enclosing a magnetic flux even if they do not touch the magnetic flux". It is described by:

$$\Delta\theta = qVt\ \hbar^{-1} \quad (1),$$

where ħ is the modified Planck's constant ($1.05 \cdot 10^{-34}$ J·s), q= the unit charge ($1.6 \cdot 10^{-19}$ A·s) and t is the duration within the voltage field. If the duration in the voltage field is a unit orbit, $1.5 \cdot 10^{-16}$ s, then for $qV \sim 2 \cdot 10^{-20}$ J the phase shift is $4.6 \cdot 10^{-3}$. Assuming the circumference of the standard Bohr orbit is $3.26 \cdot 10^{-10}$ m, the phase shift associated with 10^{-20} J would be within the range of the Compton wavelength of the electron ($2.4 \cdot 10^{-12}$ m). The phase modulation required for $2 \cdot 10^{-20}$ J is about $1.5 \cdot 10^{-12}$ m.

The Aharanov-Bohm equation can be reconfigured to solve for V if the phase shift is known. If $2 \cdot 10^{-20}$ J is assumed and θ, the phase modulation, has been estimated as shown earlier [10] then the V can be calculated by:

$$V=(\theta\hbar) \cdot (qt)^{-1} \quad (2),$$

As noted previously [10], if these appropriate parameters are inserted into (2) the resulting value for V is ~ ±4.3. One test of the validity of these quantified predictions is an experiment that allows systematic manipulation above and below the optimal value determined for the Arahanov-Bohm effect within the optocoupler circuitry that generates the magnetic field within which cells are exposed. Here we demonstrate powerful evidence for this effect.

8.2 Methods and Materials

In each experiment 6 plates (60 mm x 15 mm) each containing ~0.5 million B16 melanoma cells were placed in the middle of a 10 cm by 10 cm by 10 cm acrylic (0.7 cm thick) box within a standard incubator (NeuAir; water jacket; 188 L) maintained at 37°±1° C with 5% CO_2. The culture medium contained DMEM supplemented with FBS and antibiotics. The exposure equipment and procedures have been described in detail elsewhere [11]. In the center of each wall of the box a SPST-5VDC Reed Relay (275-0232) rated at 0.5 A at 125 VAC (250 ohms, 20 mA nominal current) had been mounted. A small nail had been inserted into each core of the solenoids to enhance the field strength concentration. The peripheral circuit was arranged such that each pair of solenoids in each plane was connected.

The presentations of the applied magnetic fields were systematically applied through all planes simultaneously. The strength of the magnetic field as measured within the centroid effective zone where the plates of cells were placed average 28 mG. The effective zone within which the largest cell effects have been demonstrated has been described previously [11]. This threshold for an effect was predicted quantitatively by Persinger and Lafrenie [12] and was based upon the magnetic field energy equivalent of the Nernst solution (26 mV) for plasma membranes independent of disparity of cation or anion concentrations. This

was considered critical because most malignant cells display plasma membrane resting membrane potentials within this range rather than the "normal" cell values of between -55 mV to -70 mV [13].

The pattern to which the cells were applied was the frequency modulated ("Thomas") pattern that has been shown to reduce the growth of several different types of malignant cells from human and mouse sources. However this manner by which the magnetic field pattern is generated does not affect the growth of non-malignant (normal) cells. The pattern which has been published several times [14,15] was composed of 849 values (numbers between 0 and 256). The transformation of 0 to 256 to -5 V to +5 V was completed through custom constructed software (© Professor Stanley A. Koren) that was applied through a digital to analogue converter (DAC) through a patented circuit involving optocouplers and Triac components. All of the circuit diagrams for this equipment have been published [3]. The programmable point durations defined as the time each voltage was presented through the circuit and ultimately to the pairs of solenoids to produce the magnetic fields to which the cells were exposed was 3 ms. This duration has been found to be most effective for slowing the growth of malignant cells as well as influx of calcium into melanoma cells where as shorter or longer point durations are less effective [16].

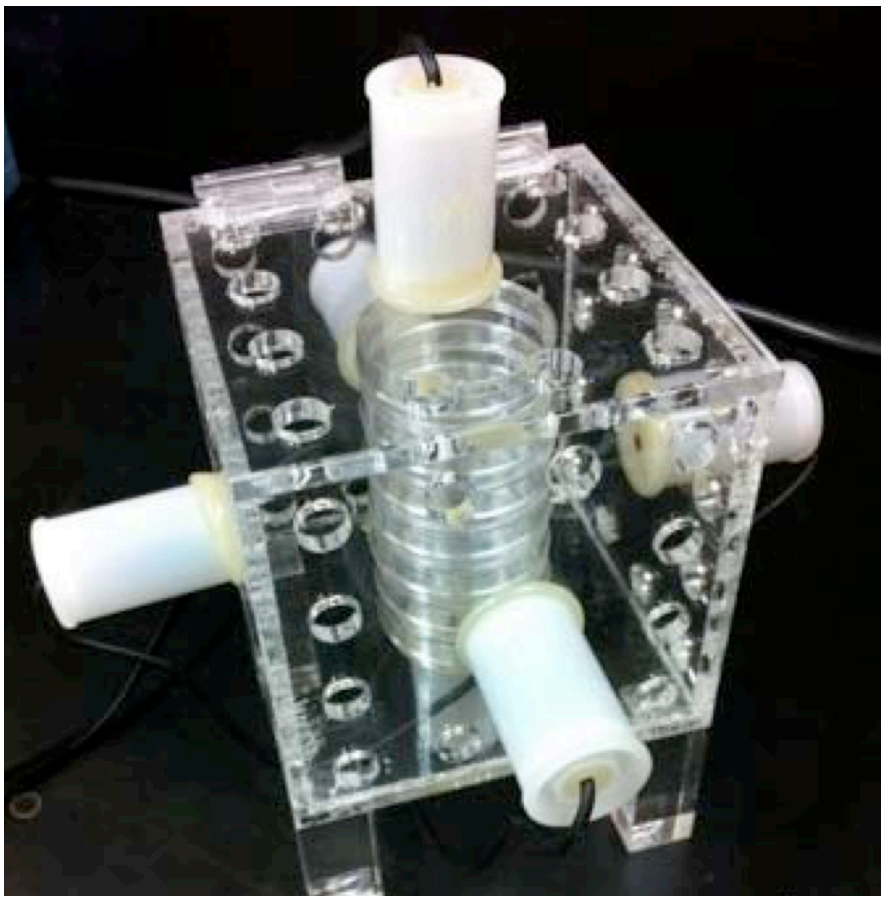

Figure 1. Exposure device within which a stack of 6 cell culture plates were placed. Each white cylinder contained the "solenoid" or reed switch. The fields were generated between opponent pairs of solenoids in each of the three spatial planes through a custom circuit composed of optocouplers, tyristors, Tirac switches and light emitting diodes. The optimal pre-optocoupler voltage predicted by the Aharanov-Bohm effect generated the largest cell effects.

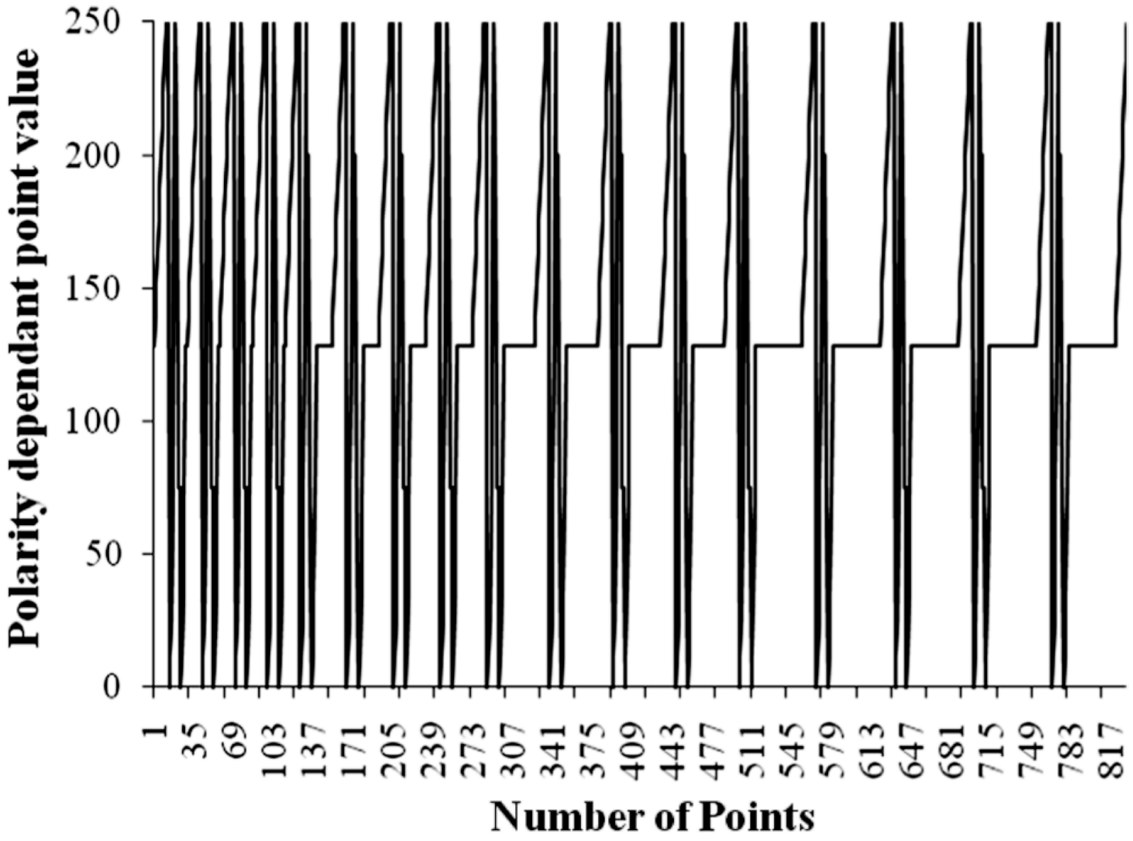

Figure 2. The temporal structure of the magnetic field pattern whose pre-optocoupler voltage by adjusted by Aharanov-Bohm solutions. Vertical axis indicates voltage that was optimally ±4.3 V. Horizontal axis reflects time in 3 ms increments for a total of 859 points for a total of 2.58 s per cycle.

Each experiment consisted of 5 successive days of 1-hour exposures to the same magnetic field pattern. The only manipulations were the calibrations that modified the peak voltage levels that were generated through the optocoupler that ultimately controlled the magnetic field intensity. The range of calibrations was 3.5 V, 4.0 V, 4.3 V, 4.5 V, 4.8 V, and 5.0 V. For any given experiment that same pre-voltage level was applied when the cell cultures were applied to every day for 5 consecutive days to the field for 1 hr. There were between 4 and 5 replicates for each pre-voltage value completed in random over a 4 months period.

8.3 Results

The results were conspicuous and reliable and were consistent with the predictions from the Aharanov-Bohm equation for a quantum of energy within the range of $\sim 2 \cdot 10^{-20}$ J which would involve the second shell energy levels most involved with the movement of protons in aqueous solutions [8]. As shown in Figure 3 the effectiveness (more than 50% dropout in malignant melanoma cells) of this patterned magnetic field was maximal when the maximum voltage was set at 4.3 V. Employing the peak voltage for the system (5.0 V) produced minimal inhibition of cell growth and was only marginally significant from no field presentation (sham controls).

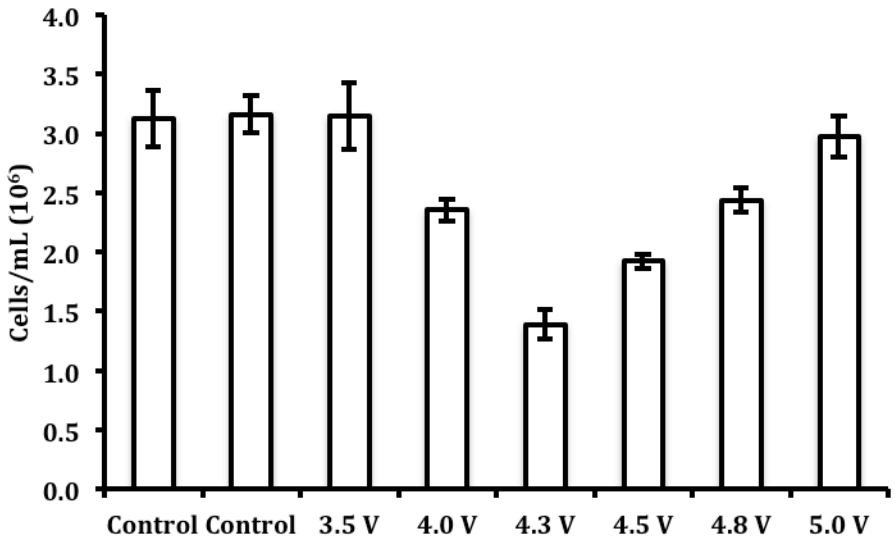

Figure 3. Numbers of cells present after 5 days of 1 hr per day exposure to the same magnetic field configurations as a function of the specific pre-optocoupler voltage. The 4.3 V predicted by the Aharanov-Bohm phase shift for the energy associated with proton movement in water (hydronium ion) produced the largest effect at this intensity and is consistent with the Persinger-Lafrenie estimate. Vertical bars indicate standard deviations.

There was also a quantitative shift in the size of the effect zone between the three pairs of solenoids within which the plates of cells were exposed. Uniquely, during the presentation of the 4.3 V configuration the effect of the field homogeneoulsy influenced all six plates stacked within the effective zone equally (see Figure 1). Typically only the two plates near the centroid zone where the imaginary lines between the three pairs of solenoids intercept showed the maxium effect.

8.4 Discussion and Conclusion

To our knowledge these experiments are the first to demonstrate the dependence of the efficacy of inhibiting malignant cell growth by optimizing the pre-voltage values that operating the optocouplers from which the magnetic flux is generated according to the precise predictions of a quantum phenomenon, the Aharanov-Bohm effect. The important feature of this effect is that neither increments of force nor energy are involved but rather than phase of the wave. This allows for the propagation of information even within shielded contexts as well as potential non-local effects. Assuming the activation energy ($\sim 10^{-20}$ J) involved with the movement of protons through hydronium ions (which in large part determine pH) and phase modulation, the calculated specific voltage was the precise value (within 0.1 V reflecting the limits of the equipment) that produced the largest

effect. The proportion of “dropout” or delayed growth was more than 60% which is the largest consistent effect that has been obtained with this paradigm.

The local effects that produce the causality within the cell cultures are most likely mediated by water. As masterfully described and pursued by Pollack and his colleagues [18, 19] water exhibits gel-like properties within discrete boundaries from surfaces, such as cell membranes. The exclusion zone (EZ) is associated with a 10 fold increase in viscosity and the creation of a layer of protons whose potential difference is up to 150 mV or the value that has been classically attributed to disparity of ion (e.g., potassium or chloride) concentrations across the plasma cell membrane. As described by Persinger and Lafrenie [12], almost all malignant cell membranes exhibit values similar to base Nernst solutions (26 mV). The magnetic field required to equate this voltage is about 28 mG, which is the average value with which we obtained are effects.

Del Giudice et al [20] have shown by calculation and application of variants of quantum theory that hundreds of water molecules exhibit simultaneous resonance in coherent domains with widths of ~100 nm which is within range of the 121.6 nm wavelengths [21] that results in $H_2O \rightarrow OH$ (N)+H producing OH radicals in their electronic ground state with the additional property of rotational quantum states that assume particular

quantum (integer) numbers, N. According to Del Giudice and Preparata [22] the application of the Dicke Hamiltonian below a specific temperature and atomic density describes a spontaneous, superradiant phase transition. This is a peculiar state where classical electromagnetic fields become trapped within ensembles of atoms oscillating in phase with the atomic transitions the specific excited states predicted by the Dicke model and ground states. A common frequency of the coherent matter in coherence domains within the 100 mV range and residing electromagnetic fields results in an energy equivalent to 0.26 eV or ~10^{-20} J. Del Giudice and Preparata [22] argued that because there is coupling between the vector potential of water and the vector potential associated with the electromagnetic fields in the environment, the phase of a system is changed by magnetic vector potentials. This is the Aharanov-Bohm effect and was demonstrated to precisely inhibit malignant growth in the current experiments.

Calculations indicate that the photons that mediate the optocoupler connections through the Triac circuit may be also represented within the center of the three-axis magnetic field within which the chemical reaction or organism is maintained. The magnetic field, if this model is valid, facilitates the containment. Persinger [23] quantified a relationship between the divergence of radiative phenomena associated with photons and the convergence within the electrical and magnetic properties of

space with each orbital rotation of an electron. He found that the order of magnitude of photon flux density ($\sim 10^{-12}$ $W \cdot m^{-2}$) that is associated with biophoton emissions in living systems when multiplied by the inverse of the product of the wave impedance applied over the hydrogen wavelength and divided by the magnetic permeability of a vacuum multiplied by the Bohr orbital frequency was $1.5 \cdot 10^{-20}$ J. Consistent with that approach is the energy per s for the more precise solution for this photon flux density ($1.9 \cdot 10^{-12}$ $W \cdot m^{-2}$) distributed over the area ($4.4 \cdot 10^{-2}$ m^2) of the neutral hydrogen line (21 cm). The energy ($8.36 \cdot 10^{-14}$ J) converges upon the equivalence for the rest mass of an electron.

The measurement of an expanded effective zone when the prevoltages determined by the phase modulation of the electron wave predicted by the Aharanov-Bohm relation were applied suggests that a standing wave emerged within the exposure containment. Typically the effect zone involves the central two plates of six stacked plates within the exposure box. The involvement of all six plates indicates that the volume of the effective zone increased by at least a factor of 3 to ~250 cc. Previous experiments whereby combinations of magnetic patterns had been employed indicated that the effective zone, within which there was zero cell growth, was about 85 cm^3 within the cross-sectional within the total volume (~1 L) of the exposure box whose external walls apposed the solenoids. Such precise tuning,

analogous to a type of emergent condensate within which coherence would occur over an unexpectedly extended space might produce the integrated domains predicted by Del Giudice and Preparata [22]. Additional explanations have been offered by Koren et al [3].

We can not exclude contributions from the background flutter of the circuit and the intrinsic frequency shifting of the applied temporal pattern. The flutter is about 10^{-9} T which is within the range of limits of measurement by our magnetometers. Assuming an ion channel exhibits a radius r ~0.5 nm in width and exhibit a current of 2 pA, which is within the range of Ca^{++} channels, the magnetic field for a cylinder, would be:

$$B=\mu I\ (2\pi r)^{-1} \qquad (3),$$

where μ is $4\pi \cdot 10^{-7}$ $N \cdot A^{-2}$ and I is current, about 10^{-9} A. From this context it is relevant that Pilla et al [24] found that the dissociation of the calcium ion from calmodulin exhibits two rates (k) equivalent to 10 to 40 Hz and 300 to 500 Hz. These are within the range of the frequency modulation of the temporal pattern of the applied magnetic field (~8 Hz to 30 Hz) and the point duration of 3 ms (333 Hz) from which the pattern is generated. Previous experiments indicate that the effect of this pattern as well as the movement of calcium through the membranes

of these cells through T-type channels [16] was not manifested when point durations are less or greater than 3 ms.

The precision of the 3 ms point duration may reflect a specific feature of proton dynamics within local and non-local space [25] that as predicted by Persinger and Lafrenie [12] may involve contributions from cosmological sources that emphasize the interaction between the photon and proton-electron interaction [3, 26]. Given the intricate relationship the viscosity of water and magnetic fields [7], the appearance of this state [27] in interfacial water, the potential role of biological water dynamics and entropy in cancer [28], a more profound biophysical origin might be responsible for this manifestation of matter. Considering the potential simultaneous particle-wave state that transports both phase and electron states from virtual particles to actual particles [29] marked precision of physical parameters within photocoupler circuits may be required to inhibit this process.

8.5 References

[1] Koren, S. A., Dotta, B. T. and Persinger, M. A. 2014. Experimental photon doubling as a possible local inference of the Hubble Parameter. Open Astron. J. 7, 1-6.

[2] Persinger, M. A. 2015. Variability of Hubble's Parameter, geomagnetic activity, and putative changes in space-mass density: implications for terrestrial cells growth. Int. Lett. Chem. Phys. Astron. 53, 137-145.

[3] Koren, S. A., Bosarge, W. E. and Persinger, M. A. 2015. Magnetic fields generated by optical coupler circuits may also be containment loci for entanglement of P-N junction-plasma cell membrane photons within exposed living systems. Int. Lett. Chem. Phys. Astron. 3(2015), 84-105.

[4] Persinger, M. A. 2010. 10^{-20} Joules as neuromolecular quantum in medicinal chemistry: an alternative approach to myriad molecular pathways. Cur. Med. Chem., 17, 3094-3098.

[5] Karbowski, L. M., Murugan, N. J. and Persinger, M. A. 2015. Novel Cosic resonance (standing wave) solutions for components of the JAK-STAT cellular signaling pathway: a convergence of spectral density profiles. FEBS Openbio, 5, 245-250.

[6] Persinger, M. A., Murugan, N. J. and Persinger, M. A. 2015. Combined spectral resonances of signaling proteins' amino acids in the ERK-MAP pathway reflect unique patterns that predict peak

photon emissions and universal energies. Int. Lett. Chem. Phys. Astron. 4(2015), 10-25.

[7] Karbowski, L. M. and Persinger, M. A. 2015. Variable viscosity of water as the controlling factor in energetic quantities that control living systems: physicochemical and astronomical interactions. Int. Lett. Chem. Phys. Astron., 4(2015), 1-9.

[8] DeCoursey, T. E. 2003. Voltage-gated proton channels and other proton transfer pathways. Physiol. Rev. 83, 475-579.

[9] Tonomura, A., Osakabe, N., Matsuda, T., Kawasaki, T. and Endo, J. 1986. Evidence of Aharanov-Bohm effect with magnetic field completely shield from electron wave. Phys. Rev. Lett. 56, 792-795.

[10] Persinger, M. A. and Koren, S. A. 2015. The Aharanov-Bohm phase shift and magnetic vector potential "A" could accommodate for optical coupler, digital-to-analogue magnetic field excess correlations of photon emissions within living aqueous systems. J. Adv. Phys. 11, 3333-3340.

[11] Karbowski, L. M., Murugan, N. J., Koren, S. A. and Persinger, M. A. 2015. Seeking the source of transience for a unique magnetic field pattern that completely dissolves cancer cells in vivo. J. Med. Sci. Engineer. 8, 531-543.

[12] Persinger, M. A. and Lafrenie, R. M. 2014. The cancer cell membrane potentials as energetic equivalents to astrophysical properties. Int. Lett. Chem. Phys. Astron. 17, 67-77.

[13] Levin, M. 2012. Molecular bioelectricity in developmental biology: new tools and recent discoveries. Bioessays 34, 205-217.

[14] Martin, L. J., Koren, S. A. and Persinger, M. A. 2004. Thermal analgesic effects from weak, complex magnetic fields and pharmacological interactions. Pharm. Biochem. Behav. 78, 217-227.

[15] Murugan, N. J. and Persinger, M. A. 2014. Comparisons of responses by planarians to micromolar to attomolar dosages of morphine or naloxone and/or weak pulsed magnetic fields : revealing receptor subtype affinities and non-specific effects. Int. J. Rad. Biol. DOI:10.3109/02699052.2014.916819.

[16] Buckner, C. A., Buckner, A. L., Koren, S. A., Persinger, M. A. and Lafrenie, R.M. 2015. Inhibition of cancer cell growth by exposure to a specific time-varying electromagnetic field involves T-type calcium channels. PLOS One, DOI: 10.1371/journal.pone.0124136.0124136.

[17] Buckner, C. A. 2011. Effects of electromagnetic fields on biological processes are spatial and temporal dependent. Ph.D. Thesis, Laurentian University.

[18] Pollack, G. H . 2003. The role of aqueous interfaces in the cell. Adv. Colloid Interface Sci. 103, 173-196.

[19] Chai, B., Yoo, H. and Pollack, G. H. 2009. Effect of radiant energy on near-surface water. J. Phys. Chem. B. 113, 13953-13958.

[20] Del Giudice, E., Spinetti, P. R. and Tedeschi, A. 2010. Water dynamics at the root of metamorphosis in living organisms. Water 2, 566-586.

[21] Clary, D. C. 1999. Interfering with water. Science 285, 1218-1219.

[22] del Giudice, E. and Preparata, G. 1994. Coherent dynamics in water as possible explanation of biological membranes formation. J. Biol. Phys. 20, 106-116.

[23] Persinger, M. A. 2015. The prevalence and significance of ~10^{-20} J and ~10^{-12} W·m^{-2} as convergent/divergent nodal units in the universe. Int. Lett. Chem. Phys. Astron. 61, 94-100.

[24] Pilla, A. A., Muehsam, D. J., Markov, M. S. and Sisken, B. F. 1999. EMF signals and ion/ligand kinetics: prediction of bioeffective waveform parameters. Bioelectrochem. Bioenerg. 48, 27-34.

[25] Persinger, M. A. 2013. Experimental evidence that Hubble's Parameter could be reflected in local physical and chemical reactions: support for Mach's principle of imminence of the universe. Int. Lett. Chem. Phys. Astron. 11, 86-92.

[26] Persinger, M. A. and St-Pierre, L. S. 2015. Compton wavelengths for the proton and electron may differ by hyperspace

geometry: are they the same particle bifurcated? Int. Lett. Chem. Phys. Astron. 61, 101-104.

[27] Verdel, N., Jerman, I. and Bukovec, P. 2011. The "autothixotropic" phenomenon of water and its role in proton transfer. Int. J. Mol. Sci. 12, 7481-7494.

[28] Davidson, R. M., Lauritzen, A. and Seneff, S. 2013. Biological water dynamics and entropy: a biophysical origin of cancer and other diseases. Entropy 15, 3822-3876.

[29] Persinger, M. A. 2015. Thixotropic phenomena in water: quantitative indicators of Casimir-magnetic transformations from vacuum oscillations (virtual particles). Entropy 17, 6200-6212.

8.6 Preamble to Chapter 9: Interfering with Generated Magnetic Field Eliminates Inhibition of Malignant Cell Effects

Electromagnetic fields represent a novel therapeutic in the treatment of cancer, though there are many intrinsic limitations, which must be considered, as is the case with any intervention. That certain materials express ferromagnetic, diamagnetic, or paramagnetic properties represents both a challenge and potential avenue for novel applications. Incubators, within which cell experiments typically take place, are lined with metals, which distort magnetic flux lines and represent a potential variable, which could alter the expected results of our paradigms. Further, replication of our work might be inappropriately conducted if other researchers were ignorant of the particular environmental variables within our laboratory. Finally, we wanted to know if materials could influence the information content of the electromagnetic field applications in ways other than simple amplitude modulation. Frequency-shifting could represent a serious problem considering the precision involved with Cosic's resonant recognition model. We endeavoured to determine whether we could interfere or enhance the effects associated with our electromagnetic fields applications by wrapping the field-producing solenoids with copper foil.

Chapter Nine

Elimination of growth inhibition of malignant cells by specific patterned magnetic fields when source solenoids are wrapped with copper: implications for quantum (Aharanov-Bohm) effects

In Preparation for Submission

Lukasz M. Karbowski, Nirosha J. Murugan, Robert M. Lafrenie and Michael A. Persinger

Abstract

Purpose: Brief daily exposures of malignant cells lines to physiologically patterned (frequency-shifting, 25 Hz to 6 Hz per 2.6 s) magnetic fields inhibit growth by approximately 50% but do not affect non-malignant cells. The effect can be maximized by employing voltage shifts predicted by the Aharanov-Bohm effect before the optocouplers generate the photons that initiate the current for the magnetic field generation. We discerned if manipulations that could affect phase-modulation of the electrons that ultimately generated the current producing the magnetic field would modify the efficacy.

Methods: Plates of mouse B16 melanoma cells were exposed the same frequency shifting ("Thomas") pattern and field strength (~2.8 μT) for 1 hr per day for 5 consecutive days. For some trials the external solenoids that generated the field between pairs of solenoid were wrapped with copper foil. This did not affect the exposure strength of the applied frequency shifting fields between the solenoids within which the cells were located.

Results: The melanoma cells that were exposed to the usual field displayed the expected 50% reduction in numbers which is typical for this paradigm. On the other hand the numbers of melanoma cells exposed to the same field when the external solenoids were

wrapped with copper foil did not differ significantly from no field (sham) conditions. Removing the exposure chamber from direct contact with the copper floor of the incubator also increased the field's efficacy.

Conclusion: Copper foil wrapped around the solenoids or solenoids' proximity to copper sources within the incubators eliminated the typical 50% reduction in malignant cells numbers following 5 days of 1 hr daily exposures. We interpreted this elimination of the onco-retarding effect as due to the disruption of the phase delay and interference generated by our field configurations by the copper shielding. The role of a Aharanov-Bohm type quantum effect in oncostasis by frequency shifting magnetic fields as well as their analgesic effects suggest a third technology in addition to chemotherapy and ionizing radiation could be developed to treat cancer patients.

9.1 Introduction

The effective diminishment of the growth of malignant cells that contribute to the proliferation of tumors or the dissemination of cancer-inducing conditions has involved two traditional approaches: pharmacological dosages and ionizing radiation. A third approach has pursued the employment of non-ionizing, time-varying electromagnetic fields whose patterns have ranged from simple sine-waves to physiologically-patterned forms with intensities within the μT to mT range. There are now multiple examples that demonstrate the equivalence between specific physiologically-patterned magnetic fields and pharmacological effects. Martin et al [1] who measured rat behavior and Murugan et al [2] who measured planarian demonstrated that both appropriate dosages of morphine and a physiologically patterned microTesla level magnetic field elicited comparable indicators of analgesia. Both types of analgesia were blocked by classic antagonists for mu receptors for morphine such as naloxone. The discovery of a "Rosetta Stone" that translates equivalences of temporal patterned magnetic fields to spatially patterned molecular structures has significant potential for future implementation of non-invasive methods to attenuate the conditions that promote cancer. However the effects of these "non-ionizing" magnetic fields upon cell

cultures are sometimes not reliable. Here we present a potential major source for this variability.

Several experimenters have demonstrated that exposure of malignant cell lines to appropriately patterned, weak magnetic fields reduces growth. Crocetti et al [3] found that MCF7 breast cancer cell lines exposed to 20 Hz, 3 mT magnetic fields for 60 min per day for three days damaged the cancer cells but not normal or non-malignant cells. Buckner [4] and Buckner and Lafrenie and their colleagues [5] reported that applications of weaker (1 to 5 μT) sharply patterned magnetic fields that repeatedly shifted across a range of 25 Hz to 6 Hz once every 2 s for one hour per day for five days reduced the proliferation of growth in a dozen different cancer cell (human and non-human) lines from several organs without affecting non-malignant cells growth in human and non-human lines. The optimal specific point duration of the voltages that generated the field was 3 ms (333 Hz). These two frequency bands are remarkably similar to the 10-40 Hz and 300-500 Hz rate equivalents for dissociation of calcium from calmodulin described by Pilla et al [6] almost twenty years ago. The maximum, reliable inhibition of growth after a few days of brief daily exposures has been about 50% for single patterns that are continuously repeated. This is effectively the same effect as that from higher intensity static fields. In other instances when tandem sequences of different patterns with

appropriate point durations were employed complete elimination of malignant cells within the effect zone of exposure occurred. However, these effects were not consistent [7].

Other experimenters have demonstrated that the efficacy of appropriately patterned magnetic fields that affect the growth of cell lines generalize to organs and organisms. Hu et al [8] showed that the same magnetic field pattern that reduced melanoma cells in vitro also suppressed their growth in mice when they were injected with these cells. Costa et al [9] employed amplitude modulated electromagnetic fields that were safe and non-invasive methods for producing antitumor effects in human patients who had been diagnosed with advanced hepatocellular carcinoma. Barbault et al [10] articulated the importance of appreciating different types of tumors emitted difference frequencies and that tumor-specific applied magnetic field patterns could be beneficial for patients diagnosed with advanced cancer.

There are multiple advantages of applying local or whole body magnetic fields rather than chemotherapy or ionizing radiation. Weak, appropriately patterned magnetic fields: 1) primarily affect malignant cells and not normal cells, 2) are inexpensive and easily applied, and 3) produce few side-effects. In fact the frequency-modulated pattern employed by Buckner et al [5] and Hu et al [8] also produces analgesia or analgesia-like

behaviours in mollusks [11], planaria [2] rats [1] and human beings [12]. Similarly patterned fields also markedly reduced depression and pain in patients who have sustained closed head injuries two or more years previously and who reported minimal improvement with antidepressants. The efficacy of these transcerebral magnetic fields applied across the plane of the temporal lobes for 1.5 hr per week for six weeks was similar to transcranial magnetic stimulation (TMS). The argument that weak (2±1 μT) magnetic fields do not penetrate through large spaces of tissue or are impeded by boundaries such as the skull has recently been refuted by measurement [13].

The problem remains that application of even appropriately patterned magnetic fields display variability between and within laboratories despite the punctilious methods of experimenters. We have found several environmental variables that include the density of GHz communication systems (wireless) within the laboratory, the filtering of power supplies operating the incubators, and melanating effects about 24 to 48 hr following strong geomagnetic (K>6) storms. These later ambient events are sufficient to increase mortality in planarian if they are housed at very specific densities [14]. Recently we identified a condition that reliably and totally eliminated the magnetic field-inhibiting influence upon malignant cells. This occurred when the external solenoids that produced the magnetic fields

within the box where the plates of cells were exposed were wrapped with copper foil. The strengths of the time-varying, patterned magnetic field within the zone within the box where the plates were placed were not affected.

The employment of the copper foil was inspired by a particularly powerful and unexpected effect we found while exploring the effects of patterned magnetic fields upon spring water that had been exposed for over 10 days in the dark within no mechanical disturbances in order to facilitate thixotropic manifestations [15]. This unusual phenomenon which is characterized by increase viscosity and the formation of coherent domains within the water matrix has been hypothesized to be centrally involved with cellular dynamics including pathology [16]. Ambient magnetic fields can contribute to these conditions [17]. In one experiment volumes (100 cc) of water were exposed in one of three positions between two Helmholtz-like coils, one of which was not activated. Pictures of the arrangement have been published.

As predicted by our quantum derived hypothesis, fluorescent spectroscopy of aliquots revealed a conspicuous peak in the "spontaneous" ultraweak photon emissions (UPE) from water around 280 nm only for the water exposed to the interface between the two coils. Additional experiments indicated that the excess photon emissions within the ultraviolet boundary of the visible

wavelength from the spring water that had been exposed to the patterned magnetic fields exhibited peak spectral power density variations that were equivalent to 10 nm, effectively the width of a cell membrane. What was not expected, as shown in Figure 1 was that when the beakers containing the water were wrapped ("shielded") by copper but not by plastic or aluminum (not shown) during the exposure the photon emissions did not occur.

This specific wavelength might be considered a signature of the presence of interfacial water compared to bulk water as reiterated many time over the decades by Pollack and his colleagues [18-19]. Interfacial water whose properties emerge spontaneously when adjacent to surfaces such as cell membranes exhibits about 10 times the viscosity of bulk water. Solutes do not penetrate into this exclusion zone (EZ). At the external boundary where interfacial and bulk water apposes concentrations of protons collect that generate potential differences that could accommodate the resting plasma membrane potential which usually attributed to disparity of potassium or chloride charges [20]. The absorption spectra from the EZ zone have been shown to peak about 280 nm [21]. The elimination of this peak for spontaneous emissions after exposure to patterned magnetic fields with point durations of 3 ms that has been argued to reflect proton involvement was considered typical of a fundamental property of matter or the space within which it exists. Recently Karbowski

et al [22] found that melanoma cells in incubators spontaneously emit photons that peak around 280 nm.

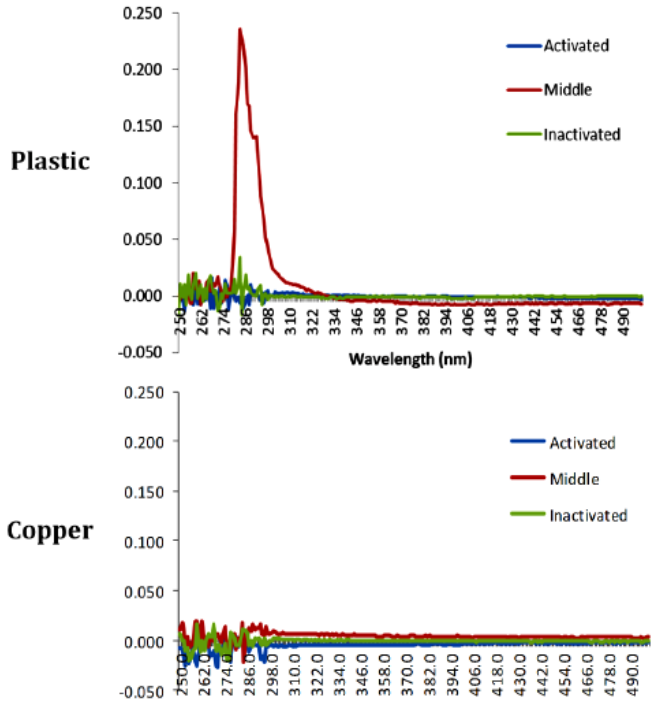

Figure 1. Relative (uv) emission fluorescence spectrometry ratios as a function of wavelength for quantities of spring water wrapped with either plastic (that did not differ from controls) or copper foil and placed within Aharanov-Bohm positions between an active and inactive coil generating the same pulse pattern as the one employed in this study. Note the elimination of the 280 nm wavelength (from Murugan et al, 2015).

In the pursuit of isolating the precise combination of parameters that could totally eliminate malignant cells but spare non-malignant cells we had found values predicted from phase-shifting quantum effects were critical to the effect. The features and characteristics of this disruption were strongly reminiscent of the Aharanov-Bohm effect [23]. According to Tonomura et al [24] this quantum effect is "the production of a relative phase shift between two electron beams enclosing a magnetic flux even if they do not touch the magnetic flux". Here we show that wrapping the source solenoids with copper foil or placing the cell culture plates near conductors within copper-jacked incubators completely abolished the robust malignant cell inhibition produced by specifically patterned magnetic fields.

9.2 Methods and Materials

A similar procedure that has been applied for the last 10 years of research in this area was followed and is described in detail elsewhere. In summary 0.5 to 1 million mouse melanoma B16 cells were exposed in stacks of six plates within custom-constructed acrylic exposure boxes which were 10 cm x 10 cm x 10 cm. The cells were grown and exposed in 65 mm by 15 mm plastic plates containing DMEM and supplemented with FBS and antibiotics. The boxes (and the cells) were maintained in NeuAir incubators (37 °C; 5% CO_2), model Nu8700 which were water jacketed with

copper shelving. The volume was 188 L. The power frequency field as measured by specific meters was less than xx mG within the exposure box within the incubators. However a xx meter indicated that the static field was about 3 G (300,000 nT) or about 6 times stronger than the earth's resultant magnetic field (~45,000 nT) at our latitude.

On each side of the box a Radioshack Reed Relay (SPST-5VDC; 275-0232) was attached (rated 0.5 A; 125 AC; coil resistance 250 ohms, nominal current 20 mA). They were encased in a plastic film canister (Figure 2). The circuit was organized such that magnetic field time-varying pattern was generated between each of the two opposing solenoids. The strength of the computer-generated time-varying magnetic field within which the stacks of 6 plates were placed averaged 28 mG and was based upon theoretical calculations [25].

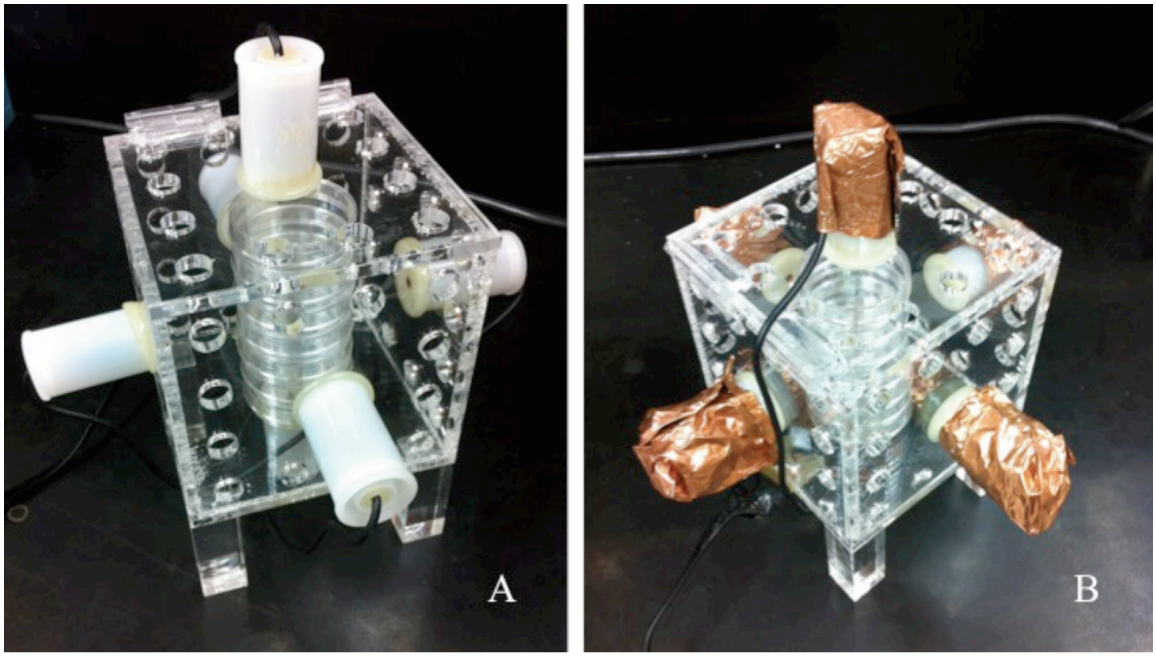

Figure 2. A) The typical plastic exposure chambers for cell cultures. Each white canister contains a solenoid. Pairs of solenoids in the same plane were connected such that the field was generated in the same plane in all three planes by the input from the unique circuit composed of optocouplers, tyristors, Triac switches and LED whose temporal patterns were controlled by the software with programmable options for the point durations producing the patterns.

The fields were generated from a digital to analogue converter circuit whose geometry and pattern have been specified elsewhere in detail in order facilitate potential reproduction by others. The pattern generated between pairs of solenoids was created by transforming a row of numbers between 0 and 256 to -5 V to +5 V with 127=0 V. There were 859 of these points within the pattern and each point duration was 3 ms. This meant that the pattern (Figure 3) repeated every 2.58 s continuously during the 1 hr exposures on each of the 5 days. The potential difference from the output of the computer was processed through custom constructed circuit composed of optocouplers, tyristors, Triac switches and internal light-emitting diodes which controlled the final current that activated the solenoids to generate the fluctuating magnetic field across the cells.

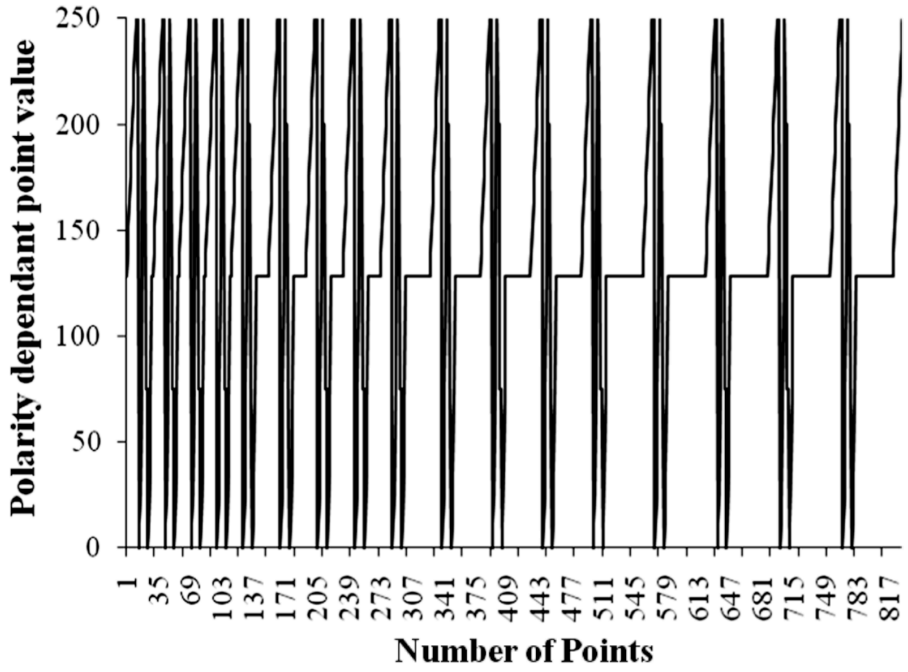

Figure 3. The temporal structure of the magnetic field pattern whose pre-optocoupler voltage by adjusted by Aharanov-Bohm solutions. Vertical axis indicates voltage that was optimally ±4.3 V. Horizontal axis reflects time in 3 ms increments for a total of 859 points for a total of 2.58 s per cycle.

To discern the effects of covering the solenoids with copper metal (Figure 2B), sheets of 99.99% pure copper foil (0.1 mm x 200 mm x 500 mm) were purchased from Fischer Scientific. Each sheet was cut into an L shaped structure for easy folding (Figure 4). During the course of experiments over the last two years we have noted varying effectiveness of the growth-inhibiting field exposures depending upon the distance of the exposure box from the copper-containing shelves within the incubator. The two positions are shown in Figure 5.

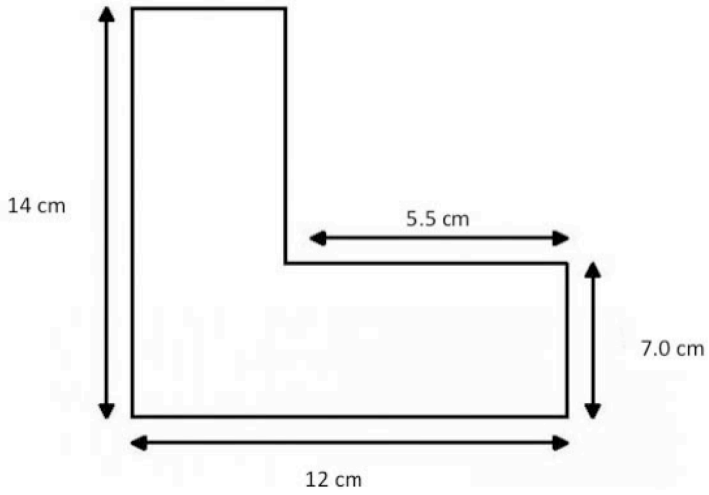

Figure 4. Shape of the copper foil sectioned for wrapping around each plastic container that contained the solenoid (See Figure 2B).

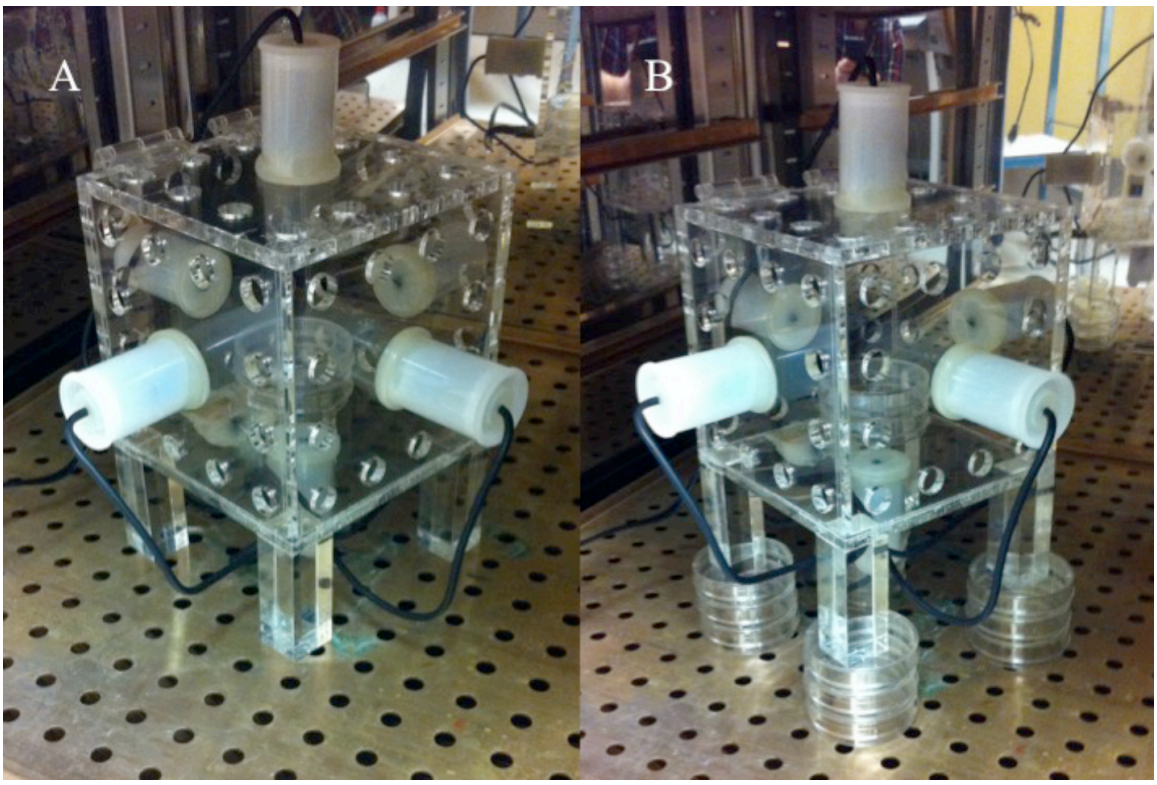

Figure 5. A) Direct contact of the exposure chamber to the copper floor of the incubator. B) Relative isolation of the feet of the exposure chamber (same size) from the copper floor of the incubator. Note: the two perspectives were not photographed with the same magnification.

The consequences of wrapping the solenoids upon the static background magnetic field were unexpected. The sensor for a MEDA magnetometer was placed inside the acrylic exposure box with and without copper wrapping of the 3 pairs of solenoids for inside the incubators and outside incubators on the laboratory counter.

The X axis was within 10 degrees of N outside the incubator and displaced by about 15 degrees inside the incubator. Measurements were obtained in the X, Y, and Z (vertical) domains in nanoTesla during 5 sec periods when the applied fields from the circuit (the one that generated the frequency shifting pattern in Figure 1) were activated or not over several dozen trials. Averages were obtained. As can bee seen in Table 1 there was no significant change in the static field (primarily the geomagnetic field) when the applied field was activated or not when there was no copper foil present outside of the incubator. Applying the copper foil produced increased the X component by 50 nT, increased the Y-component by 280 nT and decreased the vertical component by 142 nT. In other words the background static field was enhanced within the horizontal plane. Activating the applied field resulted in an additional 18 nT decrease in the vertical component.

On the other hand within the incubation chamber where all of the exposures actually occurred when the fields were off and no copper foil was applied the X plane was 95,000 nT higher, the Y axis was 16,000 nT higher and the vertical component was 10,480 nT higher. Effectively, similar to the measurement outside the incubator, the field was enhanced along the horizontal plane and diminished along the vertical plane where it is typically strongest. The activation of the applied field only increased (by

10 nT) the strength of the Y-axis. However when the copper foil was present around the external solenoids the strength of the static field when there was no applied field was 814 nT less in the X plane, 10,645 nT less in the Y plane, and 2,223 nT less in the vertical plane. The activation of the applied field with the copper foil present reduced the X plane by 4 nT, increased the Y plane by 1 nT and enhanced the vertical plane by 18 nT.

9.3 Results

The robust nature of the copper shielding of the source solenoids that the generated the effect of inhibiting growth of melanoma cells in culture is shown in Figure 6. The proportion of diminishment of proliferation was about 50% which is typical of the effect measured in 100s of trials we have measured in our laboratories over the last decade. The column on the right shows the effect of adding the copper foil around the external solenoids, a process that did not affect the magnetic field strength where the cells were exposed. The diminished growth for cells exposed to this condition was eliminated; they did not differ from non-treated controls.

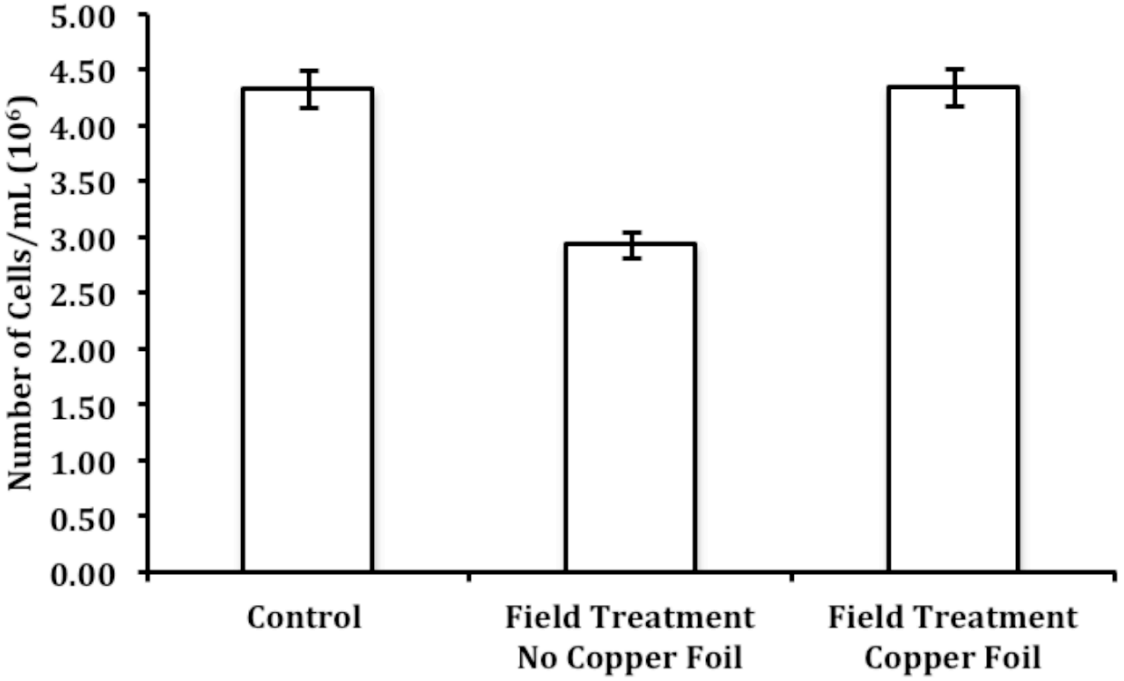

Figure 6. The number of cells per mL x 10^6 for melnaoma cells are 5 successive days of 1 hr per day exposure to sham fields (control), the typical field pattern, or the field pattern when the solenoids were simply covered by copper foil. Each group was compose of 6 to 8 different replications. Vertical bars indicate standard deviations.

The effect of moving the entire exposure chamber (Figure 2) away from the copper flooring upon growth of the melnaoma cells over the five days is shown in Figure 7. When the exposure box was elevated above the copper floor of the incubator (diamonds) the attenuation of growth was clearly apparent. The manifestation

of the magnetic field diminishing effect after day 3 is typical for this effect. Note that without this separation from direct contact with the copper floor of the incubator the growth rate even exposed to the magnetic field does not differ from sham (no) field controls. Figure 8 shows the effect of the field across the six stacks of cell plates.

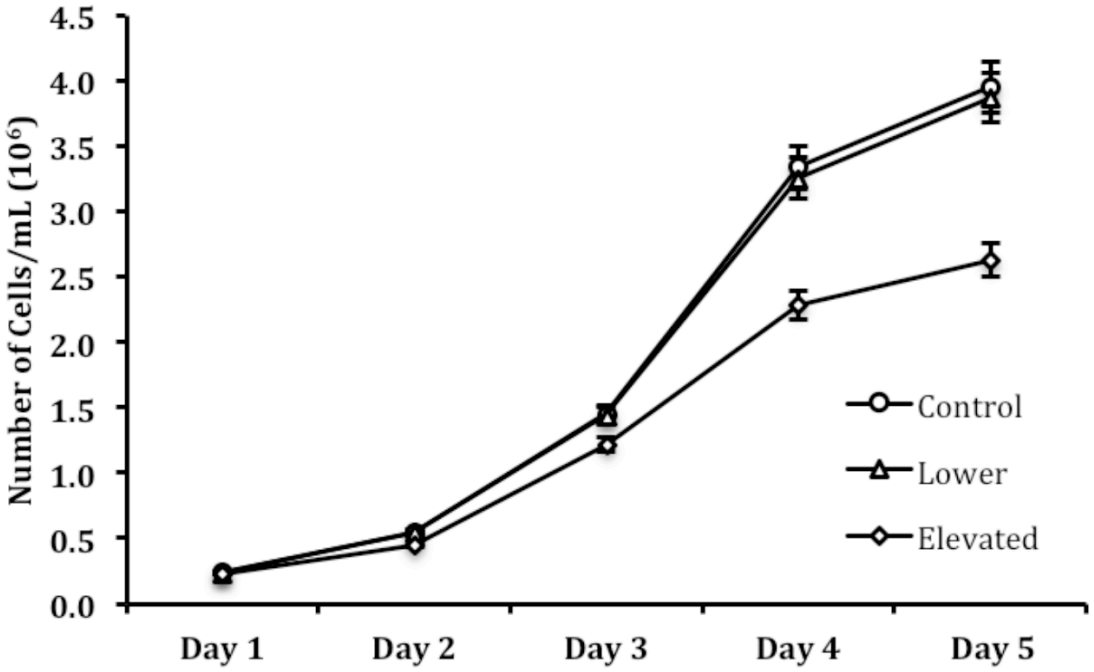

Figure 7. Numbers of cells per day over the five days of one hour exposures for the plates of cells exposed to the patterned magnetic field when the box was elvated (diamonds) or not elevated (triangle) from the copper floor of the incubator. Open circles indicate sham field controls. Vertical bars indicate standard deviations.

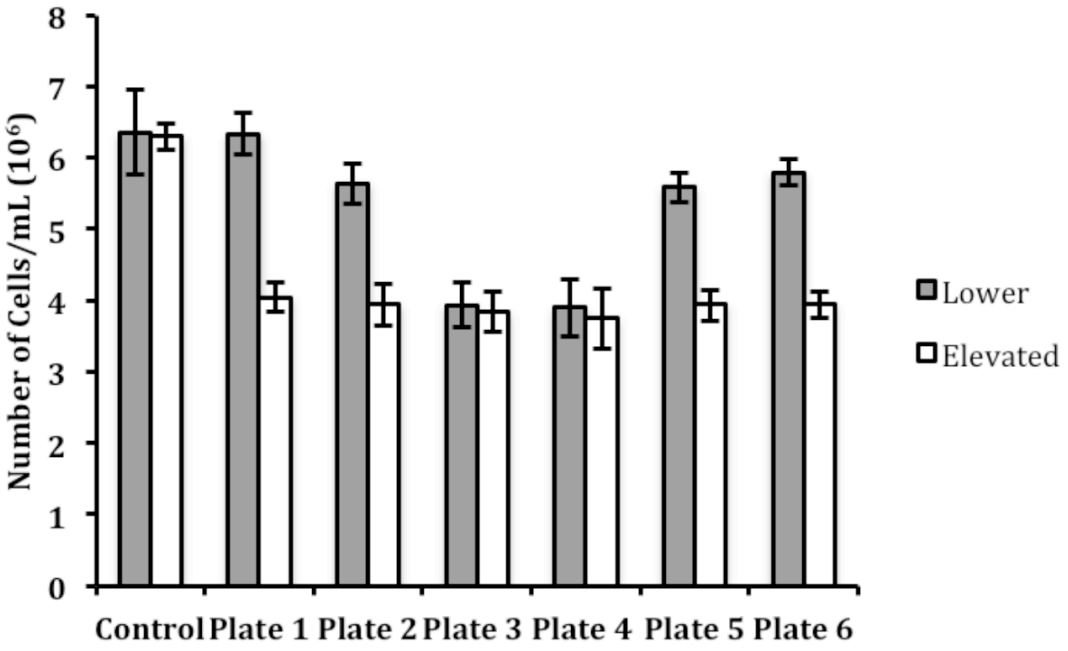

Figure 8. Numbers of cells on day 5 for sham field-exposed conditions and for the serial position (1 at top in Figure 1) of the plates when the box was either elevated (closed squares) from the copper floor or not elevated (open squares). Vertical bars indicate standard deviations.

9.4 Discussion

Traditionally there have been two major methods of diminishing the growth of malignant cells: chemical intervention and ionizing radiation. Each of these forms of therapy are associated with frank side effects and can negatively affect normal cells as well as those which are targeted. Exposure to non-ionizing low intensity magnetic fields with programmable

temporal patterns does not affect the growth of normal cells but can retard the proliferation of malignant cell lines by approximately 50%. In addition some patterns of these field produce analgesia [1, 2] during and following exposure that simulates the effects of morphine but without initiating signalling pathways that can lead to metastizes [25].

The results of the present experiment reiterate the complexity of the effective magnetic field configurations required to produce the maximum effect upon cancer cells *in vitro*. Adding copper foil around the external solenoids did not not reduce the intensity of the applied frequency-shifting field whose precise timing has been shown experimentally to inhibit mouse melanoma cell growth. However this apparently simple procedure completely eliminated this inhibtion such that there were no statistically significant differences between the sham field-exposed and copper foil wrapped solenoid-exposed cells.

We have been pursuing the potential contribution of quantum or quantum-like effects to the proliferation and the prevention of malignancy. The convenient solution for the optimal pre-optocoupler voltage based upon realistic values from the Aharanov-Bohm effect suggested that relative phase shift between the two electronic “beams” that constituted the two currents that ultimately produced the magnetic fields to which the cells were exposed may mediate this possibility. However the blocking of the

oncostatic effect by the copper foil appears to have eliminated the role of the pure Aharanov-Bohm effect [23].

According to the physics experiments most superficially similar to our configuration, such as those by Tonomura et al [24] the copper layer shields the electron wave. The elimination of the slowing effect by our configuration and generation of temporally patterned magnetic fields upon the growth of the melanoma cells would suggest that it is mediated by some feature of the electron wave function. However the Aharanov-Bohm effect requires a phase delay that contributes to interference patterns [23]. In our experiments the time-varying magnetic fields were generated between sets of solenoids (Figure 9). They were connected such that at any given time one solenoid is a "north" pole and the other solenoid is a "south" pole. This means that in addition to the flux lines directly across the space within which the cells are exposed, that is between the two apposing surfaces of the separated solenoids, there are also flux lines leaving the opposite (distal) surfaces of each solenoid to allow the pathway to be completed.

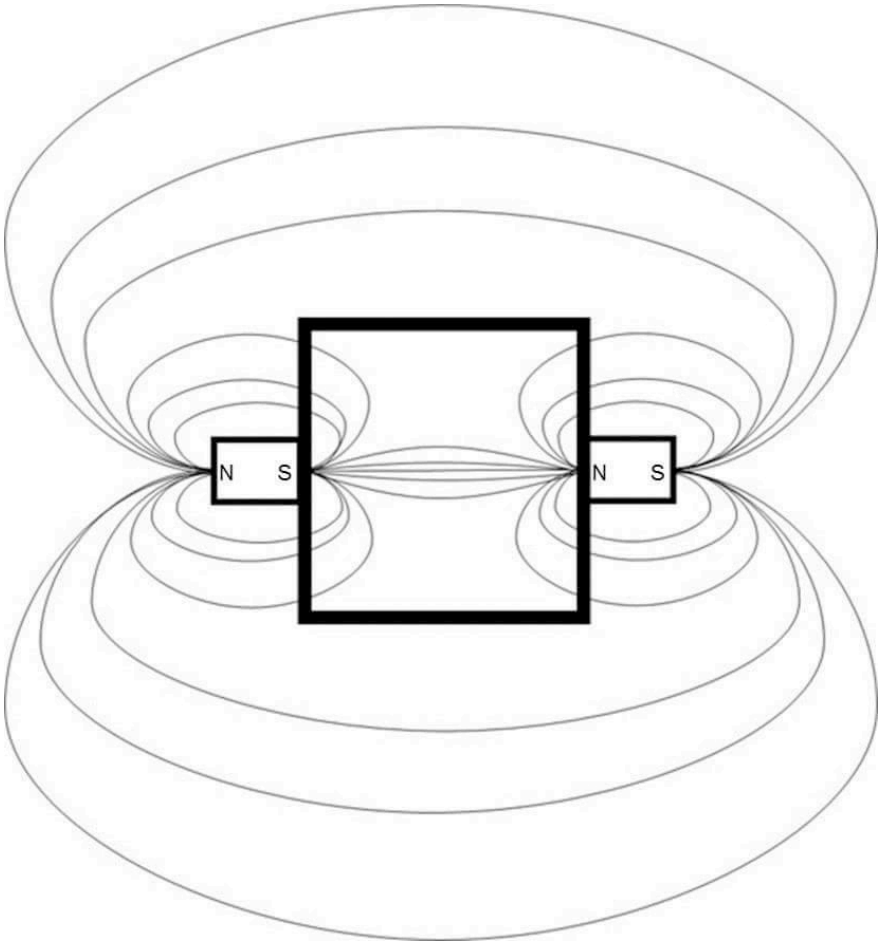

Figure 9. Depiction of flux lines propagating through and around the exposure area (black square) from the serially connected solenoids (N-S). The slight difference in convergence time would produce the interference pattens that primarily contribute to the Aharanov-Bohm effect withn the expsoure area. The cooper covering would have two solenoids would have disrupted this condition.

We suggest that the continuous collapse and production of the point durations by the Koren software through the DAC system every 3 ms produces a slight disparity between the flux generated directly between the two solenoids and those generated from the distal end of one solenoid to the distal end of the other solenoid. This is are local manifestation of the Aharanov-Bohm effect. This dynamic geometry potentially creates the condition for phase shifts and interference patterns from that component of the field within the exposure area. Consequently containing the distal portions of each solenoid with copper metal would have potentially disrupted these phase conditions within the exposure area. As a result the suppression effects upon cell growth would have been elimnated as we noted in the present study. If this mechanism is valid and can be generalized there may be an alterative explanation for how weak, time-varying magnetic fields with shifting frequencies as reported by Buckner et al [4], Hu et al [8] and Crocetti et al [3] mediated their onco-retarding effects.

There has been considerable interest in the employment of quantum-like phenomena to cancer research as well as the development of quantum biology. Historically the development of biological sciences has benefited from the reductionist approach of understanding the organ in terms of the cell and the cell in terms of the molecular pathaways that define it. This has been

the central thrust of molecular biology and its application to aberrant cellular proceses such as cancer and malignancy. The next logical step would be to pursue the more statistical and electromagnetic phenomena that have defined “quantum” physics which may exhibit macrocosmic manifestations [24]. For these models to be effective in cancer research we suspect much greater precision in the parameters that create and maintain effective magnetic field configurations must be appreciated.

9.5 References

1. Martin LJ, Koren SA, Persinger MA. Thermal analgesic effects from weak, complex magnetic fields and pharmacological interactions. Pharm Biochem Behav 2004; 78:217-227.

2. Murugan NJ, Persinger MA. Comparisons of responses by planarians to micromolar to attomolar dosages of morphine or naloxone and/or weak pulsed magnetic fields: revealing receptor subtype affinities and non-specific effects. Int J Rad Biol 2014

3. Crocetti S, Beyer C, Schade G, Egli M, Frohlich J, Franco-Obregon A. Low intensity and frequency pulsed electromagneteic fields selectively impair breast cancer cell viability. PLOS one 2013; Vol 8, Issue 9 e72944.

4. Buckner CA. Spatial and temporal magnetic fields and malignant cell growth. Ph.D. Laurentian U. 2011.

5. Buckner CA, Buckner AL, Koren SA, Persinger MA, Lafrenie RM. Inhibition of cancer cell growth by exposure to a specific time-varying electromagnetic field involves T-type channels. PLOS one 2015; DOI:10.1371/journal.pone.0124136.

6. Pilla AA, Muehsam DJ, Markov MS, Sisken BF. EMF signals and ion/ligand binding kinetics: prediction of bioeffective waveform parameters. Bioelectrochem Bioenerg 1999; 48:27-34.

7. Karbowski LM, Murugan NJ, Koren SA, Persinger MA. Seeking the source of transcience for a unique magnetic field pattern that

compeltely dissolves cancer cells in vitro. J Biomed Sci Engin 2015; 8, 531-543.

8. Hu JH, St-Pierre LS, Buckner CA, Lafrenie RM, Persinger MA. Suppression of growth of injected melanoma cells by whole body exposure to specific spatial-temporal configurations of weak intensity magnetic fields. Int J Rad Biol 2010; 86:79-88.

9. Costa FP, De Olievera AC, Meirelles R, Machado MCC, Zanescro T, et al. Treatment of advanced heaptocullar carcinoma with very low levels of amplitude-modulated electromagnetic fields. Brit J Can 2011; 105:640-648.

10. Barbault A, Costa FP, Bottger B, Munden RF, Bomhot F, Kuster N, Pasche B. Amplitude-modulated electromagnetic field treatments of cancer: discovery of tumor-specific frequencies and assessment of a novel therapeautic approach. J Exp Clin Can Res 2009; 28: 51

11. Thomas AW, Kavaliers M, Prato FS, Ossenkopp KP. Pulsed magnetic fields induces "analgesia' in the land snail, cepaenenormalis, and the effects of mu, delta and kappa opioid receptor agonists/antagonists. Peptides 1997; 18: 703-709.

12. Persinger MA, Murphy TR. Validating new techniques to treat depression, pain and the feeling of sentient beings: a reply to "neuroscience for the soul". Neurosci Med 2016; 7:27-44.

13. Persinger MA, Saroka KS. Minimum attenuation of physiologically-patterned, 1 microTesla magnetic fields through

simulated skull and cerebral space. J Electromag Analy App 2013; 5:151-155.

14. Murugan NJ, Karbowski LM, Mekers WFT, Persinger MA. Group planarian sudden mortality: is the thresold around global geomagnetic activity >K6? Comm Integrat Biol 2015; 8:6 e1095413-1.

15. Persinger MA. Thixotropic phenomena in water: quantitative indicators of Casimir-magnetic transformations from vacuum oscillations (virtual particles). Entropy 2015; 17:6200-6212.

16. Davidson RM, Lauritzen A, Seneff S. Biological water dynamics and entropy: a biophysical origin of cancer and other diseases. Entropy 2013; 15: 3822-3876.

17. Murugan NJ, Karbowski LM, Persinger MA. Serial pH increments (20 to 40 ms) in water during exposures to weak, physiologically-patterned magnetic fields: implications for consciousness. Water 2014; 6:45-60.

18. Pollack GH. The role of aqueous interfaces in the cell. Adv Colloid Inter Science 2003; 103: 173-196.

19. Chai B, Yoo J, Pollack GH. Effect of radiant energy on near-surface water. J Phys Chem 2009; 113: 13953-13958.

20. Persinger MA. 10^{-20} Joules as the neuromolecular quantum in medicinal chemistry: an alternative to the myriad molecular pathways. Cur Med Chem 2010; 17: 3094-3098.

21. Chai Bh, Zheng Jm, Zhao Q, Pollack GH. Spectroscopic studies of solutes in aqueous solution. J Phys Chem 2008; 112: 2242-2247.

22. Karbowski LM, Murugan NJ, Persinger MA. Experimental evidence that specific photon energies are "stored" in malignant cells for an hour: the synergism of weak magnetic field-LED wavelength pulses. Biol Med 2016; 8:1 BM-162-16.

23. Kregar A. Aharanov-Bohm effect. Seminar-.4 letnik, Ljubljana, 2011.

24. Tonomura A, Osakabe N, Matsuda T, Kawasaki T, Endo J. Evidence for Aharanov-Bohm effect with magnetic field compeltely shielded from electron wave. Phys Rev Lett 1986; 56: 792-795.

25. Murugan MJ, Karbowski LM, Persinger, M. A. Weak burst-firing magnetic fields that produce analgesia equivalent to morphone do not initiate activation of proliferation pathways in human breast cells in culture. Int Can Sci Therapeut 2014; 1(3):47-50.

9.6 Preamble to Chapter 10: Investigating Other Forms of Generated Low-level Electromagnetic Fields

Suppose two spaces could be effectively linked by electromagnetic fields where events within space A could physically interact with events in space B. This is essentially what the phenomenon of excess correlation represents. Many experiments involving controlled chemical reactions, human brain-to-brain communication, as well as cellular interactions have been conducted within our laboratory. Given our interest in malignant cells and their various interactions with electromagnetic field applications, we sought to induce growth inhibition in melanoma cells by remotely introducing a stress-inducing, potentially lethal chemical compound within a space spatially separate from the cell culture though sharing the same rotating electromagnetic field application. In principle, the two spaces would share properties such that a noxious stimulus in position A could induce cell growth inhibition in position B.

Chapter Ten

Experimentally-Induced Inhibition of Growth in Melanoma Cell Cultures Separated by ~Two Kilometers When Both Share Excess Correlation Magnetic Fields: Macroscopic Evidence of Free-Space Quantum Teleportation?

Published in Journal of Signal and Information Processing (2015) – Vol: 6 (1). Pg. 39-48

Reproduced with Permission from Scientific Research

Lukasz M. Karbowski, Nirosha J. Murugan and Michael A. Persinger

Abstract

In multiple experiments plates of melanoma cells separated by either 3 m or 1.7 km were placed in the centers of toroids. A specific protocol of changing, angular velocity, pulsed magnetic fields that has been shown to produce excess correlation in photon durations and shift in proton concentrations (pH) in spring water were generated around both plates of cells. Serial injections of 50 µL of standard concentrations of hydrogen peroxide into the "local" plates of cells during the 12 min of field activation produced conspicuous cell death (reduction of viable cells by about 50%) with comparable diminishments of cell numbers in the non-local plates of cells within 24 hr but only if both loci separated by either 3 m or 1.7 km had shared the "excess correlation" magnetic field sequence. The non-local effect did not occur if the magnetic fields had not been present. Higher or lower concentrations of peroxide or concentrations that eliminated all of the cells or very few cells in the local dishes were associated with no significant diminishment of non-local cell growth. The data indicate that there must be a critical number of cells remaining viable following the local chemical reaction for the excess correlation to be manifested in the non-local cells. We suggest that this specific spatial-temporal pattern of fields generated within the paired toroidal geometries promote transposition of

virtual chemical reactions as an information field. Calculations of the energy available per cell and per volume of the quantity of reactants injected into the local space from the intensity of the changing velocity toroidal magnetic field supported previous measurements and derivations that the units of information transposition may involve discrete quantities that represent equivalents of photons, electrons and protons.

10.1 Introduction

One of the most important possibilities for 21st century transposition of information within different localities is the technical production of reliable excess correlations without the direct involvement of an apparent medium. Whereas electromagnetic communication requires the assumptions of locality with spatial characteristics defined by magnetic permeability and electric permittivity from which the velocity of light can be derived, non-locality does not require an obvious medium. The occurrences of excess correlations of function between two non traditional localities, often described as "entanglement" [1], are likely to involve multiple, different mechanisms. Traditional understanding of these processes have indicated this type of "entanglement" could only occur within subatomic and quantum domains. Here we report evidence that the survival of cancer cells in two distant loci display powerful correlations when the two spaces share specific types of circularly generated magnetic fields with changing angular velocities. The effect may be sufficient to develop practical applications for information "transfer" over distances through properties of photons for both electronic and living systems.

Quantum entanglement is a phenomenon whereby joint measurements of at least two systems exhibit stronger correlations than expected by classical explanations [2].

Quantum teleportation which involves the process of quantum communication has been demonstrated at distances that have ranged from 55 m to 16 km [3]. Hotta et al [4] have calculated that quantum teleportation could occur without limitation by distance. Olson and Ralph [5] have shown that time-like entanglement could be extracted from a subcomponent of the quantum vacuum which has been interpreted in manner that is conducive to this process [6,7]. As indicated by Vaziri et al [8] the primary means for producing quantum communication for the foreseeable future will involve photons. According to most quantum approaches co-existence at some particular space-time coordinate is essential for the later display of entanglement properties, such as the reversal of polarity of one photon when the other's polarity is altered. However Megidish [9] and his colleagues indicate that entanglement could occur between photon that never co-existed. Presumably this condition would require a shared third factor.

Julsgaard et al [10] demonstrated experimentally that entanglement can occur between two macroscopic objects, specifically caesium gas samples containing about 10^{12} atoms. That macroscopic objects could display excess correlations at non-classical distances was further explored by Dotta et al [11]. They based their design upon unpublished statistical analyses by Persinger and Lafreniere [12] who had noted that conjugate points in geomagnetic coordinates, when both exhibited properties of

circular rotating fields within the larger angular momentum of the earth's rotation, displayed evidence of "superimposition". Dotta et al [11] found that when two cultures of melanoma cells separated by 10 m were simultaneously exposed to circularly rotating magnetic fields the application of light flashes to one dish resulted in the emission photons as measured by photomultiplier tubes from the other. This "excess correlation" did not occur when the circularly rotating fields were not present.

Persinger and his colleagues [11,13] developed an experimental protocol based upon the theoretical considerations by Tu et al [14] that the photon displayed a non-zero rest mass. If this presumption were valid then the group and phase velocity of photons would be dissociated, thus creating additional vectorial features and properties of electromagnetic fields. We assumed that if the processes were isotropic their simulation could affect photon behaviour. The challenge was to build and to develop equipment that could create the conditions within a macroscopic context. Koren, Dotta and Persinger [15] devised a system by which electromagnetic fields with specific point durations generated by computer software could be generated around a circular array of eight solenoids. The rate of change of the circular angular velocity, which would technically be a

second derivative, could be increased or decreased by the same software.

While discerning if photons themselves were the operational unity of the "excess correlations" between either cerebral or cellular activity [11] by measuring the non-local photon radiant flux density during chemoluminescent reactions (hydrogen peroxide and sodium hypochlorite solutions), Dotta and Persinger [13] identified one particular effective sequence. Doubling of the power densities of photon emissions occurred when both loci in which the chemoluminescent reactions occurred were first exposed to circularly moving magnetic field whose group velocity was accelerating and phase velocity decreasing and then to a circularly moving magnetic field whose group velocity was decelerating but phase velocity was increasing. In these instances the single injection of a reactant (hydrogen peroxide) into each locus of hypochlorite solutions resulted in a doubling of photon output as if the two loci were the same space and hence had been injected with twice the amount. The excess correlation was demonstrated at distances of 10 m and 3 km.

Clusters of cultured cells (~10^5 to 10^6) emit photons at radiant flux densities in the order of 10^{-12} $W \cdot m^{-2}$ [16]. The photons are more than by-products of metabolism and have been argued to be the primary mode of inter-cell communication [17, 18]. Melanoma cells emit copious amounts of photons during their

habituation to room temperature after removal from incubation. The peak wavelengths of photons within the visible range shifted predictably as a function of the time since the removal from incubation [19]. There is direct and indirect evidence that these bursts of photons affect the activity of similar cells within their proximity. Drugs such as morphine elicit remarkably strong bursts of photons from malignant cell cultures [20]. In the present experiment novel equipment (toroids) was developed that captured the characteristics of the array of eight solenoids but was operated by easy-to-construct Arduino systems rather than the required custom constructed digital-to-analogue convertors (DACs) required in previous studies.

10.2 Materials and Methods

A total of 27 separate experiments (trials) were completed over a period of two months. B16-BL6 murine melanoma cells (~10^5) were cultured using 2.5 cc of DMEM culture media in 35 mm x 10 mm standard plastic dishes. For each experiment 2 plates of cells were placed in the center of the two toroids (1 plate per toroid), labeled as local or non-local. The exposure equipment and control systems are shown in Figures 1 and 2. A schematic of the experimental design and circuit has been published elsewhere [21]. Each toroid was composed of a plastic ring whose diameter was 25.4 cm. It was wrapped with 225 turns of

16 gauge copper wire (for stereo speakers) and covered with black, vinyl electrical tape. The width between the bottom and top of the wire and plastic ring combined was 3.8 cm.

The local and non-local toroids were separated by either 3 m or 1.7 km (distance between the university lab and the local research hospital). The dish of cells was always placed in the middle of a solenoid at room temperature after being removed from standard incubation (37°C). The toroid that was designated as local or non-local was counterbalanced within each treatment series. Local refers to the toroid within which the cells received small (50 µL) injections of hydrogen peroxide. Non-local referred to the toroid within which the cells never received any peroxide. Control plates (n=2, per trial) were placed outside of the incubator for the same duration as those cells exposed to the experimental magnetic fields at distances where power meters indicated there was no discernable changes from the experimentally-generated magnetic fields.

Both pairs of plates containing cells were exposed to the excess correlation paradigm using decreasing and increasing phase (frequency) modulated magnetic fields. Their shapes have been published elsewhere [22]. The fields were controlled using an Arduino microcontroller system and laptop (Figure 2) similar to that described in more detail by Rouleau et al [22]. By orienting the diode the current (fields) were rotated in the

counterclockwise direction. Eight separate 3 ms pulses were generated in two patterns. For the decreasing frequency or phase modulating condition the 3 ms pulses (p) were generated in this manner: p, 20 ms, p, 22 ms, p, 24 ms, p, 26 ms, p, 28 ms, p, 30 ms, p, 32 ms, p, 34 ms. The sequence was then repeated for the duration that it was programmed. For the increasing frequency or phase modulating condition the 3 ms pulses were generated in this manner: p, 20 ms, p, 18 ms, p, 16 ms, p, 14 ms, p, 12 ms, p, 10 ms, p, 8 ms, p, 6 ms before the cycle repeated.

Consequently although the current within the copper wire was being generated continuously (and presumably moving ~10^8 $m \cdot s^{-1}$) there was a superimposed changing angular velocity implicitly associated with the different completion times for the generation for one sequence of the signals for decreasing (203 ms) and increasing (128 ms) angular velocity programs. The only additional component was an amplifier that was added to the circuit so that the strength of the field within the area occupied in the center of each toroid by the cells was 3 to 5 μT as measured directly by a power meter.

The paradigm was 12 minutes in duration. The first injection of 50 uL of either 300 uM, 800 uM, or 1 mM of hydrogen peroxide (diluted with culture media) was placed in the local dish 4 minutes after the initiation of the decreasing frequency modulated field. The pattern was then changed to an increasing

phase (frequency) modulated field for 8 more minutes. Every 1 min for the next 5 minutes the same amount of hydrogen peroxide was injected into the local plate of cells. Hence there were a total of 6, 50 µL injections. After 12 minutes had elapsed form the activation of the fields, the Arduino systems for both loci were turned off and the cells were placed back into the incubators for 24 hours. After the 24 hours, cells from the plates were counted using the standard haemocytometer/Trypan protocol (Figure 3). The media containing the cells was centrifuged. The pellet containing the cells was then re-suspended in PBS (phosphate buffer solution). Within each chamber (Figure 3) 15 µL of the solution was injected. The average (mean) of 8 grids was calculated and expressed in traditional formats (per 1.5 mL).

All experiments for local and non-local pairs for the distances of 3 m and 1.7 km were repeated five to six times. Only one experiment was completed per day. The experiments were also repeated when the excess correlation protocol was activated for both locations (separated by 1.7 km) for local and non-local reactions but only the volume (50 µL) of media (no hydrogen peroxide) was injected into the cells in order to control for injection artifacts. All results are presented as means and standard deviations (SDs) for each condition within the different experiments. Because of the conspicuous nature of the effects and the absence of overlap between the standard deviations we did not

pursue traditional statistical analyses because all effects would be p <.01.

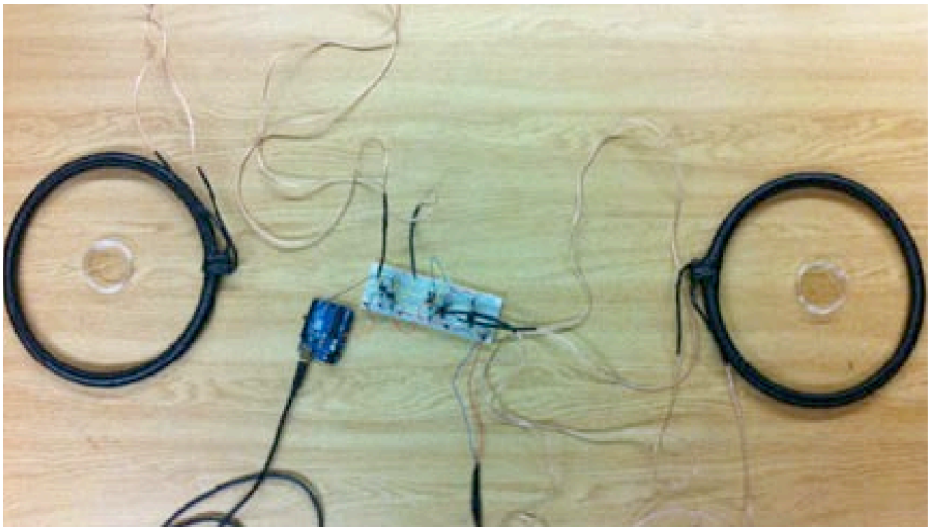

Figure 1. Pictures of the actual toroids and microcontroller system employed to generate the changing angular velocity pulsed magnetic fields.

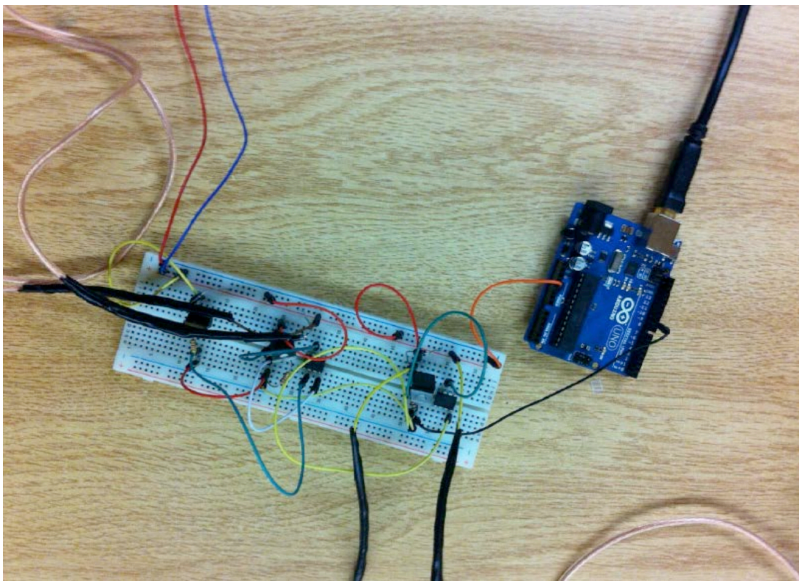

Figure 2. Closer view of the micro-control (Arduino) system that operated the toroids

10.3 Results

The results were conspicuous and reliable. Figure 4 shows the means and standard deviations (SDs) for the cells remaining 24 hr after the serial (every min) injections of 50 uL of 800 µM hydrogen peroxide (local) into the dish and in the dish that did not receive any injections when both shared the same decreasing and increasing frequency (phase)-modulated magnetic fields delivered through different toroids separated by 3 m. Although one would expect the reduction of cell numbers in the cultures injected with the peroxide, the non-local cultures that were not injected but shared the changing angular velocities of magnetic fields displayed a reduction of cells that was approximately 50% (about 60 to 70 cells per 1.5 mL or about $1.2 \cdot 10^5$ cells) compared to the control cells (those that were removed from the incubator and placed near the local and non-local spaces but beyond the intensity of the fields. The difference between the local and non-local effect was about 10 cells per 1.5 mL or about 1 to $2 \cdot 10^4$ cells.

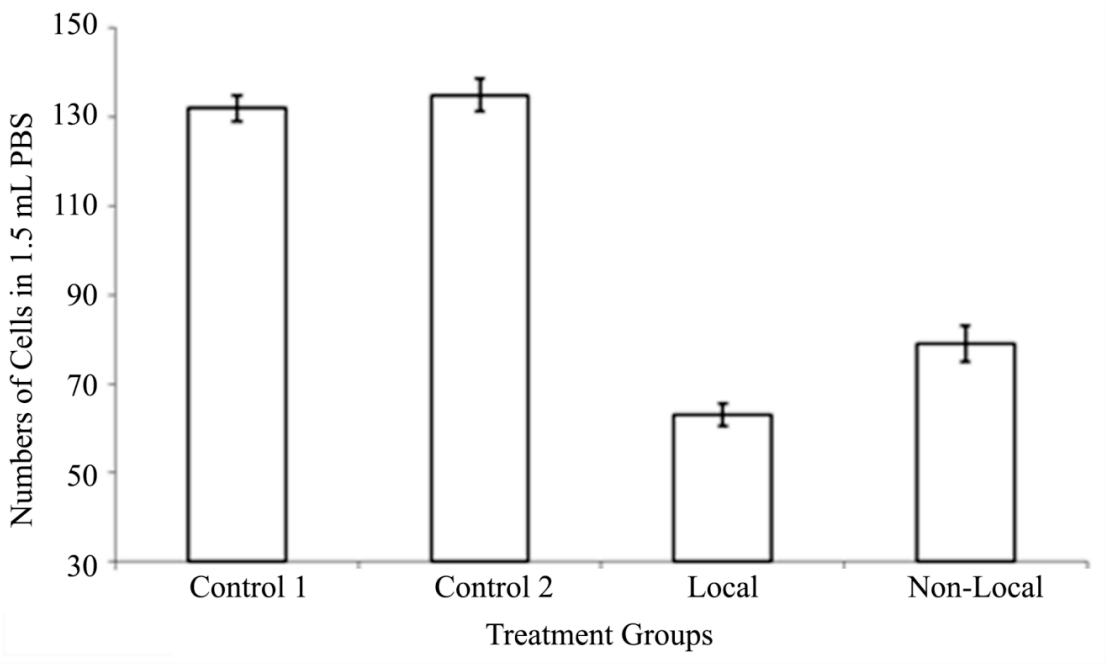

Figure 3: Means and standard deviations (for 5 experiments) for the numbers of cells sampled from 15 µL of cell suspensions 24 hr after a single (12 min) exposure to the excess correlation rotational magnetic fields in pairs of toroids separated by 3 m. The local cells dishes were injected with hydrogen peroxide while the non-local was not. Control cells were not exposed to the paired fields or the hydrogen peroxide but had been removed from the incubator for the same duration.

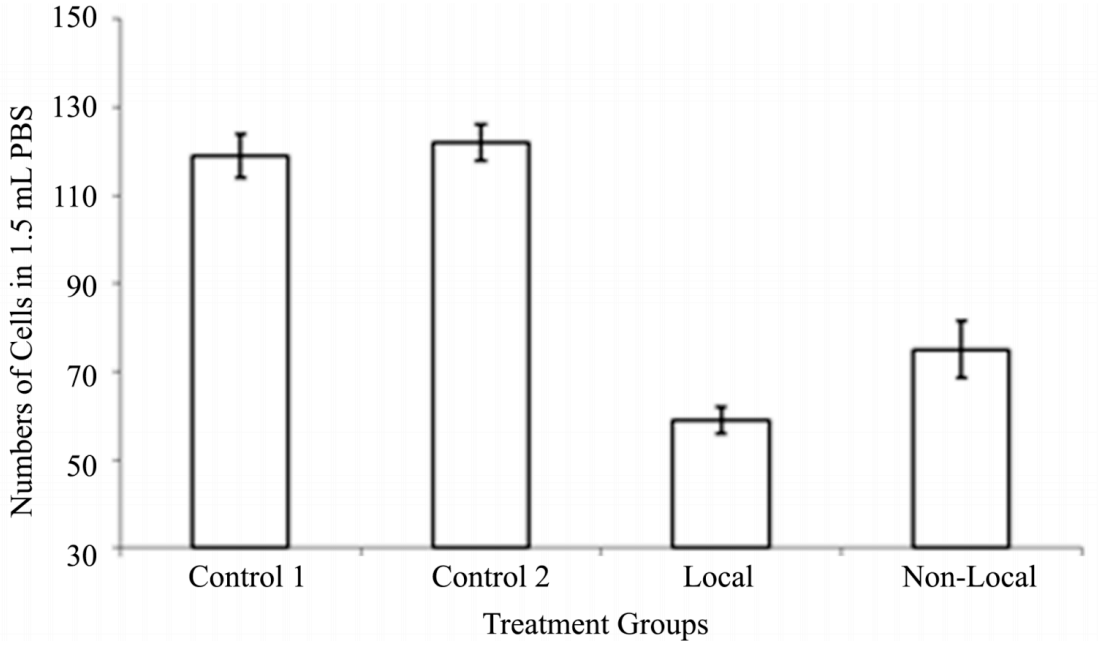

Figure 4: Means and SDs (for 6 experiments) for the numbers of cells sampled from 15 µL 24 hr after a single (12 min) exposure to the excess correlation rotational magnetic fields in pairs of toroids separated by 1.7 km. The local cells dishes were injected with hydrogen peroxide while the non-local cells were not. Control cells were not exposed to the paired fields or the hydrogen peroxide but had been removed from the incubator of the same duration.

Figure 5 shows the means and standard deviations for the numbers of cells measured within the local and non-local plates 24 hr after the single exposure (12 min) to the excess correlation protocol when the toroids were separated by 1.7 km. The control conditions were dishes that were also removed from the incubators but not exposed to the excess correlation fields. Although the similarity of the cell effect for the cells exposed to the local condition would be expected because they were injected with the same amount of hydrogen peroxide, the cell loss within the non-local condition, even though the toroids were separated by 1.7 km rather than 3 m, was also very similar.

Figure 6 shows the effects of injecting different concentrations of hydrogen peroxide (same unit volume of injection) into the local plates of cells. As expected increased concentrations of hydrogen peroxide was associated with more cell death in the injected (local) populations. However the non-local effect was *non-linear*. Compared to the dishes of cells from the control conditions, the non-local effect were marginally lower when the local cells were injected with either 300 µM or 1 mM of hydrogen peroxide. The maximum non-local effect in this experiment occurred when the concentration of peroxide injected into the local cells was 800 µM as was found in the previous experiments.

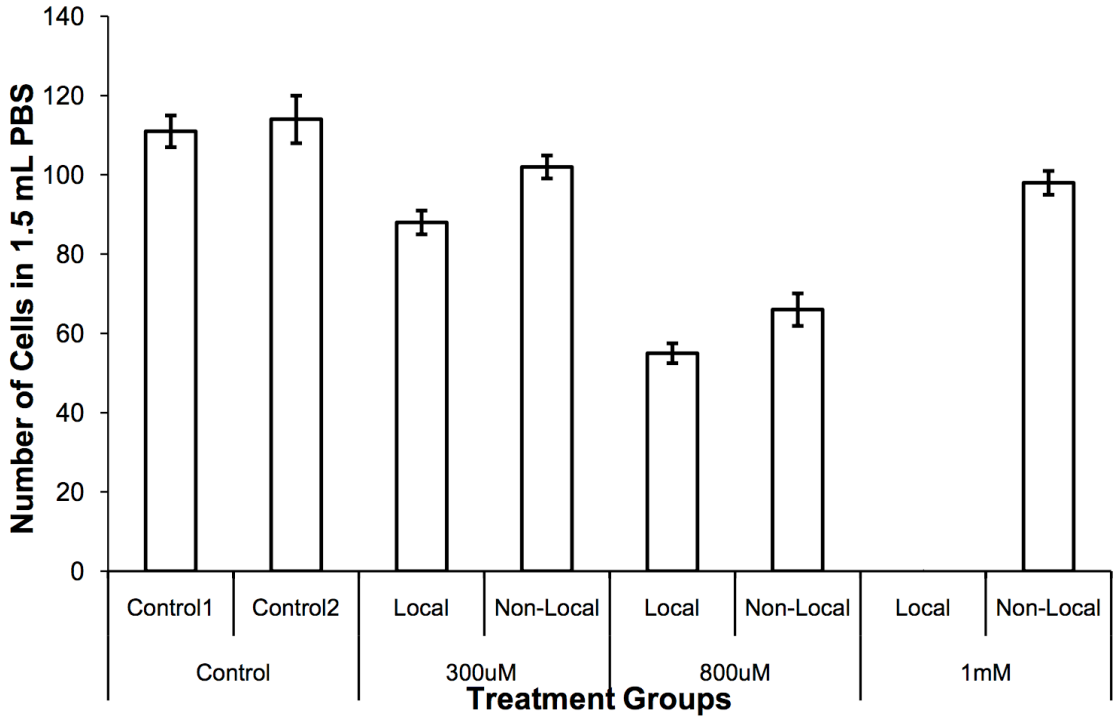

Figure 5. Means and SDs for the numbers of cells sampled from 15 µL 24 hr after they had been exposed to control conditions or after the local cells were injected with either 0.3, 0.8 or 1 mM of hydrogen peroxide. Note that when the local cells were completely eradicated by the hydrogen peroxide there was no evidence of excess correlation. The distance between local and non-local cell plates was 1.7 km.

The means and SDs for the results of 5 experiments for numbers of cells within the control and local and non-local sites when only media was injected (no peroxide) are shown in Figure 7. There was no conspicuous suppression of cells numbers (cell loss) even when the toroidal fields were activated when just media was injected (rather than hydrogen peroxide) into the cells within the local condition. There was also no non-local effect.

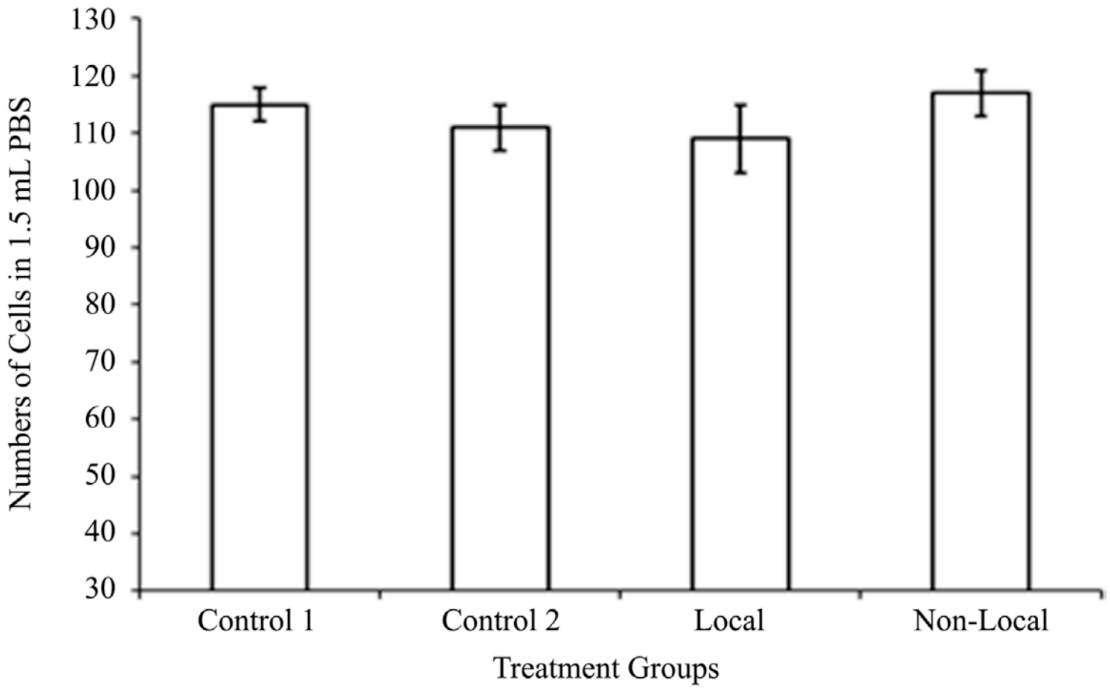

Figure 6: Means and SDs for the numbers of melanoma cells after the serial 50 uLs of media were injected into either the control or to the local and non-local dishes separated by 1.7 km.

10.4 Discussion

Direct and practical application of the variants of excess correlation will likely be one of the most important innovations for information superimposition between non-traditional distances in this century. Although the measurement of temporally congruent changes in properties of clusters of photons simultaneously in two different loci have been described as “macro-entanglement” or “teleportation”[4], the essential operation is the superimposition of information in its most fundamental form. We are assuming, as has Vaziri et al [8] that this fundamental form involves photons. Previous research has shown that excess correlation can occur over tens of meters to several kilometers for discrete photon emissions from controlled chemiluminescent reactions.

The results of the present experiments demonstrated that robust, reliable excess correlations occurred with a very specific sequence of changing angular velocities of discrete (3 ms) pulsed magnetic fields generated through double-circular geometry, i.e., a toroid. This unique configuration can be conceived as a three dimensional extension of a circle, a helical pattern, that is then contained within a circle. When the current generated with this double-circular geometry is pulsed, with the features of a “quantum well”, and the inter-pulse durations change systematically to simulate changing angular velocity (and

momentum), the conditions are created to allow potentially Mach's principle to be manifested as well as additional properties of photons if they display non-zero rest masses [14].

The combination of Mach's principle that emphasizes angular momentum [23] as an important contributor to the process by which a change in any subset of the universe affects the entire universe or set and the "extensional" properties of a photon may be one substrate for the occurrence of excess correlations. We have suggested that specific duration of pulsed magnetic fields is derived from the largest and smallest features of the universe reflected by Hubble's parameter and Planck's constant. Persinger and Koren [24] had shown that the time required for the width of a proton to expand one Planck's length would be about 3 ms. The required duration for an electron would be about 1 ms. Experimental evidence from photon emissions from chemo luminescent reactions supported this values [23].

We designed the temporal parameters for this experiment to be very specific such that the 3 ms pulse would satisfy the proton condition. The differential between the addition or subtraction of 2 ms for the inter-pulse duration could be considered a persistent derivative (or rate of rate of change) that resulted in a beat frequency. This beat frequency or subtraction between the 3 ms and 2 ms durations would be 1 ms, or the predicted duration for the electron. If our model is correct

the two basic components of matter, the proton and electron, and their spatial arrangements that determine molecular structure and activity and ultimately the properties of the living cell would be congruent.

Although the empirical support for such integration across quantum and macro-level processes will require more verification, the energy quantities that would be associated with the non-local effects reliably demonstrated in the present experiments can be tested by calculations. The median strength of the magnetic fields generated from the toroids within the center that was occupied by the plates of cells only once for 12 min was about 5 μT. According to the classic formula:

$$E=B^2 \cdot (2\mu)^{-1} \cdot m^3 \qquad (1),$$

where B is the magnetic field strength, μ is the magnetic permeability ($4\pi \cdot 10^{-7}$ $N \cdot A^{-2}$) and m^3 is the volume, the energy available within the volume of a melanoma cell with a diameter of 12 μm or a volume of 9×10^{-16} m^3 would be $\sim 10^{-20}$ J. This value is associated with the energy of forces over the distances between the potassium ions that are attributed to the resting membrane potential and the exchange of "information" between receptors and ligands [25]. This value is well within the quantity of energy associated with average force within the universe per Planck's

voxel (about 10^{-19} N) applied across the most ubiquitous wavelength of neutral hydrogen (21 cm) or $2.1 \cdot 10^{-1}$ m [26]. Although interesting, the solution is not easily tested empirically.

However the potential bases for the narrow band of cell loss in non-local space that was associated with injection of the specific concentration of 800 μM of hydrogen peroxide into local space could be pursued quantitatively. The numbers of molecules injected during the protocol would have been 6 injections ($5 \cdot 10^{-5}$ L per injection) $\cdot$ ($8 \cdot 10^{-4}$ M/L) $\cdot$ ($6.023 \cdot 10^{23}$ molecules per M) or $1.45 \cdot 10^{17}$ molecules. Our previous research has indicated that the proton, specifically the one associated with the hydronium ion, is a major mediator of the magnetic field effects. At pH 7.4, which would be the mode value of the cell culture as verified by the color of the media, the molarity would be $3.98 \cdot 10^{-8}$. Hence the total number of protons involved with this total protocol would be $5.77 \cdot 10^{9}$.

This becomes important when the magnetic energy from the applied toroid fields is calculated for the total volume of hydrogen peroxide injected. According to equation (1) for a 5 μT field the energy within $3 \cdot 10^{-7}$ m^3 (300 μL from 6, 50 μL injections) would be $3 \cdot 10^{-12}$ J. This means that per second on average the synchronized energy from the two toroidal magnetic fields would be the quotient or $0.521 \cdot 0^{-21}$ J. When applied over

the total protocol duration of 12 min or 720 s, the total energy available to the system would be $3.67 \cdot 10^{-19}$ J.

This quantity may be essential for understanding the process. When the value is divided by Planck's constant ($6.626 \cdot 10^{-34}$ J·s) and this product is divided into the velocity of light in a vacuum, the wavelength is ~545 nm. This wavelength is within the visible range. In unpublished (and replicated) experiments we found that the average of the split spectrum of peak wavelengths of emissions of photons that were measured from melanoma cells during the 60 min period after they were exposed to other forms of pulsed magnetic fields was ~545 nm.

If a type of "experimental teleportation" [4] is involved with this protocol, then the properties of the electron should also be accommodated. The total numbers of cells in the re-suspended pellet in 1.5 mL of PBS, can be estimated quantitatively. Assuming an average of 130 cells in the control condition (e.g., Figure 4) which was from 8 fields the product multiplied by 18/8 (where 18 was the total number of fields occupied by 15 µL, the numbers of cells in 1.5 mL would be $2.3 \cdot 10^{5}$. The total number of cells multiplied by the unit energy per H^{+} from the peroxide reaction was $3.7 \cdot 10^{-19}$ J for the total exposure. Hence the total energy for the system was $8.6 \cdot 10^{-14}$ J. This is a particularly significant value because (when divided by the velocity of light squared) the mass equivalence is $9.5 \cdot 10^{-31}$

kg, effectively the rest mass of an electron. For this value to occur very specific molarities of reactants and associated pH would be required as noted in our experiments. The convergence of the total energy within the system with a single electron classical mass could create the conditions for coherence [2]. It would also metaphorically become a type of "condensate" where by the state of the unit (electron) reflects the entire unit (the system).

Although the intricacies of such convergent reactions must still be isolated, these calculations may help explain the non-linear effect and why 800 µM of peroxide produced the greatest effects while 300 µM did not. For the latter the critical numbers of molecules were not available to produce the energy per molecule from the toroidal magnetic field to produce the energies that would be associated with the critical photon wavelength or the "condensate" of total energy of the entire population of cells. If all of the cells died from the peroxide, then there would be no source for the information to be mediated by the excess correlation.

The injection of the hydrogen peroxide into the cells is very likely to have promoted a variant of the well known reaction within hypochlorite ions that would have been available from the interaction of sodium and chloride with oxygen proximal to the cells' plasma membranes. Our interpretation is that the

emissions of these photons from the local cells were ultimately represented within the cells 3 m or 1.7 km away in the non-local spaces. Whether or not these photons occurred during the 12 minutes of exposure or later when cells from both the local and non-local sites were likely to have emitted photons because both had been exposed to the magnetic fields remains to be tested. The latter condition would suggest that once experimental "entanglement" had occurred the photon transpositions between spaces could occur during any subsequent time.

Another more information-based approach involves the quantum of energy associated with the dissipation of a bit of information into entropy. There could be the consequent transformation of virtual particles into matter determined by this information from the zero point vacuum oscillations into a non-local space [27]. Landauer's solution derived from $\ln 2 \cdot kT$ where k is the Boltzmann constant and T is absolute temperature for the incubation temperature would be $4.2 \cdot 10^{-21}$ J per bit. If we assume the total energy in the system from the magnetic field energy, as calculated previously was $8.6 \cdot 10^{-14}$ J, then there would be $\sim 2 \cdot 10^{7}$ bits available for the system. Because about 10^{5} cells in the non-local space were eliminated, this would involve about 200 bits per cell. If this sufficient to initiate a cascade that results in cell death must be verified experimentally.

These results are consistent with but not proof our hypothesis that macro-excess correlation can be demonstrated in the laboratory. The narrow-band nature of the concentration of reactants that produced comparable effects at distances of 3 m and 1.7 km are also consistent with the superimposition of two loci into the same space such they behave as the same space. One interpretation of our results is that the excess correlation protocol produced the conditions by which the changes in protons and electrons within the local cells due to the peroxide injections resulted in transpositions of protons and electrons (or the virtual particles from which they originated) into both loci.

10.5 Conclusion

Specific sequences of changing angular velocities of serial point duration magnetic fields generated within toroids separated by 3 m or 1.7 km produced excess correlation from experimentally-induced changes in the viability of about 10^5 cells or the equivalent of 2 to 5 x 10^{-8} kg. One day after only 12 min of exposure to chemical reactions (local cells) that reduced cell numbers by 50% similar numbers of cells were reduced in plates of non local cells but only if both local and non-local spaces shared the excess correlation protocol. The specific molarity of hydrogen peroxide that produced the maximum effect was associated

with the numbers of protons in hydronium ions whose energy per molecule from the specific intensity of the magnetic fields would allow the conditions for photon emissions and production of the rest mass of an electron. Both phenomena may be manifestations of or means by which fundamental bits of information can be transposed in separate spaces. The results are consistent with transposition of the chemical reactions in the local cells to the non-local cells.

10.6 References

[1] A. D. Aczel, "Entanglement: The Greatest Mystery in Physics", Raincoast Books, Vancouver, 2002.

[2] I. Afek, O. Ambar and Y. Silberberg, "High-NOON states by mixing quantum and classical light," *Science*, Vol. 327, 2010, pp. 878-881.

[3] X.-M. Jin, Ji-G. Ren, B. Yang, Z.-H. Yi, F. Zhou, et al "Experimental free-space quantum teleportation" *Nature Photonics*, Vol. xx, No. xx, 2010, pp. xx-xx.

[4] M. Hotta, J. Matsumoto and G. Yusa, "Quantum energy teleportation without limit of distance," *Physical Review A*, Vol. 89, 012311, 2014.

[5] S. J. Olson and T. C. Ralph, "Extraction of timelike entanglement from the quantum vacuum,"

[6] M. A. Persinger, "A Possible Explanation for the Vacuum Catastrophe," *International Journal of Astronomy and Astrophysics*, Vol. 4, 2014, pp. 178-180.

[7] M. A. Persinger, "Discrepancies Between Predicted and Observed Intergalactic Magnetic Field Strengths from the Universe's Total Energy: Is It Contained Within Submatter Spatial Geometry?", *International Letters of Chemistry, Physics and Astronomy* Vol. 11, 2014, pp. 18-23.

[8] A. Vaziri, G. Weihs and A. Zeilinger, "Experimental two-photon, three dimensional entanglement for quantum

communication," *Physical Review Letters*, Vol. 89, No. 4, DOI:1103/PhysRevLett89:240401.

[9] E. Megidish, A. Halevy, T. Shacham, T. Dvir, L. Dorvat and H. S. Eisenberg, "Entanglement between photons that have never co-existed,"

[10] B. Julgaard, A. Kozehekin and E. S. Polzik, "Experimental long-lived entanglement of two macroscopic objects," *Nature*, Vol 413, 2001, pp. 400-403.

[11] B. T. Dotta,

[12] M. A. Persinger and G. F. Lafreniere, "Space Time Transients and Unusual Events," Nelson-Hall, Chicago, 1977.

[13] B. T. Dotta and M. A. Persinger, "'Doubling' of local photon emissions when two simultaneous, spatially separated, chemiluminescent reactions share the same magnetic field configurations," *Journal of Biophysical Chemistry*. Vol. 3, 2012, pp. 72-80.

[14] L.-C. Tu, J. Luo and G. T. Gilles, "The Mass of the Photon," *Reports on Progress in Physics*, Vol. 68, 2005, pp. 77-130.

[15] S. A. Koren, B. T. Dotta and M. A. Persinger, "Experimental Photon Doubling as a Possible Local Inference of the Hubble Parameter," *The Open Astronomy Journal*, Vol. 7, 2014, pp. 1-6.

[16] B. T. Dotta, C. A. Buckner, D. Cameron, R. F. Lafrenie and M. A. Persinger, "Biophoton Emission from Cell Cultures:

Biochemical Evidence for the Plasma Membrane as the Primary Source," *General Physiology and Biophysics*, Vol. 30, 2011, pp. 301-309.

[17] D. Fels, "Cellular Communication Through Light," *PLOSone*, 4, 2009, doi: 10.137`/journal.pone.0005086.

[18] R. Bajpai, L. Brizhik, E. Del Giudice, F. Finelli, F.-A. Popp, and K-P. Schlebusch, "Light as a Trigger and a Probe of the Internal Dynamics of Living Organisms," *Journal of Acupuncture Meridian Studies*, Vol. 3, 2010, 291-297.

[19] B. T. Dotta, N.J. Murugan, L. M. Karbowski, R. M. Lafrenie and M. A. Persinger, "Shifting Wavelengths of Ultraweak Photon Emissions From Dying Melanoma Cells: Their Chemical Enhancement and Blocking Are Predicted by Cosic's Theory of Resonant Recognition Model for Macromolecules," *Naturwissenschaften*, Vol. 101, 2014, pp. 87-94.

[20] N. J. Murugan, B. T. Dotta, L. M. Karbowski and M. A. Persinger, "Conspicuous Bursts of Photon Emissions in Malignant Cell Cultures Following Injections of Morphine: Implications for Cancer Treatment," *International Journal of Current Research*, Vol. 6, 2014, pp.

[21] N. Rouleau, T. N. Carniello, and M. A. Persinger, "Non-Local pH Shifts and Shared Changing Angular Velocity Magnetic Fields: Discrete Energies and the Importance of Point Durations," *Journal of Biophysical Chemistry*, Vol. 5, 2014, pp. 44-53.

[22] N. Rouleau and M. A. Persinger, "Local Electromagnetic Fields Exhibit Temporally, Non-Linear, East-West Oriented 1-5 nT Diminishments Within a Toroid: Empirical Measurement and Quantitative Solutions Indicating a Potential Mechanism for Excess Correlation " *Journal of Electromagnetic Analysis and Applications* (in submission).

[23] M. A. Persinger, "Experimental Evidence that Hubble's Parameter Could Be Reflected in Local Physical and Chemical Reactions: Support for Mach's Principle of Imminence of the Universe," *International Letters of Chemistry, Physics and Astronomy*, Vol. 11, 2013, pp. 86-92.

[24] M. A. Persinger and S. A. Koren, "A Theory of Neurophysics and Quantum Neuroscience: Implications for Brain Function and the Limits of Consciousness," *International Journal of Neuroscience*, Vol. 117, 2007, pp. 157-175.

[25] Persinger, M.A. (2010) 10^{-20} Joules as a Neuromolecular Quantum in Medicinal Chemistry: An Alternative Approach to Myriad Molecular Pathways. Current Medicinal Chemistry. 17. 3094-3098.

[26] M. A. Persinger, S. A. Koren and G. F. Lafreniere, "A Neuroquantological Approach to How Human Thought Might Affect the Universe," *Neuroquantology*, Vol. 6, 2008, pp. 262-271.

[27] Bordag, U., Mohideen, U. and Mostepanenko V.M. (2001) New developments in casimir effect. Physics Reports. 353. 1-205.

Chapter Eleven

11.0 Discussion and Conclusion

After aggregating and summarizing the results presented here, three significant advances can be discerned. First, malignant cells can be detected using combinations of highly specialized spectral analysis techniques as well as combinations of filters which isolate wavelength-specific photon signatures characteristic of aberrant biological processes. The data indicate that the critical threshold of 1% malignancy within a medium consisting of 99% non-malignant cell culture is associated with a particularly conspicuous signature in this regard. Other experiments demonstrated that stored photon energies are reliably emitted and detected once probed by interacting stimulations of electromagnetic fields and applied light. Together, these discoveries suggest that discernment of malignant cells (cancer detection) by means of a photon signature is possible both in principle and in practice.

As a matter of practical application, these technologies and methods could be used to detect malignancy at earlier stages relative to those associated with current methods. In addition to simple detection, the prospect of a type of photon-biopsy, wherein light is applied directly to the tissue, re-emitted, and assessed by a researcher or clinician is now feasible. With the application of specific energies to the tissues in question,

photon signatures can be assessed and compared to normative databases in order to infer pathology. These inferences are characteristically early-staged and non-invasive.

The second advance is important for reasons which are theoretically fundamental. Because wavelength-specific activation values of a molecule can be predicted based upon Cosic's resonance model, entire biomolecular pathways can now be characterized as unique arrays of spatially distinct units, unbound by chemical restraints. That is to say, biochemical probes are not necessarily required in order to infer the presence of molecules now that molecular structure can be reduced to basic geometrical patterns with predictable signatures of photon emissions. It is conceivable that with the appropriate, careful dissection of each cellular pathway, a full and complete characterization of biomolecular pathways can be achieved within the context of resonance recognition.

This advance would significantly narrow the focus of photon detection and application paradigms relevant to cancer and other biological paradigms. From here, future research should attempt to demonstrate the parity which would be evident in a systematic comparison of chemical and resonance-based analyses of biomolecular pathways. By knocking out individual molecular components within a cell and tracing the resonant consequences of said knock-outs by means of the resonant recognition model (RRM),

cellular maps of resonant “hot spots” could be generated to target particular regions of interest within cells using photon-based applications of energy. In this regard, we could paint the target before taking aim and destroying it.

The third and final advance which can be discerned based upon the works presented here consists of a significantly improved and precise understanding of the consequences of applied, complex electromagnetic fields upon malignancies. Our experiments indicate that by a targeted expansion-contraction of malignant cells, complete dissolution can be achieved which is not observed in healthy, non-malignant cells. This finding bodes well as current cancer therapies are relatively crude, targeting non-specific though critical biomolecular processes such as those involved in mitosis. By increasing the precision of cancer treatments, collateral damage at the level of tissue will be reduced which in turn decreases the likelihood of secondary malignancies or associated complications.

Examining the physical bases for our effects, we observed some key details which will inform future developments in this area of research and clinical application. One significant observation was that selective shielding of components of the solenoids which emit the electromagnetic fields can reduce or modulate the field application in ways which are biologically relevant. This method of tuning suggests that the distribution of

ferromagnetic and paramagnetic materials within the vicinity of the exposure area can dramatically alter the magnitude of the effects observed. For instance, we observed that elevating the exposure chamber and thereby increasing the distance between the exposed material and the copper-laden environment increased efficacy.

Further, and perhaps most importantly, we systematically identified the optimal point duration associated with our particular exposure paradigm: 3.2 ms. By achieving this value, we have both highlighted the importance of millisecond-precision and noted a further parameter of electromagnetic field exposures which requires "tuning". Finally, our experiments further demonstrated that non-local techniques could be used to destroy cancer cells by means of alternative electromagnetic field applications. Though this discovery indicates a potential avenue for further research, the full implications of this latter finding are not entirely evident at present.

Because research in this area indicates that non-local processes can be generated both naturally and by synthetic means, it is entirely possible that we have replicated a process which is already abundant in nature. That is, our non-local approach is perhaps a demonstration of a phenomenon that is already happening all the time: the communication between cellular systems across non-traditional spaces as relating to pathology. If this is the

case, further research should aim to identify ways in which unintended communication between cells can be reduced, thereby decreasing noise within the cellular microenvironment and potentially reducing pathological conditions as a consequence of non-local, cellular mixed messages.

In summary, these advances provide a solid basis for further research relating to the detection, targeting, and destruction of cancer. With the development of highly-precise technologies and with ever-increasing spatial and temporal resolutions, these advances will become increasingly relevant within the clinical setting. It is entirely possible that within the foreseeable future, clinics and hospitals will make use of photon detection as well as resonant models to diagnosis and treat cancers in humans.

Our research has provided a path to this end by systematically identifying principles which govern these technological applications. Biomolecular pathways are and always have been characterized by both chemical and physical properties. By reconciling these perspectives, advanced techniques can be developed to fight cancers in ways currently unimagined. Though we have performed many experiments in pursuit of these advances, there is still important work which can and must be done.

With regard to photon detection, it is imperative that future research incorporate extensive normative data which can be

referred to when investigating pathological cellular states. For instance, spectral power frequency-shifts of even fractions of 1 Hz increments can be critically important when discussing molecules whose spatial and temporal parameters upon which wavelength will operate at incredibly fine levels of discourse approaching those of atoms. These shifts, if reliably detected, could be used to discern even the difference between a given molecule and its acetylated or methylated counterpart. If such precision can be approximated in photon detection, entire genomes could be mapped by resonant signatures. This will be relatively inexpensive once the equations are tuned and the normative databases are assembled.

With regard to treatment, future research must attempt to streamline the effects associated with applications similar to those presented here. Our physiologically-patterned electromagnetic field exposures, though efficacious under most conditions, can demonstrate unreliable results if particular parameters are not tuned. Future research should aim to identify further tuning parameters in addition to means by which these parameters can be carefully adjusted.

By incorporating many “sliding” parameters into the hardware and software, our exposure paradigms could be tuned to target tumors of particular depths, within particular tissues of particular densities while factoring in variables such as

vascularization, the presence of inorganic depositions and other such individualities. Tailoring treatment to suit the individual has becoming increasingly important within the medical field as researchers and clinicians begin to accept that standardized dosages and procedures based upon means necessarily ignore individual differences which might significantly impact the efficacy of both diagnosis and treatment. Our approach is well-suited to individualized application.

If cancer is inextricably tied to the fundamental processes which govern normal, healthy cellular life cycle, attempts to inhibit cancer must either be accompanied with the accepted notion that there will be significant collateral damage or that increased precision is needed. We have favoured the latter approach. It is the responsibility of bioengineers to take these advances seriously and to develop new technologies which take into consideration the influences of electromagnetic field intensity, pattern, frequency, phase, application geometry, as well as environmental factors which might modulate these conditions.

That copper significantly influences our exposures is unsurprising, though often overlooked due to conventional thinking. The media within which our cell exposures take place are subject to changes in viscosity dependent upon surface features. The incubators involved in regulating the external

environment in such a way as to maintain homeostasis sufficient to study these phenomena are lined with potential confounding instruments such as mechanical pumps, motors, as well as ferromagnetic and paramagnetic materials. Just as anti-microbial environments are maintained by means of UV-radiation and various disinfectant methods within laboratories which employ cell models, laboratories of the future which attempt to expand upon the research presented here will need to take into consideration the many factors which influence electromagnetic fields.

These future laboratories will need to account for cellular communication within incubators – where light and electromagnetic radiation are no doubt continually absorb and re-emitted by cells, as our experiments have demonstrated. These invisible though entirely physical factors have perhaps already contributed to countless negative results as researchers have attempted to replicate interesting though perhaps less reliable or subtle effects reported by others. These false-negatives will have set back this line of research; this is a consequence of confounds unforeseen and not accounted.

Secondary to the advances presented here, reiterated and summarized explicitly, there are implicit concepts, which must be considered. Most notable: Are traditions impeding progress? Our observations would suggest that biomolecular sciences would benefit from an equal representation of biophysics. The

implications of combining concepts in molecular biology and biophysics will be a more complete understanding of life sciences in general.

The study and eventual intimate understanding of cancer marks the beginning of a new chapter in a scientific pursuit of immortality. The physical bases of chemistry, biology, and each progressive step along the continuum of natural aggregates must be further characterized before death becomes a forgotten, however unpleasant, reality of the past. The advances outlined here might provide a blueprint to this end.

10.1 Future Direction

Replication of fundamental properties and effects of low-level electromagnetic fields on living systems have been shown to be more difficult than anticipated. As the chemical components of molecules have been shown to be highly dependent on the structural molecular complexity, the same principles apply with respect to generated electromagnetic fields where the complexity and structure of a specific temporal pattern dictate successful outcomes. A major component of this thesis provides support for the specificity of temporal patterns and its highly conservative nature with respect to its effects. Several factors such as intensity, point duration and others influence the specificity of a generated temporal pattern where its proper application becomes

crucial in replications. Future work considers on developing these principles of proper field replication and field theory with respect to the engineering of electromagnetic field generation and applications. The major component of appropriately generated electromagnetic fields is highly dependent on the electrical circuitry within the digital to analogue converters (DACs) and its respected coils or solenoids. Focusing on the understanding of proper field propagation shows great promise in enhancing the low-level electromagnetic field effects observed in cancer therapeutics, longevity and tissue regeneration.